COPY C.

YIELDING AROUND NOTCHES IN TENSILE SPECIMENS

A thesis

presented by

Prabir Kumar Basu, B.Tech.(Hons.)

for the

Degree of Doctor of Philosophy

August 1967.

Department of Metallurgy,
Royal School of Mines,
Imperial College,
London, S.W.7.

ABSTRACT

Detailed investigations have been carried out on the effect of notch shape on the mode of deformation in the elastic-plastic strain stage and on the ultimate strength and ductility properties of flat tensile specimens of 3% Si-Fe (average grain diameter = 0.15 mm). A wide range of notches have been covered, with three different root radii (r = 0.015", 0.004" and 0.0015") and ranging in depth from 4.5% to 73%. To test the effect of material characteristics, supporting experiments have been carried out on two other materials - a high-nitrogen steel and a coarse-grained 3% Si-Fe (grain diameter = 0.4 mm). Plastic zone formations were revealed by the dislocation etching technique and these have been compared with the predictions of a numerical analysis using the finite difference method.

These studies have revealed that the mode of deformation in the region of high non-uniform stresses in the vicinity of the notch is determined directly by the notch geometry, but that farther away it is determined by the yield characteristics of the material. Theoretical predictions of yield zones are in close agreement with experimentally etched zones in Si-Fe. Results indicate that whilst Si-Fe obeys the

von Mises criterion of yielding, mild steel follows that of Tresca. Notch strength and ductility results reveal a region of weak notches between notch depths of 36% and 55%. These variations can be related to the mode of deformation as determined from etch-pit observations.

CONTENTS

CHAPTER 1

INTRODUCTION

The presence of stress concentration in the form of notches, holes, cracks, and surface irregularities in structural components has been a constant source of concern to the design engineer. Since structural requirements are precisely the factors responsible for surface irregularities, the problem of non-uniform stress has to be accepted. Scientific research has, therefore, been directed at investigating the true nature of the non-uniformity, and in this respect notches of various geometry have been used extensively to simulate service conditions.

The behaviour of a notched specimen depends in a complex way on a number of factors, e.g., the shape of the specimen, the notch geometry, the elastic and plastic properties of the material, its texture, strength and the laws governing their dependence on the speed and temperature of testing. It has been established, however, that notching has two fundamental effects:-

a) it gives rise to a stress concentration in the immediate vicinity of the notch, and

b) it introduces a triaxial state of stress.

The triaxial stress state existing below a notch may be divided into a "hydrostatic" component, which is the mean stress, $\bar{\sigma} = (\sigma_x + \sigma_y + \sigma_z)/3$ and "deviatoric" components, $\sigma'_x = (\sigma_x - \bar{\sigma})$, $\sigma'_y = (\sigma_y - \bar{\sigma})$ and $\sigma'_z = (\sigma_z - \bar{\sigma})$. It is the deviatoric component of stress which is responsible for plastic flow. Plasticity theory assumes that the hydrostatic component has no effect on the yielding. It is, therefore, generally believed that any material will tend to behave in a brittle manner if the triaxility of tension becomes sufficiently great, i.e., if there is a sufficiently close approach to a state of "hydrostatic tension" in which the transverse tensile stresses equal the longitudinal stress.

Earlier on it was thought that catastrophic service failure resulted from completely brittle conditions and therefore metallurgists and engineers devoted their efforts to simulating brittle characteristics on the laboratory level by using very sharp notches, high strain rates and low temperatures and devising elastic solutions to predict failure.

Quasi-brittle materials like metals, however, behave more in an elastic-plastic than an elastic-rigid manner. Through experiments it has been established now that in these materials no "brittle failure" in practice is entirely brittle and that a certain amount of plastic deformation is

associated with all types of failures. This happens when the maximum stress at the root of the notch or crack exceeds the yield point of the material owing to the stress concentration effect and the elastic strain stage transforms to the elastic-plastic stage, since the material in the vicinity of the notch begins to deform plastically, even though in the centre of the specimen deformation continues to be elastic. In this case the load which is being carried by the notched specimen will depend on the position of the boundary between the elastic and plastic regions.

The ability of continuum plasticity to predict the position of the elastic-plastic boundary and associated redistribution of elastic stresses is limited because of the inherent falsity of its assumptions. Metal deformation is an atomistic process and whilst in simple metallic structures the criterion of yielding is simply the critical resolved shear stress in the planes of crystallographic slip, it is difficult to extrapolate this concept because of the grain boundary complexity effect and the inconsistencies of polycrystalline yield behaviour. Methods of dealing with this problem are suggested by the idealized theoretical proposals of von MISES and similar workers, but any study of the nature of deformation in the elastic-plastic strain stage must, therefore, include some experimental means of delineating

the elastic-plastic interface to verify and adjust the hypothetical model.

Because of the relative simplicity of analysing plane systems, investigations in notch-deformation characteristics are usually done under conditions of plane strain or plane stress, depending on the particular type of information sought.

The purpose of the present work is to investigate the influence of notches of various geometry on the nature and path of yielding under essentially equilibrium conditions. Low strain-rates and substantially plane stress conditions were therefore selected.

CHAPTER 2

INVESTIGATION

The investigation was undertaken with a view to studying the deformation modes in notched tensile specimens in the initial stages of yielding, and correlating the yield behaviour with subsequent strength properties of the notched material.

Because of their well-known dislocation etching characteristics the materials chosen for the investigation were:-

(a) a fine grained 3% Si-Fe

(b) a coarse grained 3% Si-Fe

(c) a nitrogen bearing mild steel.

A variety of notches were used varying in depth and root radius.

The experimental programme can, conveniently, be divided into two sections:

a. where specimens were tested to destruction to provide a measure of the notch strength, and

b. where specimens were tested to various degrees of elastic-plastic strains and an electro-etching technique was used to delineate the propagation of plastic zones with increasing stress.

The experimentally determined modes of deformation have been compared with the predictions of a suitable theoretical model. For this purpose a programme has been developed for the IBM 7090 to solve the governing differential equations for the elastic and elastic-plastic states by a finite-difference representation.

Apart from the geometry of the notch, other factors which influence the manner of deformation at a notch can broadly be classified as:

a) The material yield characteristics, arising from inherent structural factors, e.g., available slip systems, dislocation density, impurity content and atomic bonding.

b) The specimen geometry, i.e., thickness and width, - in determining whether the macroscopic yield mode is characteristic of, e.g., plane strain or plane stress.

c) The conditions of testing, e.g., temperature and strain-rate. Lower temperatures and higher strain-rates make greater demands on the ability of the material to yield plastically in preference to fracture.

Of these, the material yield characteristics is of greatest importance in a study of deformation such as this.

The experimental programme was, therefore, planned to include notch investigations in two particular grain sizes of silicon-iron and a high-notrogen mild steel, in which plastically deformed areas can be revealed by the Fry's reagent.

The other parameters, viz., the specimen size, the temperature and strain rate were kept constant throughout the experimental routine.

The choice of the specimen size was guided by convenience of handling; a suitable width/thickness ratio was selected to approximate to plane stress conditions.

Since conditions were chosen to aid the study of plastic rather than brittle behaviour, all tests were carried out at room temperature under a strain-rate sufficiently low as to allow plastic strain in the material to exist in equilibrium with the applied strain.

CHAPTER 3

LITERATURE SURVEY

The study of notch effects can be conducted on a microscopic level in which the material is considered to be discontinuous with a finite grain structure, or it can be conducted on the engineering level in which material is considered to be continuous and homogeneous and to be composed of identical elements of finite dimensions. The former is the domain of metallurgists and the latter has direct applications in engineering design.

A summary of related work pertaining to the two different approaches has been presented in the following sections.

3.1 THE ENGINEERING APPROACH

Most work in this field has been aimed at understanding the phenomenon of brittle fracture, its initiation and propagation. The most important factor in this respect is the stress state generated ahead of a notch or crack and a number of theoretical analyses are available. Some of the relevant ones have been presented in Chapter 7.

Since this work deals with plastic deformation occurring at notches, only some important findings which can help in

understanding the notch effects, mainly the stress concentration factor and the transverse stresses, are included here.

3.1.1 The Stress Concentration Factor.

The stress concentration factor, α_k, has been found to be independent of the absolute value of the nominal stress as well as of the material provided that the latter remains elastic and that the profile of the notch is not too sharply curved (NEUBER (1)). The above two conditions must be sufficiently fulfilled in that the loading is not so great that the maximum stress exceeds the elastic limit. In the classical theory of elasticity a hypothetical model is used, wherein the material is structureless and made up of infinitely small elements. When the root radius, r, of the notch is large compared to the crystalline structure of the material no error becomes evident because the stress gradient occurs over sufficiently large distances relative to the structure. In the case of very sharp notches, however, the stress variations occur over very small distances having the order of magnitude of the crystals and hence the existence of a finite crystal structure can no longer be ignored.

The law of stress gradient essentially states that the higher the stress peak at a point the more sharply (at small

distances away from the point) it fades out bringing about considerable relaxation of stresses around the margin of the highly loaded zone (NEUBER). Accordingly, only that part of the surface of the notch which belongs to the most highly loaded zone will essentially affect the maximum stress. Hence for round notches, the curvature of the base will be of primary importance in determining the stress distribution, while for a sharp notch the flank angle will play a much more important role.

(a) Effect of notch depth.

In the case of "shallow" notches (not defined exactly), the stress variation is distributed only in the immediate vicinity of the notch, while at a greater distance it is merely a case of uniform stress distribution regardless of the notch. GREEN and HUNDY (2) have defined a shallow notch for the case of an externally notched prismatic bar in bending as $d/a < 1.4$, where d is the notch depth and a the depth of material below the notch, called the ligament. Within the shallow range, therefore, the depth of notch is the more important factor as regards the stress distribution than the actual width of the specimen. On the other hand, for a deep notch the stress variation will extend over the entire narrowest section and therefore, the width of the

narrowest section will determine the stress concentration factor, while the notch depth itself becomes less important. For both the limiting cases, i.e., when the depth of notch, d, equals zero and when the ligament ($a \to 0$) becomes so slender that the immediate vicinity of the narrowest section can be regarded as a straight bar, the stress concentration factor, α_k, becomes equal to unity.

(b) Calculation of the stress concentration factor.

NEUBER (1) has derived formulas for α_k as a function of the non-dimensional ratios a/r and d/r and presented them in the form of nomographs for notches removing from 0 to 100% of the crossectional area and for a variety of loading conditions.

Values of α_k can also be determined from a number of analytical elastic solutions described in Chapter 7.

Experimental values of the stress concentration factor can be calculated by dividing the yield stress of an unnotched material by the nominal applied stress at which the first sign of yielding is detected under the notch. While in principle this is justified, because transverse stresses at the root are zero and yielding should start when the $(\sigma_x)_{max}$ reaches the yield stress in tension, the problem of developing a sufficiently accurate method for detecting slip initiation is considerable.

Experimental measurements of α_k have been made by FROCHT (3), DIXON (4) using the photo-elastic technique and by KNOTT (5), WILSHAW (6) and GRIFFITHS (7) using etch-pitting techniques. KNOTT found experimental values of α_k were much lower than those predicted by theory, but since his results were based on fracture tests this might be expected if fractures were not completely brittle. It has been suggested that even small amounts of plastic strain reduce the stress concentration factor (SACHS et al (8)).

WILSHAW,(6), using a sharp notch in bending plotted plastic zone sizes against stress level according to a theoretical relationship developed by DUGDALE (9) (equation 3.1)

$$\rho/d = \sec\left[\frac{\pi}{2} \cdot \frac{\sigma_n}{\sigma_y}\right] - 1 \qquad (3.1)$$

where ρ is zone size, d is the notch depth, σ_n the nominal stress and σ_y the yield stress. Extrapolating the curve to $\rho = 0$ enabled the value of α_k to be deduced and WILSHAW found that the value predicted by his material, mild steel, was too high when compared with his experimental value and with that computed from NEUBER's nomographs.

In similar notch bend tests, GRIFFITHS (7), using a more sensitive etching technique has found slip bands at loads predicted from NEUBER's theoretical values of α_k.

3.1.2 The Tranverse Stress.

It is a familiar experimental observation that in a notched bar the mean stress in the neck, measured at the yield point, is greater than the yield stress with an unnotched specimen. The notch strength (maximum load/ original notch cross-section) too, has been found to increase, linearly, with notch depth in a ductile and homogeneous metal (8, 10). This linear relationship has often been found to terminate for a fairly sharp notch, having nearly a 100% notch depth, in a value approximately twice the ultimate strength of the metal. The reason for this phenomenon is, broadly, that the lateral contraction which would accompany a uniform extension in the neck is partially inhibited by the adjoining bulk of material; a lateral tension is thereby induced, in the face of which the requisite shear stress for yielding is only attained by means of an increased axial tension. The transverse notch contraction thus represents an average estimate of the lateral stress. By plotting notch contraction against the conventional longitudinal strain for the value of e_x/e_y and using it in the von MISES criterion, LECQUEAR and LUBAHN (11) obtained a measure of the biaxiality through the thickness of their specimens. They found that the biaxiality reduced

to half its value from the central plane to the side surface.

Results (12) have also indicated that the transverse stress in the restrained notch section is little affected by notch radius between zero and some critical value. When the notch radius becomes rather large, however, the notch strength and correspondingly the transverse tension decreases with increasing radius, while the notch ductility (contraction in area) increases.

Experiments in axially symmetric and flat notched specimens have produced higher fracture strengths in the former than in the latter (KENYON and BURNS (13)). This has been attributed to a more rapid increase in transverse stress during local contraction in the axially symmetric than in the flat specimen (13).

3.1.3 Fracture at Notches.

On the occurrence of fracture at notches, two generally accepted criteria for a brittle initiation exist:-

(a) Brittle fracture would occur if the maximum tensile stress attained a critical value before the shear stress necessary to bring about yielding. The presence of a notch enhances the possibility of brittle fracture by increasing the ratio of maximum tensile stress to shear stress.(DAVIS, PARKER and BOODBERG (14), YUKAWA and

McMULLIN (15), BARTON and HALL (16)). The temperature and strain-rate dependence of brittle fracture has been ascribed entirely to the dependence of the yield stress on those parameters (HENDRICKSON et al (17)).

(b) The maximum normal stress and a large ratio of the maximum normal stress to maximum shear stress are the most important factors determining brittle fracture, which was most likely to be initiated at the mid-thickness of a plate where the tensile stress in the thickness direction is a maximum (JENKINS et al (18), COTTRELL (19)). In a qualitative discussion GRINTER (20) has reasoned that in a plate of sufficient thickness the tensile stress in the thickness direction can attain values of the order of the yield stress.

In analysing the notch properties of high strength sheet alloys, WEISS, SESSLER and others (21, 22) found that the stress gradient is the predominant factor influencing notch strength. Other factors, such as specimen geometry and elastic stress-concentration factors, are significant only in so far as their contribution to the magnitudes of the stress gradient and the maximum stress in the region of the notch root.

Other tests (SACHS et al (8, 10, 12)) , particularly on high strength materials have indicated that maximum

embrittlement occurs with notches removing between 30% and 60% of the cross-sectional area. The observation was explained on grounds of higher stress concentrations developed in these notches and the inherent lack of ductility of the materials, which helps the stress concentration effect to be retained even at late stages of yielding.

Stress analyses based on classical elastic theory give results that are probably very near the truth, but with the onset of plasticity the picture becomes very confused because different materials under different conditions of testing, yield in widely different manners and it is not feasible to apply a general model which could embrace the yield behaviour of a wide range of materials. This is the disadvantage of the engineering approach, which has to assume an idealised material to which the above restrictions do not apply.

The engineering yield stress represents a state where there is already a large amount of plasticity on a microscopic scale. To understand the dependence of the yield stress on various external parameters it becomes essential to understand the phenomenon of micro-yielding, its onset and nature of development in real materials. This is where an engineering analysis has to be supplemented by more fundamental research into yield propagation through dislocation motion and the barriers resisting a free flow of dislocations.

3.2 METALLURGICAL APPROACH

In relation to the onset of plasticity the most significant points on the stress-strain curve for a conventional tensile test are:-

(a) The stress, σ_E, at which the first sign of a loop in observed on unloading. This has been said to be the true elastic limit, as a loop represents an energy loss (BROWN and EKVALL (23)).

(b) The stress, σ_A, at which the loop is open, represents the limit of anelasticity. A deviation from linearity can be measured at this stage, and this is usually the same as the limit of proportionality (BROWN and EKVALL).

(c) The stress, σ_{yd}, at which there is macroscopic flow, usually initiated by the break-down of grain boundary resistance at some stress called the "first slip break-through stress" (WORTHINGTON and SMITH (24)).

The region between the elastic limit and the macroscopic yield stress is known as the region of microyield. Micro-yielding and its relationship with the yield stress is dealt with after defining some of the characteristic features of the yield stress itself.

3.2.1. The Yield Stress.

It is well known that b.c.c. metals will in general exhibit the phenomenon of abrupt yielding and that the stress at which this occurs varies with material properties, such as, grain size, impurity content and also with testing conditions, such as, temperature and strain rate. To explain the dependence of the yield stress on these parameters various theories have been proposed on the mechanism of yielding.

(i) The mechanism of yielding.

The well-established dislocation locking concept of COTTRELL (25) has helped considerably in understanding the phenomenon of yielding and the yield drop. Evidence in support of the mechanism is found in the direct observation of particles formed on dislocations by electron microscopy and in the dependence of the yield drop and discontinuous yielding on interstitial impurities (LOW and GENSAMER (26)). Other evidence, such as the Lüders strain and the Lüders band velocity (FISHER (27)) cannot be adequately explained by the unlocking concept. The grain-size dependence of unlocking presents other difficulties. While the observed $d^{-\frac{1}{2}}$ dependence of the lower yield stress is in accord with the unlocking theory (HALL (28), PETCH (29)), it frequently is not influenced by test temperature in the manner

prescribed (CONRAD and SCHOEK (30), KAZINCZY et al (31), STROH (32)). Furthermore, the same dependence is displayed by f.c.c. metals in the absence of discontinuous yielding (BALDWIN (33)). Finally, the PETCH interpretation of $d^{-\frac{1}{2}}$ in terms of unlocking and pile-ups does not provide for yield points displayed by single crystals (SCHWARTZ and LOW (34)).

These difficulties have directed attention to an alternative view - developed by JOHNSTON and GILMAN in their studies in LiF. They found that LiF crystals exhibit a prominent yield drop but show no evidence of unlocking. The dislocations responsible for slip were heterogenously nucleated (GILMAN and JOHNSTON (35)) and multiplied rapidly. KOEHLER (36) first proposed the hypothesis that after a given Frank-Read source had produced a number of loops and the process of generation had failed to carry through, further development could proceed by a process of cross-slipping of the screw components from the active plane without the need of further primary source activation. Following this JOHNSTON and GILMAN (37) accounted for the yield drop quantitatively simply in terms of the rapid multiplications of dislocations and the stress dependence of the dislocation velocity.

STEIN and LOW (38) have shown that in 3% Si-Fe the macroscopic yield stress corresponds to the stage where dislocations attain a critical velocity of the order of 10^{-3} cm/sec. Other evidence such as rapid multiplication of dislocations by the cross-slip mechanism have also been found (HOLDEN (39)). The JOHNSTON and GILMAN interpretation of the yield phenomenon has been extended to include Fe, 3% Si-Fe and other related b.c.c. metals by STEIN and LOW (38), HULL (40), HAHN (41), TAKENTI and IKEDA (42).

(ii) Relationship of σ_{yd} with other parameters.

When plastic deformation occurs by slip, it has been established by HALL (28) and PETCH (29) that the lower yield stress, σ_{yd}, is related to the grain size, d, by the relationship:

$$\sigma_{yd} = \sigma_i + kd^{-\frac{1}{2}} \qquad (3.2)$$

where σ_i and k are material constants for a given set of testing conditions.

PETCH based his interpretation of the results on the idea that the lower yield stress was the stress required to propagate a Lüders band from grain to grain by the stress concentration of an array of dislocation piled up at a grain boundary. He used an analysis given by ESHELBY (43) where the shear stress at a distance l directly ahead of a slip band is:

$$(\tau - \tau_i)(d/41)^{\frac{1}{2}} \qquad (3.3)$$

where τ is the applied shear stress, τ_i the lattice friction shear stress and d the grain size.

Thus if τ_c be the critical shear stress to operate a source l ahead of the band,

$$\tau_c = (\tau - \tau_i)(d/41)^{\frac{1}{2}} \qquad (3.4)$$

or
$$\tau = \tau_i + 2\tau_c l^{\frac{1}{2}} d^{-\frac{1}{2}} \qquad (3.5)$$

Since the early theoretical considerations (PETCH (29), COTTRELL (44), CODD and PETCH (45)) were based on a model where both slip planes and directions in each grain were assumed to make angles of 45° with the tensile axis,

$$\sigma = 2\tau = 2\tau_i + 4\tau_c l^{\frac{1}{2}} d^{-\frac{1}{2}} \qquad (3.6)$$

In relation to equation 3.2, this gave an equivalence of σ_i with $2\tau_i$ and k with $4\tau_c l^{\frac{1}{2}}$. Subsequently equation 3.6 has been modified (ARMSTRONG et al (46), WILSON and CHAPMAN (47)) to take into account the different orientations of grains in a ploycrystalline aggregate, and expressed as

$$\sigma = m\tau_i + m^2\tau_c l^{\frac{1}{2}} d^{-\frac{1}{2}} \qquad (3.7)$$

where $m > 2$, is an average orientation factor. Some recent etch-pit observations (WORTHINGTON and SMITH (24, 48)) on polycrystalline 3% Si-Fe have provided experimental support for the relation.

WORTHINGTON (49) suggests that the equation 3.2 is based on the model of sharp slip bands. In order to account

for blunted slip bands they further modified the equation by introducing a factor, q, in the calculation of the shear stress ahead of a blunted band. The shear stress then becomes equal to

$$q(\tau - \tau_i)(d/4l)^{\frac{1}{2}} \qquad (3.8)$$

where $q < 1$ is a parameter which measures the degree of blunting.

From extensive experimentation HESLOP and PETCH (50) concluded that the σ_i term in the HALL-PETCH equation could be resolved into two components: the first, σ_i', increases linearly with the total impurity content and is independent of temperature, whilst the second, σ_i'', is independent of the impurity content, but increases rapidly with decreasing temperature. They suggested, rather tentatively, that the temperature dependent component, σ_i'', could be identified with the stress required to move a dislocation through the perfect lattice, that is, with the Peierls-Nabarro stress.

The most common methods of measuring σ_i are (a) extrapolation backwards of the strain-hardening portion of the stress-strain curve to its intersection with the elastic line and (b) extrapolation of the yield stress-grain size curve to infinite grain size. ROSENFIELD (51) has shown that the two methods of measurement can be regarded as equivalent.

3.2.2 Micro Yielding.

The process of plastic yielding in a polycrystalline aggregate involves the co-operative shear displacement of individual grains; the conventional engineering yield point represents on the strain axis, only a summation of a very large number of these events. It has become increasingly apparent that there is much to be learned about the nature of these processes at strain levels where these events are still relatively isolated. Because of its well known dislocation etch characteristics, Si-Fe has been used extensively for investigations in the pre-yield range of strain.

(i) The elastic limit.

In 1941 KUZNETSOV (52) put forward the theory that there is no absolute elastic limit. His conclusions were based on experiments which showed that as the accuracy of measuring devices increased, deformation was discovered at progressively lower stresses. A number of authors (AVERBACH et al (53, 54), BROWN and LUKENS (55), FINKEL and BEREZOVSKIY (56)) have, since, come to the same conclusion. According to BROWN and LUKENS (55), for instance, plastic variations begin from a deformation of around 10^{-12} per cent.

SHTREMEL (57) has suggested that plastic deformation appears at extremely low stresses but up to the "elasticity

threshold", about 10^{-4} to 10^{-6}% strain, it is quantitatively negligible and associated with reversible movements of dislocations unable to withdraw to the surface of the grain.

FINKEL and BEREZOVSKIY (56) have reported evidence of such reversible movement of dislocations in a 4% Si-Fe at a stress level of 18 - 20 kg/mm^2. They recorded reversible displacements of dislocations, of the order of 2 to 3μ, along sub-grain boundaries by employing a technique of dislocation etching during loading.

(ii) Elasticity threshold : micro-yield point.

At the elasticity threshold (10^{-4} - 10^{-6}% strain) a permanent displacement of dislocations has been seen in Ni, Fe and 3% Si-Fe by BRENTNALL and ROSTOKER (58) using an etch-pitting technique. They called this stress the micro-yield point.

The threshold stress also corresponds to the stress, σ_E (corresponding to a 4 x 10^{-6}% strain), at which ROBERTS and BROWN (59), BROWN and EKVALL (23) first detected a loop on unloading. From LOW and GUARD's (60) observation in iron that edge dislocations move more readily than screw dislocations, BROWN and EKVALL (23) suggested that at this stress only edge dislocations move and that this be the true friction stress of the material.

Nucleation Sites.

As to where slip is initiated, two views exist :

(a) a random distribution of active sites in grains determines slip initiation (SUITS and CHALMERS (61), BROWN and LUKENS (55)),

(b) that slip is initiated at grain boundary sources (MCLEAN (62), WORTHINGTON and SMITH (24), CARRINGTON and MCLEAN (63)).

Observations made by BRENTNALL and ROSTOKER (58) of etch pits in a clean 3% Si-Fe and in iron with a high inclusion content have provided some illumination in this respect. They found that in the unclean material differences in thermal expansion during cooling had generated sufficient stress around the inclusions to cause the initiation of short range slip within grains. In the clean material slip originated at grain boundaries. They also found the micro-yield stress to be grain size dependent in the clean Si-Fe. A high population of inclusions in the iron seemed to negate the grain size dependence effect. SUITS and CHALMERS' (61) observation of a grain size-independent slip initiation stress in Si-Fe suggests a strong resemblance between their material and the unclean iron used byBRENTNALL and ROSTOKER (58).

At this, the elasticity threshold stage, slip bands are confined to a very small region (order of 1μ) near the grain boundary.

(iii) Slip-band formation stress.

Only a small stress increment, about 20% at the most, is required to cause a slip-band to grow in length from 1μ to the size of a grain (WORTHINGTON (24)). This is the stress required to push dislocations against the lattice friction stress across favourably oriented grains and has therefore been identified with the friction stress, σ_i, of the material by MCLEAN (62), WORTHINGTON (48, 49), SUITS and CHALMERS (61). Whether this might or might not be a more accurate description of the friction stress than the σ_E of BROWN and EKVALL (23), it is the more useful parameter from the experimental point of view, and probably corresponds to the stress, σ_A, at which the first sign of permanent deformation is detected on the strain axis on unloading.

From etch-pit observations, particularly of slip bands less than a grain size in length WORTHINGTON and SMITH (24) concluded that two conditions must be satisfied before a slip band traverses a grain:-

(a) The applied stresses arising from a difference in elastic constants between neighbouring grains and magnified by local stress concentrators such as ledges or precipitates must be sufficient to operate a dislocation source at a grain boundary.

(b) The applied stress, resolved along the operative slip system in the grain, and again modified by stresses arising from a difference in elastic constants between neighbouring grains must exceed the lattice friction stress.

Perhaps the only other important stress level before the σ_{yd} is the stress at which slip bands first propagate out of a favourably oriented grain and this has appropriately been called the "first break-through stress."

(iv) The effect of grain size on micro-yield.

SUITS and CHALMERS (61) investigated micro-yielding in 3% Si-Fe with two different grain sizes - 0.17 mm and 0.02 mm in diameter. They found two important differences in the yielding of the two materials:-

(a) The coarse grained material showed no distinct yield drop. The fine grained material in contrast to the coarse had a high yield stress and deformed inhomogeneously showing an upper and lower yield stress.

(b) Slip activity started in both at a stress of about 30 kg/mm^2, but whereas in the coarse grained specimens, at a relatively small further increment of stress, yielding was brought about homogeneously by expanding clusters of yielded grains both at the fillet and the bulk of the specimen, in the fine grained samples deformation was

confined to the fillet until the upper yield stress, when there was a yield drop attended by heavier deformation at the fillet. This was followed by propagation of the bands along the gauge length at the lower yield stress.

The type of non-uniform deformation seen by SUITS and CHALMERS in their fine grained Si-Fe is also typical of mild steel. CRUSSARD (64) has distinguished between the two types of bands by referring to the pre-yield bands which cross the specimen at the fillets in a direction at right angles to the tensile axis as "cross bands", and those that propagate along the gauge length at the lower yield stress as "oblique bands" because these bands progress with their fronts at an angle of about 45° to the tensile axis.

The change in yield behaviour from uniform to non-uniform with decreasing grain size is interesting and a parallel effect has been observed in Si-Fe by increasing the temperature from $23^{\circ}C$ to $100^{\circ}C$ (STEIN and LOW (65)) and in other b.c.c. metals such as Nb, Mo, 0.2C steel (66-70). HAHN(41) has treated this in greater detail.

BRENTNALL and ROSTOKER (58) by varying the grain diameter in Si-Fe between 1.8 mm and 0.2 mm agreed with SUITS and CHALMERS (61) that the differential between detection of micro-yield and macro-yield was least in their

coarse grained material and increased with finer grain sizes. In variance with SUITS and CHALMERS' observations, however, they found no yield drop in any of their material and no evidence of non-uniform yielding. Just before the yield elongation effect, they observed slip to have been activated in every grain even in their finest material.

By comparing their fine grained material with that of SUITS and CHALMERS, BRENTNALL and ROSTOKER attempted to explain the disparity in the matter of what proportion of grains develops slip activity before the yield point is reached by using an idea developed by PETCH (71). PETCH argued that the nucleation of a Lüders band at the upper yield point begins in a grain grouping of 10-100 grains, the size of the grouping being essentially independent of grain size. As the size of the Lüders band nucleus approaches the grain population per unit volume, the upper yield point decreases until at the point of equality, the upper and lower yield are indistinguishable.

From dislocation velocity considerations the grain size dependence of the micro-yield phenomenon can be explained in the following manner:

In a large grain dislocations nucleated at a grain boundary are able to move through it as the applied shear stress exceeds the friction stress, τ_i, of the material.

With increasing stress the dislocations gather speed and when they meet the opposite boundary of the grain they have attained a sufficiently high velocity to propagate through it without much loss in velocity. In a coarse-grained material, therefore, macroscopic yielding takes place very near the friction stress as grain boundaries do not offer effective resistance to dislocations, which move at increasing velocities until a critical velocity for macroscopic yielding is reached.

In a small grain a dislocation would start to move at the friction stress, but before it can attain a critical break-through velocity it meets the opposite boundary and is stopped. The grain boundary acts as an effective locking site and the stress rises. New dislocations are generated at high stresses and move faster until a critical velocity for break-through is attained. A number of these events happen in the specimen and the strain rate of the specimen catches up with the applied strain rate and the stress stops rising. However, multiplication continues with increasing strain producing more than enough dislocations and the stress drops until the dislocation motion is so slow that the strain rate of the specimen equals the applied strain rate again.

Three conditions must therefore be satisfied for the occurrence of a yield drop (HULL (40)):

(a) The initial dislocation density must be small.

(b) The dislocation velocity must not increase too rapidly with increasing stress.

(c) The dislocation must multiply rapidly.

In silicon iron, probably because of a high density of mobile dislocations, a distinct yield drop is not usually seen. However, a very small grain size could presumably provide sufficient barriers to initial movement and thus bring about the yield drop.

3.3 YIELDING AT NOTCHES

When a notched specimen is stretched plastic deformation starts at the root and develops into the specimen. Two distinct forms of zones result and because of their appearance they are usually classified as - (a) wedge-type zone and (b) hinge-type zone.

3.3.1 Wedge-type Zone.

This looks like an inverted triangle with its base at the root of the notch and its apex a little below it (Fig. 3.1). It can therefore, effectively deepen and sharpen a blunt notch. This type of deformation has been predicted by slip-line field analysis for plane strain deformation in notched bars in bending (LIANIS and FORD (72)) and shown

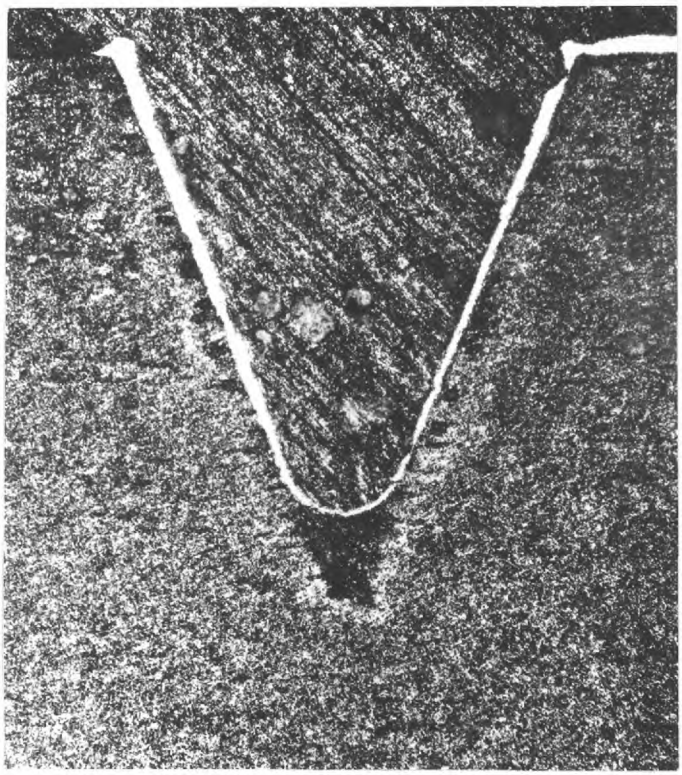

Fig. 3.1. Wedge-type zone (WILSHAW (6)).

experimentally by WILSHAW (6) in plane-strain bending, by KOMHOLOV and USHIK (73) in axially symmetric tension and by DUGDALE (9) and HAHN (74) in plane-stress tension.

The "wedge" probably represents a tensile tearing of the notch, actual separation being prevented by the constraining influence of the surrounding material (DUGDALE (9)). Several factors may serve to intensify this tearing effect. First, such an effect should be enhanced by plane strain conditions and this view is supported by the observations of WILSHAW (6) in three-point bending of Charpy specimens. By etching successive surfaces he found that the wedge was most pronounced in the mid-thickness. Second, flank angle is important. KOCHENDORFER and SCHURENKAMPER (75) showed that the effect of reducing flank angle is to increase the available amount of hydrostatic stress, and this causes a more marked development of the wedge pattern.

Yielding is normally initiated by the formation of a wedge and under brittle conditions further deformation by "hinges" often develops from the tip of the wedge rather than the notch root (KOMHOLOV and USHIK (73)).

3.3.2 Hinge-type Zone.

These are far-reaching arcs of plastic deformation which distribute the high local strain over a large distance. As

such they have also been called accomodation zones (COTTRELL (76)). Their appearance arrests brittle fracture by the relaxation of maximum stresses and lowering of the high stress gradients.

The forms of these zones vary considerably with the stress state arising from the geometry of the notch and the type of loading, temperature, strain rate and material.

Generally, high strain rates (KNOTT (77), WILSHAW (6)), low temperatures, high triaxiality (KOMHOLOV and USHIK (73)), - in other words brittle conditions - favour the formation of thin arcs extending from the notch in a direction roughly at 45^{o} to the longitudinal axis. Low strain rates, higher temperatures and biaxial stress rates, on the other hand, permit zones to develop along the notch or slit axis (DUGDALE (9), HAHN (74)).

The two extreme cases of hinge formation are called the plane strain and plane-stress mode of formation because the direction of shear in the former is mainly in the plane of the specimen, while in the latter it is oblique to the specimen plane.

By comparing theoretical limit loads for plane strain (from slip-line field solutions given by LEE (78)) and plane stress conditions with yield loads in aluminium and mild steel specimens having different thickness (t)/net width (a)

ratios, DRUCKER and FINDLEY (79) found that conditions approximated very closely to plane stress when $t/a \leq \frac{1}{2}$, whereas plane strain conditions required enormous thicknesses ($t/a > 6$). While these limiting values are useful they are not adequate description of the plane strain and stress conditions, the experimental determination of which must employ some means of revealing the actual development of the plastic zones. Etch-pitting techniques have shown that real materials usually exhibit a mixture of both characteristics.

The importance of material yield characteristics in the development of plastic zones in identical specimens under identical conditions of loading has been shown by many authors.

In aluminium, DIXON (4) using a V-notch in tension and BATEMAN, BRADSHAW and ROOKE (80) using a central slit in tension found that hinges were broad and spread in a direction oblique to the tensile axis. DIXON by using a photo-elastic coating found maximum shear strain patterns for a range of notches in good agreement with ALLEN and SOUTHWELL'S relaxation solutions. In mild steel on the other hand, the hinges were narrow and developed along the slit axis (DIXON and VISSER (81), BATEMAN et al (80)) by simple shear as previously seen by DUGDALE (9).

DIXON and STRANNINGAN (82) extended their investigations to include a wider range of sheet materials, such as, copper, aluminium, Ti, brass, austenetic steel and mild steel. By using the photo-elastic coating technique they found that except for mild steel the shear strain distribution for all materials was similar in form to the elastic solution. Using a very sharp slit DIXON and VISSER (81) showed that below a stress, $\sigma_n/\sigma_{yd} = 0.4$, the shear strain distribution in mild steel was of the elastic type, but that this type of distribution broke down at higher loads by the development of plastic zones extending into the specimen along the slit axis.

DIXON et al (81, 82), ROOKE et al (80) concluded that this behaviour was peculiar to mild steel because of its yield point instability.

BILBY, COTTRELL and SWINDEN (76) investigated the distribution of dislocations in front of a sheared crack of length 2c, and the relation between the distance from the crack tip to the farthest dislocation in the distribution as a function of the ratio of the applied stress, σ_n, to the stress for general yield, σ_{yd}. They found the relation to be identical to that developed by DUGDALE (9) (equation 3.9) for the spread of plastic deformation from a sharp notch.

$$\rho/c = \sec\left\{\frac{\pi}{2} \cdot \frac{\sigma_n}{\sigma_{yd}}\right\} - 1 \qquad (3.9)$$

where ρ is the zone size, and c the crack length.

DUGDALE verified the relationship against experimental zone sizes in mild steel.

Etch-pit observations in 3% Si-Fe (HAHN (74), HAHN and ROSENFIELD (83)) seem to indicate that both the plane stress and the plane strain modes are possible. The bands spread slowly with wide-spread relaxation in neighbouring grains and often the entire region between the two limiting plane strain and plane stress directions show yield. TETELMAN (84) has suggested that this is because of a high density of active or lightly pinned dislocation sources in silicon iron.

The two distinctly different types of hinge formation in mild steel and 3% Si-Fe can be related to the non-uniform and uniform yield modes exhibited by the respective unnotched materials. The slit-axial zones seen in mild steel are the equivalent of cross bands that are characteristic of the non-uniform yielding exhibited by unnotched samples of the material. It should, therefore, be possible to predict the form of hinges from the stress-strain curves of materials. It is interesting to note that the very fine grained (0.02 mm) 3% Si-Fe used by SUITS and CHALMERS (61) yielded in a non-uniform manner. It is very likely that deformation patterns in notched samples of very fine grained Si-Fe would be similar in appearance to those in mild steel.

CHAPTER 4

EXPERIMENTAL PROGRAMME

An account is given here of the experimental sequence, the materials used, the dimension and production of the notched specimens, the heat treatments and the etching techniques employed.

4.1 MATERIAL

The experimental materials employed in this investigation, i.e., Si-Fe and mild steel, were both chosen for their expediency of etching plastically deformed areas.

Both materials have been known to exhibit discontinuous yielding and have similar stress-strain curves. On the other hand, whilst mild steel deforms on any of the slip systems $\langle 111 \rangle \{110\}$, $\{112\}$, $\{123\}$, the principal slip plane in Si-Fe seems to be the $\{110\}$ plane (BARRETT, ANSEL and MEHL (85)). The reason for this has been attributed to a lower mobility of screw dislocations in Si-Fe (LOW and GUARD (60)); this restricts cross-slip and inhibits slip on the $\{112\}$ and $\{123\}$ planes. Lower temperatures of testing and higher silicon contents enhance this inhibiting effect.

In the complete absence of carbon a 3% Si-Fe is ferritic, but additions of as little as 0.05% carbon causes some γ-iron

to be present. The 3% Si-Fe used here was in the ferritic range with sufficient carbon present (0.005%), however, for the decoration of dislocations.

The materials used in the experiment and their states prior to the machining of the specimens were:-

(a) A fine-grained Si-Fe alloy containing 2.91% Si and traces of carbon. This was obtained in the form of 0.1" thick cold-rolled sheets from the Steel Co. of Wales, and had an average grain size of 0.15 mm.

(b) A coarse-grained Si-Fe alloy containing 2.85% Si and traces of carbon. This was produced from a stock of 99.9% pure Japanese electrolytic iron and appropriate additions of silicon and carbon, melted and cast under vacuum in the form of 10 lb ingots. These ingots were subsequently hot pressed at about 1100°C into 1" thick slabs and finally hot rolled down to a thickness of 0.1". The sheets were cut into strips and annealed in vacuum for 2 hours at a temperature of 950°C to reduce the background dislocation density. The resultant average grain size was 0.4 mm.

(c) The nitrogen-bearing mild steel was of the following composition:

C	Mn	N	S	P
0.10/0.15	0.2	0.018	trace	trace

This was obtained from N.C.R.E. Rosyth in the form of ½" square-section bars. They were hot rolled down to a thickness of 0.1" and annealed in vacuum for 1 Hour at 850°C to give a uniform grain size of 0.10 mm.

4.2 PREPARATION OF SPECIMENS

The dimensions of the specimen adopted for the investigation is shown in Fig. 4.1. It had an overall length of 3¼" and a gauge section of 1" x ¼". The thickness of the specimens was kept constant at 0.050". Although the use of thinner specimens would have meant a closer approximation to plane stress conditions, this was not possible because of the risk of introducing strain at the roots while machining the notches and in subsequent handling of the specimen before actually proceeding with the tests.

The notches were Izod-type, with a flank angle of 45°. This type of notch falls between the 90° V-notch and the edge-slits that have been used by other workers in this field; it was thought that information on this specific geometry would provide some useful light on the effect of flank angle on the deformation modes.

The experimental programme was planned to cover a wide variety of notches, having three different root radii (r = 0.015", = 0.004", = 0.0015") and ranging in depth from

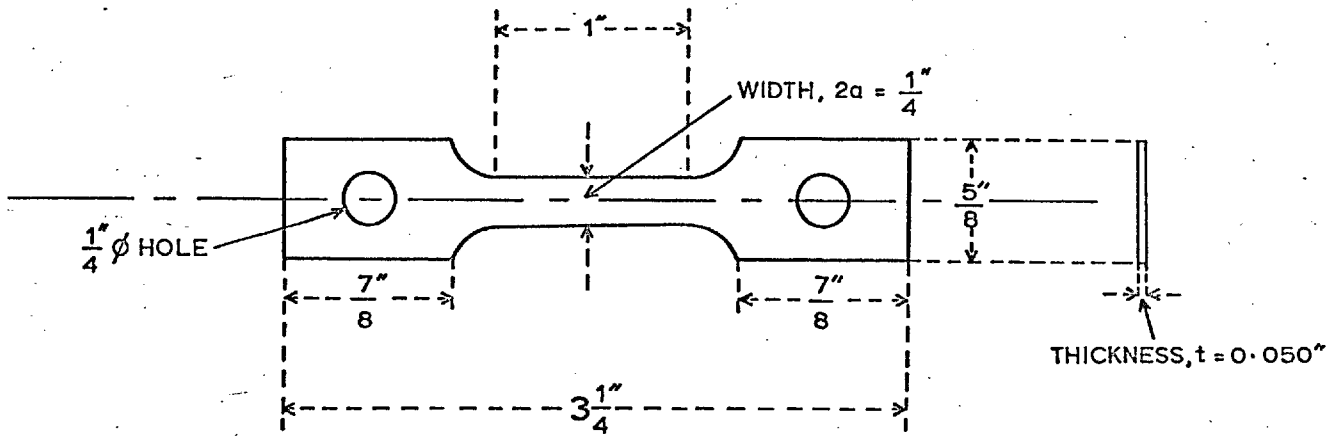

FIG. 4.1. SPECIMEN DIMENSIONS.

Notch Depth %	Root Radius		
	γ = 0.015"	γ = 0.004"	γ = 0.0015"
4.5	1M1 - 1M5	1'M1 - 1'M5	1"M1 - 1"M5
9.0	2M1 - 2M5	2'M1 - 2'M5	2"M1 - 2"M5
22.5	3M1 - 3M5	3'M1 - 3'M5	3"M1 - 3"M5
36.0	4M1 - 4M5	4'M1 - 4'M5	4"M1 - 4"M5
45.0	5M1 - 5M5	5'M1 - 5'M5	5"M1 - 5"M5
54.5	6M1 - 6M5	6'M1 - 6'M5	6"M1 - 6"M5
63.5	7M1 - 7M5	7'M1 - 7'M5	7"M1 - 7"M5
73.0	8M1 - 8M5	8'M1 - 8'M5	8"M1 - 8"M5

TABLE 4.1 Specimen notation for fine-grained Si-Fe (M).

4.5% to 73%. Identical specimens in groups of 5 (for the fine-grained Si-Fe), and 4 (for the mild steel) were manufactures for each combination of notch depth and root radius.

The specimen notation used is explained in Table 4.1. The first number in the notation refers to the notch depth in the order of increasing depth, the number of apostrophes to the root radius in decreasing order, the middle letter refers to the type of material - M for the fine-grained Si-Fe, C, E and F for the coarse-grained Si-Fe and S for the mild steel, and the last number refers to a particular specimen in each group of identical specimens.

4.3 MACHINING OF THE NOTCHES

In order to minimize work-hardening at the roots and to obtain clean, accurate notch profiles the notches were introduced by grinding.

The surface of the specimen was first ground to a smooth flat surface and then mounted on its central longitudinal axis on a special purpose jig. To maintain accuracy in notching, opposite edges at the centre of the gauge length, were ground to a width of 0.220" by rotating the specimen through 180°. Notches were then ground on a Jones and Shipman surface grinding machine. For this purpose a master template was made of the notch form for each root radius, and the notch

form was then developed on the grinding wheel by means of a diamond dressing pantagraph. The notches were then introduced in each specimen, the depth being controlled by a micrometer adjustment forming part of the grinding wheel head. Alignment of the notches was ensured by the central-axis mounting of the specimen.

After notching the specimens in this manner, the flat surfaces were again ground and finally polished on successive grades of emery paper down to the desired thickness. The notch depth and alignment was finally checked on a Reichert projection microscope to an accuracy of $\pm 0.0005"$.

All notched specimens were then given a stress-relieving anneal at 600°C for 5 hours.

The Si-Fe specimens were next heated to a temperature of 900°C, furnace cooled to 550°C and then air cooled. This last treatment has been found to render Si-Fe more amenable to etching, probably by a process of supersaturation of carbon (GRIFFITHS (86)).

4.4 TENSILE TESTS

All tests were done on an Instron testing machine, the specimens being vertically mounted by means of Hounsfield pin grips which allowed free movement about two horizontal axes, at right angles to each other. By this means self-alignment of the specimens was ensured.

A cross-head speed of 0.05 cm/min was used for all tests, but full scale deflection on the load axis and the chart speed was adjusted for each experiment to give the maximum accuracy of recording. Proper seating of the specimen was checked thoroughly before commencing each test and the Instron machine was calibrated after every two tests in order to ensure a correct trace on the chart.

Of every batch of identical specimens one was tested to fracture. The remaining specimens were strained to produce varying degrees of yield between that corresponding to yielding of the first grain and general yield. The mode of yielding was revealed by a dislocation etch-pitting technique.

4.5 ETCHING TECHNIQUES

4.5.1 Si-Fe.

Following the straining routine the Si-Fe specimens were aged at 160°C for about 15 to 30 minutes to permit decoration of slip dislocations by segregation of carbon. The specimens were then polished on a fine grade of emery paper and were prepared for electropolishing by stopping off all but the notched area by a thin coating of Lacomit enamel.

Electro-polishing and etching was done in MORRIS's chromic-acetic electrolyte of the following composition:

Glacial acetic acid (99.5% by weight).....133 ml

Chromium trioxide..... 25 gm

Water..... 7 ml

The solution deteriorates on prolonged standing and hence necessitates the frequent preparation of fresh solution.

During electro-polishing, the electrolyte was contained in a glass dish with a stainless steel sheet at the bottom to act as the cathode. The specimen was mounted on a rotating magnetic holder. The temperature of the electrolyte was kept between 17 and 19°C.

The voltage employed was that at which the current just stopped rising with increasing voltage and for a gap of a $\frac{1}{4}$" between the anode and the cathode, this was about 22 volts the current then being 0.6 amp. Best polishing results were obtained with fresh solutions and an electrode gap of a $\frac{1}{4}$". At least 25μ of the surface had to be removed in this way in order to remove the emery scratches; this involved polishing for about 20 to 25 minutes.

After completion of polishing the specimen was etched for about 3 minutes by reducing the voltage to less than half that required for polishing. Best etching response was obtained by diluting the MORRIS's solution slightly - about 4 ml distilled water in every 100 ml of polishing solution. This had the effect of increasing the current to about 0.3 amp at 8 volts.

4.5.2 Mild steel.

Following the deformation the mild steel specimens were aged for 12 hours at a temperature of 160° -170°C and were subsequently polished on a fine grade of emery paper to remove the surface relief introduced by straining.

Plastic deformation was then revealed on the surface of specimens by chemically etching with FRY's (88) reagent, the tec hnique being only successful on steels which contain 0.005% nitrogen.

The etchant contains 45 gm cupric chloride, 180 ml hydrochloric acid and 100 ml water.

The mechanism of the etch is supposedly by the diffusion of nitrogen on aging and precipitation on fresh dislocations as Fe_8N (FISHER (89)). Iron nitride is readily soluble in hydrochloric acid and presumably copper is deposited where the nitride has been leached out.

This technique does not reveal individual dislocation pits but results in a preferentially darkened area on a macroscopic scale.

CHAPTER 5

TENSILE PROPERTIES

This chapter relates to preliminary investigations into the macroscopic strength and ductility values of those notched specimens that were tested to failure.

Except for a decrease in strength when the notch depth was between 36% and 55%, the general effect of increasing notch depth was to increase the strength of the notched specimens. The dependence of ductility on notch depth was found to be almost opposite to that of strength. These effects havebeen discussed with respect to the expected notch tensile properties.

5.1 RESULTS

The results of the tensile tests for the fine grained 3% Si-Fe (M), the coarse-grained 3% Si-Fe(C,E,F), and the high-nitrogen (0.018%), 0.14% carbon steel (S) are presented in a tabulated form in Tables 5.1, 5.2 and 5.3.

5.1.1 Notch Strength and Notch Ductility.

The notch strength values were obtained by dividing the maximum load supported by the notched specimen by the original area between the notches. To allow better

Specimen No.	Notch Depth %	Yield Stress kg/mm^2	Notch Strgh. kg/mm^2	Notch Strgh. Ratio	Notch Dctly. R.A. %	Notch Dctly. Ratio	Elongation %
M	0	39.59	51.52	1.000	43.82	1.000	-
1M5	4.5	41.49	53.71	1.042	38.47	0.878	-
1'M5	4.5	41.79	53.70	1.042	33.79	0.771	-
1"M5	4.5	42.58	54.80	1.064	32.25	0.736	-
2M5	9.0	43.46	55.12	1.069	36.63	0.836	-
2'M5	9.0	43.98	55.80	1.080	30.15	0.688	-
2"M5	9.0	44.20	55.69	1.081	29.36	0.670	-
3M5	22.5	44.46	56.57	1.099	35.10	0.801	-
3'M5	22.5	44.07	58.08	1.128	27.21	0.621	-
3"M5	22.5	43.94	58.52	1.136	25.63	0.585	-
4M5	36.0	45.17	57.61	1.118	36.68	0.837	-
4'M5	36.0	42.22	60.12	1.167	29.14	0.665	-
4"M5	36.0	47.73	57.41	1.132	26.55	0.606	-
5M5	45.0	38.45	58.01	1.127	39.61	0.904	-
5'M5	45.0	47.35	59.71	1.160	31.51	0.719	-
5"M5	45.0	45.53	60.70	1.179	27.91	0.637	-
6M5	54.5	47.42	59.74	1.161	39.96	0.912	-
6'M5	54.5	48.37	60.12	1.167	29.49	0.673	-
6"M5	54.5	46.01	60.52	1.174	27.83	0.635	-
7M5	63.5	-	-	-	-	-	-
7'M5	63.5	46.27	62.43	1.212	27.87	0.636	-
7"M5	63.5	49.04	63.48	1.233	28.09	0.641	-
8M5	73.0	40.47	61.02	1.184	34.75	0.793	-
8'M5	73.0	44.51	65.95	1.281	23.66	0.540	-
8"M5	73.0	49.37	64.82	1.258	24.89	0.568	-

TABLE 5.1. Notch Tensile Properties of Fine-Grained 3% Si-Fe.

Specimen No.	Notch Depth %	Yield Stress kg/mm^2	Notch Strgh. kg/mm^2	Notch Strgh. Ratio	Notch Ducty. R.A.%	Notch Ducty. Ratio	Elongation %
C	0	32.29	45.48	1.000	70.26	1.000	
E	0	35.54	45.93	1.000	54.79	1.000	
F	0	32.16	44.46	1.000	41.91	1.000	
1C5	4.5	32.31	46.68	1.026	49.87	0.723	35.8
1'C5	4.5	33.85	48.17	1.059	52.42	0.746	36.7
1"C5	4.5	31.35	43.97	0.967	69.91	0.995	38.8
2C5	9.0	33.29	48.50	1.066	47.81	0.679	32.8
2'C5	9.0	35.51	48.96	1.077	25.90	0.368	30.3
2"C5	9.0	35.15	48.82	1.073	43.81	0.623	30.8
3C5	22.5	34.65	52.03	1.144	29.48	0.418	16.8
3'E5	22.5	36.83	55.92	1.218	37.61	0.686	21.1
3"C5	22.5	38.75	53.98	1.187	49.41	0.703	20.8
4F5	36.0	35.67	53.76	1.209	34.45	0.821	10.4
4'F5	36.0	35.79	53.63	1.206	43.98	1.044	11.5
4"F5	36.0	36.28	54.26	1.220	29.25	0.857	11.9
5F5	45.0	37.01	52.95	1.191	43.51	1.038	8.0
5'F5	45.0	36.92	55.25	1.243	46.41	1.100	7.8
5"F5	45.0	34.64	52.27	1.176	46.46	1.107	7.6
6F5	54.5	38.36	53.09	1.194	51.13	1.220	6.0
6'F5	54.5	39.39	60.18	1.354	46.70	1.112	6.9
6"F5	54.5	36.24	54.29	1.221	44.06	1.051	5.9
7E5	63.5	33.99	56.03	1.220	57.70	1.051	4.6
7'E5	63.5	41.80	64.68	1.408	50.76	0.925	5.4
7"E5	63.5	40.07	59.73	1.301	57.22	1.043	4.9
8E5	73.0	39.52	55.24	1.203	42.85	0.780	4.1
8'E5	73.0	40.62	61.33	1.335	42.47	0.775	3.8
8"E5	73.0	40.14	61.38	1.336	42.85	1.022	4.4

TABLE 5.2. Notch-Tensile Properties of Coarse-grained 3% Si-Fe.

Specimen No.	Notch Depth %	Yield Stress kg/mm^2	Notch Strgh. kg/mm^2	Notch Dctly. Ratio	Notch Dctly. R.A. %	Notch Dctly. Ratio	Elongation %
S	0	26.39	40.87	1.000	65.24	1.000	-
1S5	4.5	25.67	41.96	1.027	59.30	0.909	45.8
1'S5	4.5	26.68	44.37	1.086	46.22	0.708	49.6
1"S5	4.5	27.54	44.76	1.095	46.41	0.711	49.6
2S5	9.0	27.08	43.11	1.055	56.68	0.869	40.4
2'S5	9.0	27.39	45.01	1.101	37.99	0.582	39.1
2"S5	9.0	28.10	45.39	1.111	41.93	0.643	38.3
3S5	22.5	25.29	44.58	1.091	54.89	0.841	25.8
3'S5	22.5	29.78	47.63	1.165	33.48	0.513	28.0
3"S5	22.5	29.38	47.22	1.155	38.14	0.585	24.0
4S5	36.0	26.46	45.77	1.120	53.79	0.825	17.9
4'S5	36.0	28.40	47.10	1.152	37.71	0.578	17.0
4"S5	36.0	29.18	49.08	1.201	37.34	0.572	16.6
5S5	45.0	25.74	46.32	1.133	56.35	0.864	13.0
5'S5	45.0	29.44	48.54	1.188	36.94	0.566	12.4
5"S5	45.0	27.56	48.72	1.192	37.78	0.579	12.0
6S5	54.5	25.96	45.16	1.105	57.75	0.885	7.9
6'S5	54.5	29.77	49.73	1.217	35.51	0.544	8.0
6"S5	54.5	27.58	50.74	1.242	38.61	0.592	7.6
7S5	63.5	19.73	47.55	1.163	57.34	0.879	5.8
7'S5	63.5	31.14	50.39	1.246	34.81	0.534	6.4
7"S5	63.5	28.46	52.53	1.285	38.67	0.593	6.0
8S5	73.0	21.60	48.07	1.176	52.58	0.806	4.8
8'S5	73.0	29.18	51.82	1.268	33.72	0.517	5.1
8"S5	73.0	-	-	-	-	-	-

TABLE 5.3. Notch-Tensile Properties of High-Nitrogen Steel.

comparison of the effect of notches in materials having different strength levels, the notch strength has also been presented as the notch strength ratio, which is defined as the ratio between the notch strength, above, and the U.T.S. of the unnotched specimen. To make for better understanding of the effect of notching on strength properties the notch strength ratio (N.S.R.) curves for each material have been presented together with the notch ductility or reduction in area, measured after fracture, in Figs. 5.1, 5.2 and 5.3. The latter has also been expressed as a ratio of the unnotched ductility of each material.

(i) Fine-grained Si-Fe.

The general effect of increasing notch depth in this material is that the notch strength increases, attains a maximum, and then decreases over a short region (about 10% on the abscissa), before increasing again (Fig. 5.1). Increasing the root radius from 0.0015" to 0.0040" does not have any appreciable effect on the character of the curves, but for the blunt-notched specimens (r = 0.0150") the strength curve is displaced as a whole towards lower strength.

The first reversal in strength occurs with notches of intermediate sharpness at about 40% and in the sharp-notched specimens at 45% while the second reversal occurs at about

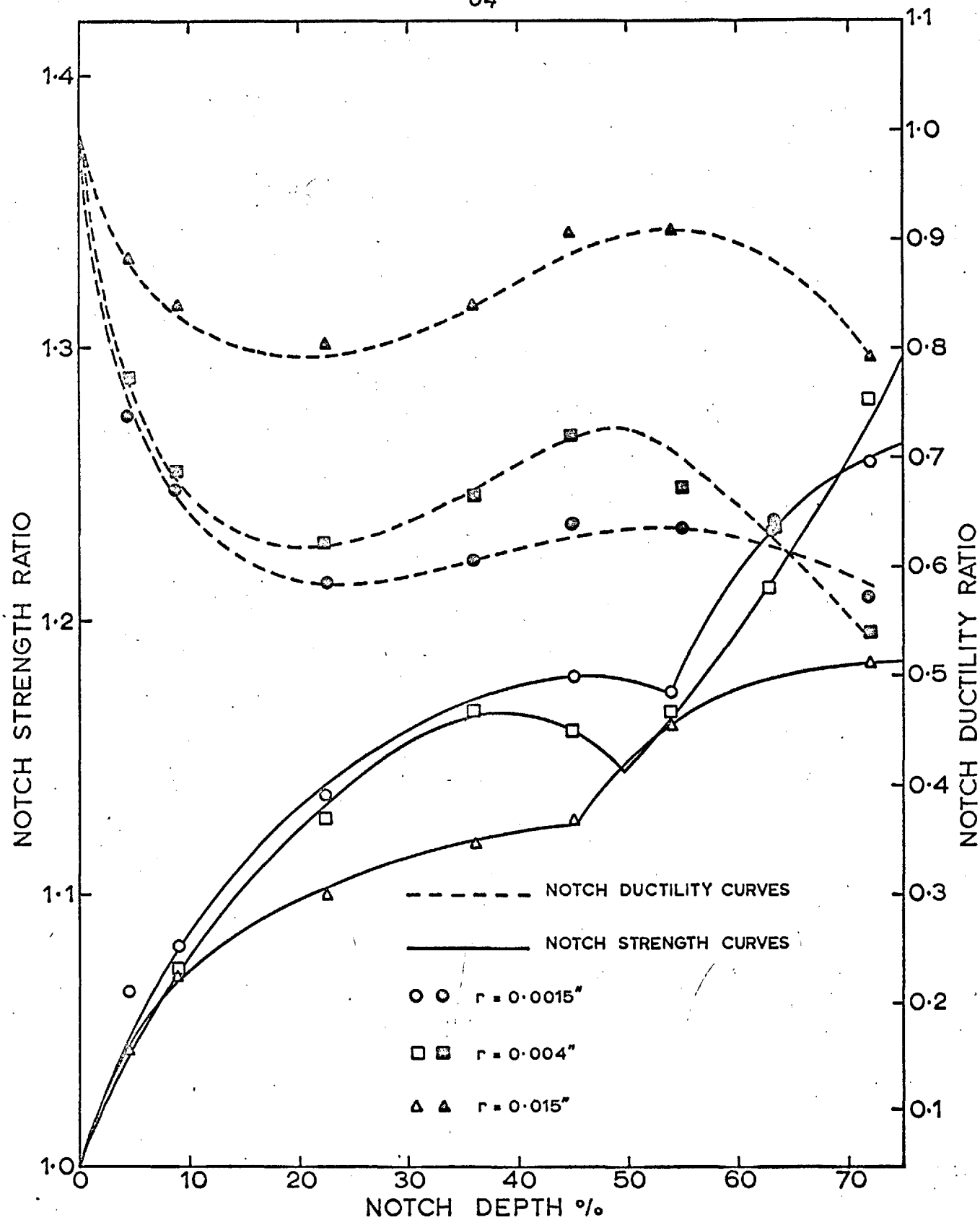

Fig.5.1. THE EFFECT OF NOTCH DEPTH AND SHARPNESS ON STRENGTH AND DUCTILITY IN FINE-GRAINED Si-Fe.

50% in the former and 55% in the latter. The curves for these specimens with the sharper notches are close together and noticeably higher than that for the blunt notched specimens, which does not exhibit a region of decreasing strength at all. Another feature of interest is that the reversals in the strength curve for the notches of intermediate sharpness occur at smaller notch depths than in that for the sharp notches.

It is indicated from these curves that an effect causing a decrease in strength comes into the picture and becomes increasingly effective over a range of notch depth between 40% and 55%, but is subsequently overshadowed by the strengthening effect of progressively deeper notching. This effect is also revealed in the notch ductility curves (Fig. 5.1) by an increase in ductility between notch depths of 20% and 60%. Although these points of reversal do not coincide exactly with those for the notch strength, it is considered that they are equivalent evidence of the same effect.

The effect of increasing root radius on notch ductility is to displace the curves towards higher values of ductility.

(ii) Mild steel.

The notch strength and ductility curves for mild steel (Fig. 5.2) exhibit the same basic characteristics as those for the fine-grained Si-Fe.

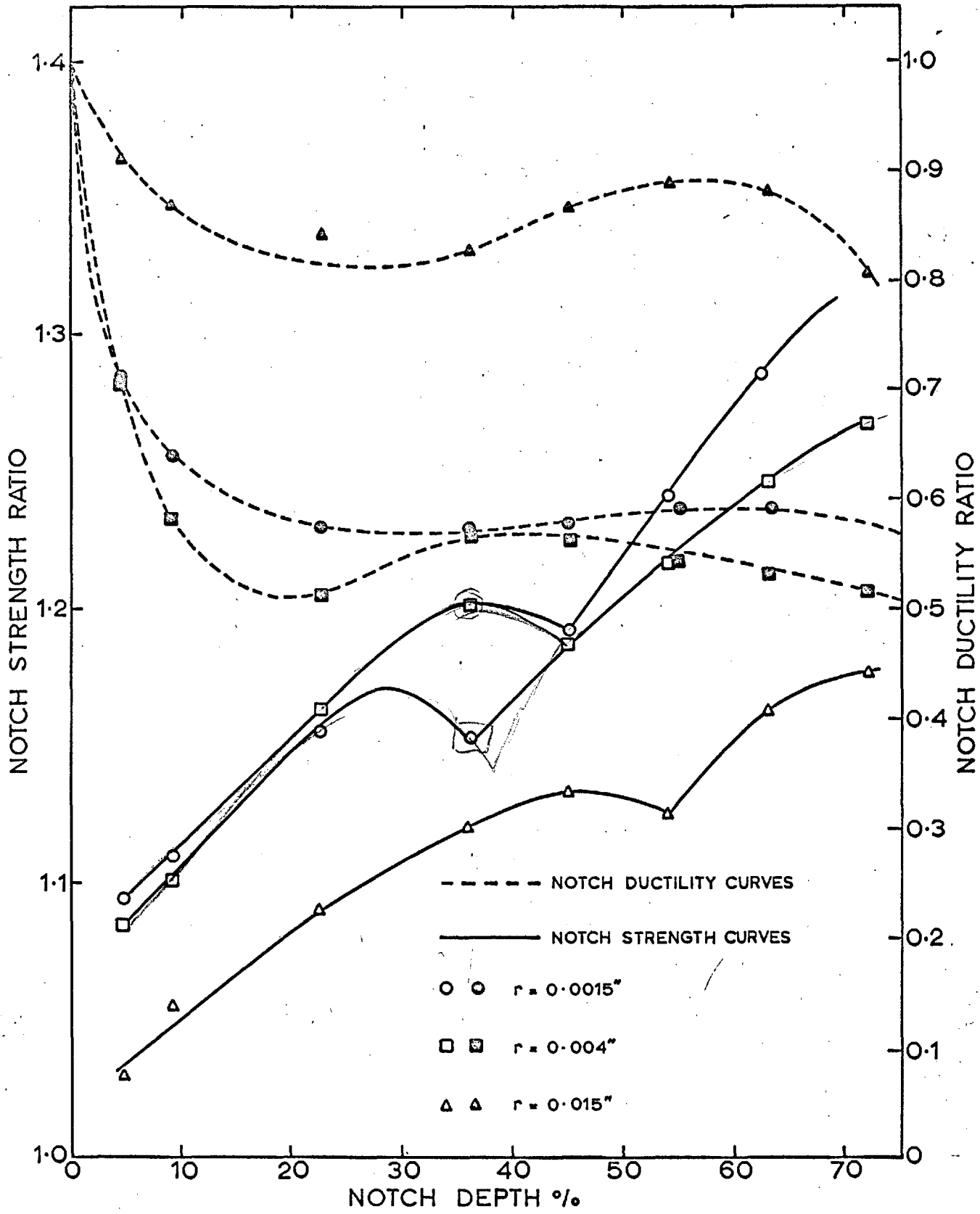

Fig.5.2. THE EFFECT OF NOTCH DEPTH AND SHARPNESS ON STRENGTH AND DUCTILITY IN MILD STEEL.

In the sharper notches, the reversals in strength occur earlier, at 30% and 36% depth innotches of intermediate sharpness and at 36% and 45% depth in sharp notches - but the blunt notched specimens too show a definite sign of decreasing strength between 46% and 54% notch depths.

The notch ductility curves show the corresponding reversals at about the same places on the abscissa as in the fine-grained Si-Fe, except in the case of the intermediate sharp notches where the second reversal occurs at about a depth of 40% as compared to its occurrence at a 50% depth in Si-Fe. Another point of interest in the notch ductility curves is that the curve for the intermediate sharp notch, contrary to expectations, is lower than that for the sharp notch.

(iii) Coarse-grained Si-Fe.

The notch strength and ductility curves (Fig. 5.3) show the same tendencies as the other two materials, but unlike the others, the slopes of the curves are much steeper, they cover a much larger range of strength and ductility, and the region of weak notches - between 27% and 40% depth in the intermediate sharp, 32% and 48% depth in the sharp and 37% and 48% depth in the blunt notches - is perhaps a little larger.

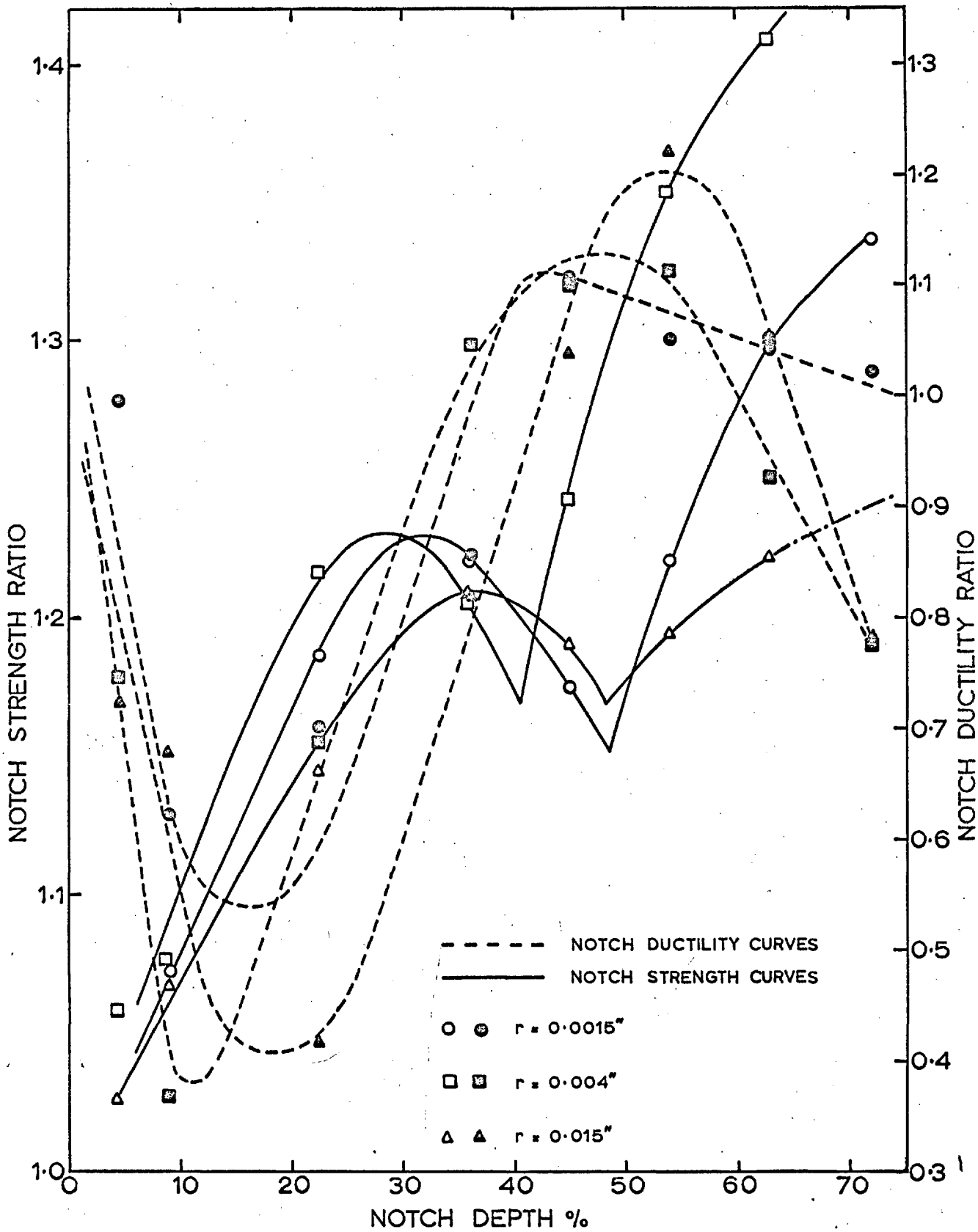

Fig.5.3. THE EFFECT OF NOTCH DEPTH AND SHARPNESS ON STRENGTH AND DUCTILITY IN COARSE-GRAINED Si - Fe.

The reversals in ductility occur roughly at the same points on the abscissa as in the previous materials, the first occurring between 10% - 18% depth and the second between 45% - 55% depth. Curiously, when the notch depth is 45% and above, all but three specimens, viz., two of intermediate sharpness and 63% and 73% depth and a 73% deep blunt notch, showed greater ductility than the unnotched sample.

Neither the ductility nor the strength curves for the blunt notched specimens are set apart sufficiently from those for the sharper notches to justify a distinction due to the effect of root radius.

From a comparison of the Figs. 5.1, 5.2 and 5.3, it is seen that while the effect of deeper notching is quite clear in every case, the effect of root radius is not nearly so obvious. Some of the observed effects of varying root radius are , therefore, worth repeating.

(i) Along the notch depth axis, reversals in strength occurred first in the case of the notches of intermediate sharpness, then in the sharp and finally in the blunt notched specimens.

(ii) Except in the coarse-grained Si-Fe, the notch strength values for the two sharper notches were comparable, but the blunt notched samples had much lower strength.

(iii) The reversals in ductility at particular values of notch depth was little altered by varying root radius. The reversals for the intermediate sharp notched samples, however, tended to occur earlier.

(iv) No systematic relationship between the ductility and notch radius of the sharper notched specimens was observed, but the blunt notched specimens were decidedly more ductile than those having a smaller root radius in the fine-grained Si-Fe and the mild steel.

5.1.2 Elongation.

Elongation values were calculated by dividing the cross-head displacements required to reach the U.T.S. by the original gauge length (= $\frac{1}{2}$") of the specimens and expressed as a percentage.

In an unnotched specimen where the strain is uniformly distributed over the entire gauge length, elongation measurements provide information on the ductility characteristics of the material. In a notched specimen, however, the plastic strain is non-uniformly distributed only over a certain portion of the gauge section around the notch, whilst the rest remains undeformed. Since the longitudinal spread of this non-uniform strain mainly contributes to the elongation of the gauge length, it is expected that the

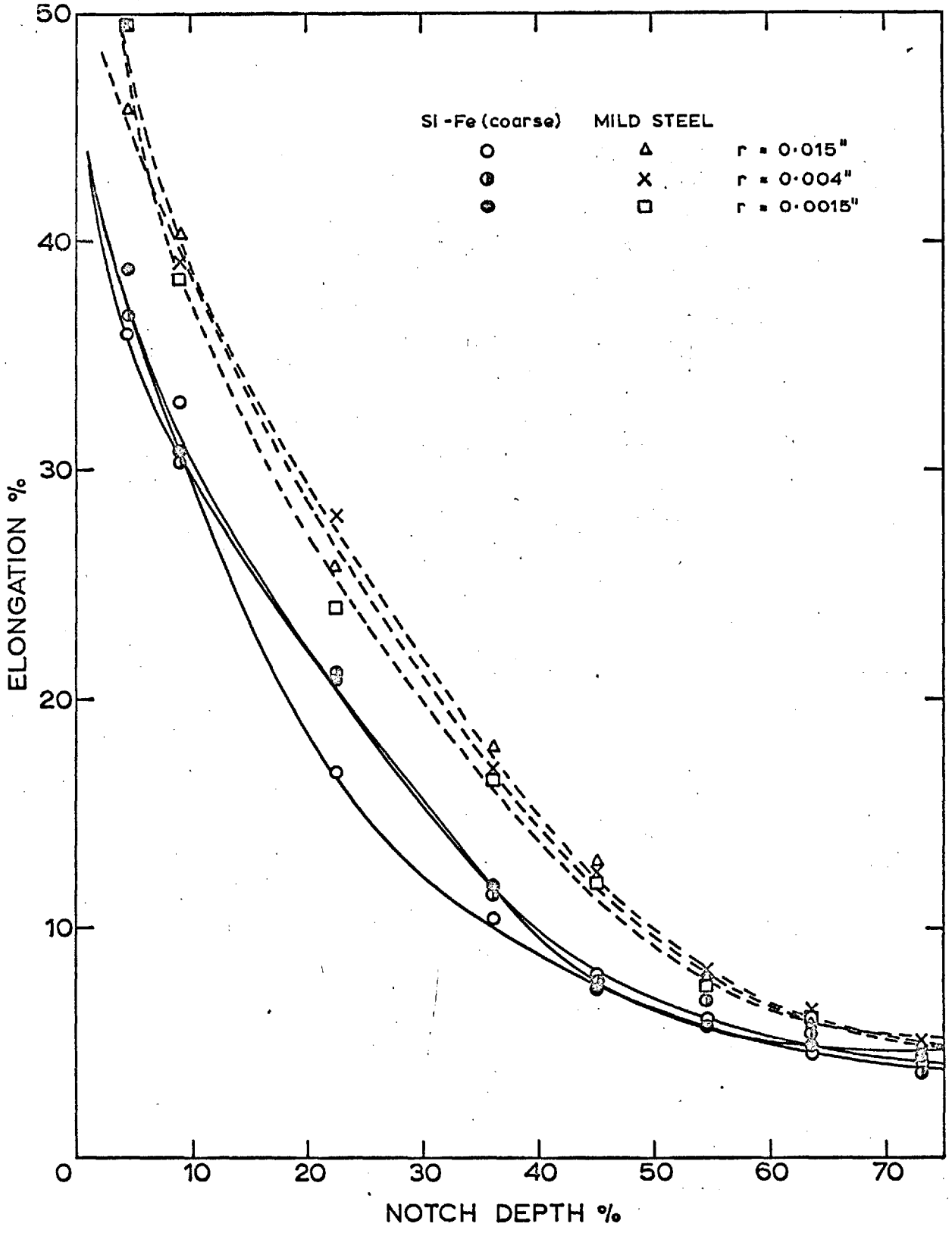

Fig. 5.4. THE EFFECT OF NOTCH DEPTH AND SHARPNESS IN Si - Fe AND STEEL

measurement of elongation would provide a relative measure of the preferential yielding around notches.

Fig. 5.4 shows the elongation curves for the coarse-grained Si-Fe and mild steel. They are characterised by a continuous decrease of elongation to a flat minimum as the deformation changed from a uniform distribution along the length of an unnotched sample to a highly non-uniform localized strain in a deep notched sample.

5.1.3 Yield Strength

The yield strength values included in the tables correspond to the nominal stress at which plasticity was first detected, visually, under the notch. This seemed to be the most suitable means of observing the approximate macroscopic limit of elastic behaviour, since none of the notched specimens (excepting those of 4.5% and 9.0% depths) exhibited an observable point of transition to plastic behaviour on their load-deflection curves. The yield strength values obtained in this way, however, were not found to be accurate enough to elicit any useful information on the effect of notches on the yield strength.

5.2 DISCUSSION

5.2.1 Load-Deflection Curves.

(i) Si-Fe.

Apart from such information as has already been presented in Tables 5.1 and 5.2, the load-deflection curves showed another interesting feature on the basis of which the distinction between "very shallow" and "shallow" notches was made.

The unnotched specimens and those with a depth of 4.5% and 9% showed a sharp change from elastic to plastic behaviour marking a yield point. This is expected, since for shallow notches the non-uniform stress is concentrated in a very small volume in the vicinity of the notch; in the remainder of the specimen the deformation follows the "general" mode characteristic of unnotched specimens. This effect was most marked in those specimens having sharp notches with increasing depth up to 9%; distinct yield drops were found to occur marking an upper and a lower yield stress (Fig. 5.5). This is presumably because the sharp notches give rise to higher and more localized stress peaks. The higher peak of longitudinal stress, σ_x, would mean that the notch starts to yield while the rest of the specimen is still at a low stress level. This would allow a longer time for higher values of the upper yield stress, σ_{uy}, to be attained before

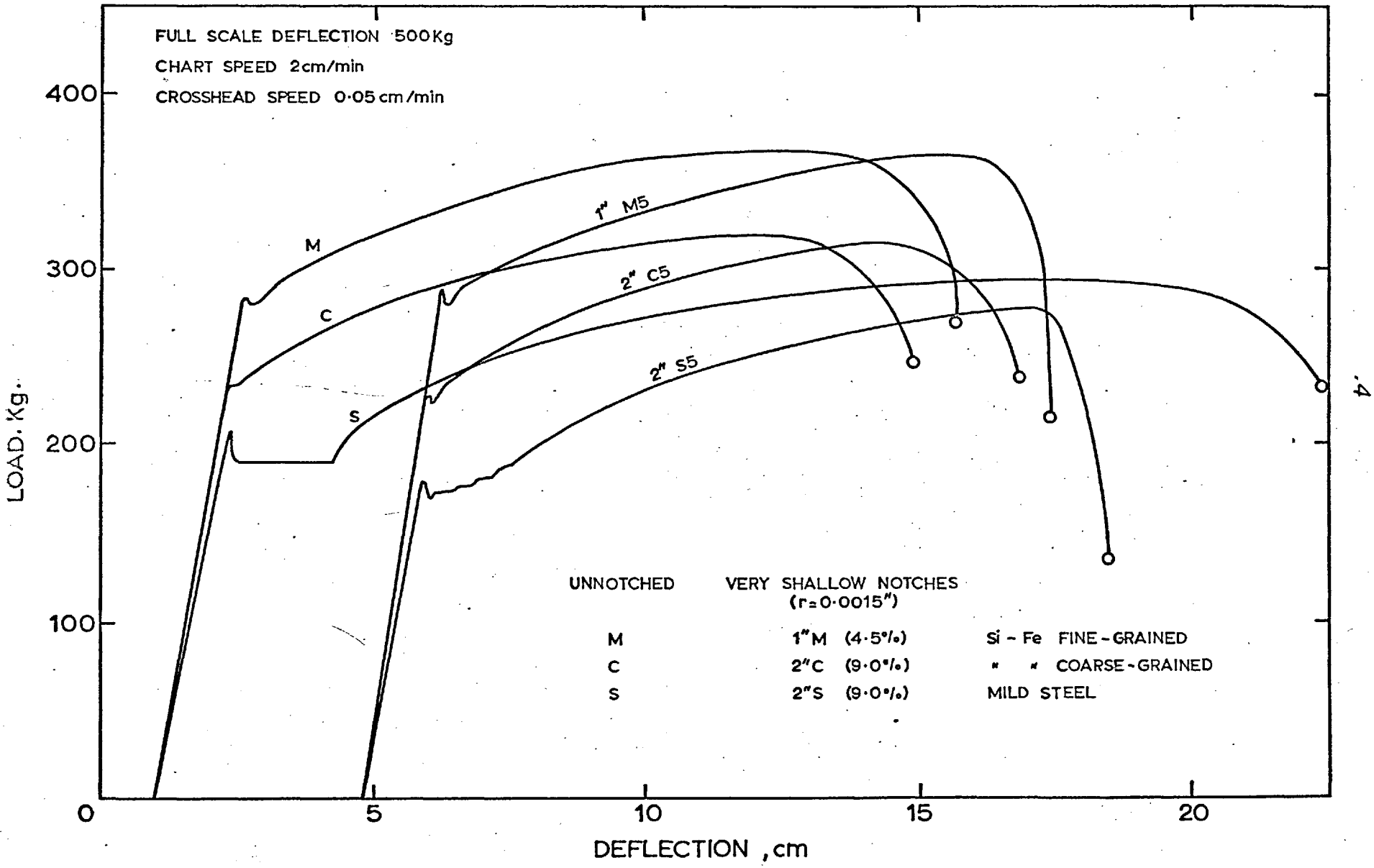

Fig.5.5. LOAD-DEFLECTION CURVES FOR UNNOTCHED AND VERY SHALLOW NOTCHED SPECIMEN

the average flow stress is reached. A necessary condition for a yield drop to occur in anotched specimen would then appear to be that the yield nucleus at the notch is restricted from spreading until a critical stress (σ_{1y}) is attained in the bulk of the specimen. This condition requires (a) the peak of the transverse tension to have a sufficiently high value to restrict the yield nucleus from expanding and (b) that it occurs sufficiently close to the notch that the effect of the stress peaks does not extend far enough inside the specimen to alter the "general" mode of yielding. This sort of yielding, where notching does not effectively alter the overall behaviour from that characteristic of unnotched specimens, was found to occur up to a depth of 9% for all root radii investigated and they have been labelled as "very shallow" notches (Fig. 5.8).

As the notch depth increased beyond 22.5% no yield point was observed at all and the change from elastic to plastic behaviour became more and more gradual while the overall extension along the deflection axis decreased progressively.

(ii) Mild steel.

As far as a qualitative comparison goes the load-deflection diagrams for the steel samples were a little different from those for the Si-Fe samples in that the increased yield drop tendency with increasing depth within

the "very shallow" range of notches was not observed in this case. All specimens yielded very inhomogeneously and the overall extension for corresponding specimens was higher in steel than in Si-Fe.

In the samples with very shallow notches (4.5% and 9%), Lüders bands spread sharply across the minimum section with a consequent yield drop. This was followed by the development of more bands from the notches in a direction at about 45° to the tensile axis and these spread outwards along the gauge length. During the progress of these bands the stress was not quite constant, but varied as fresh Lüders bands developed or when these encountered stress raisers in the form of surface irregularities or fillets. A diagrammatic representation of the mode of deformation and the corresponding variations on the load-deflection curves is given in Fig. 5.6 for different notch depths.

In the case of the shallow and intermediate notches, yielding did not take place quite as suddenly across the minimum cross-section and once it had yielded the growth of the zone was restricted to the notched section for some time before deformation bands from the notches spread across the specimen to the opposite edge.

For the deep notches yielding was completely confined to the notched area till fracture occurred.

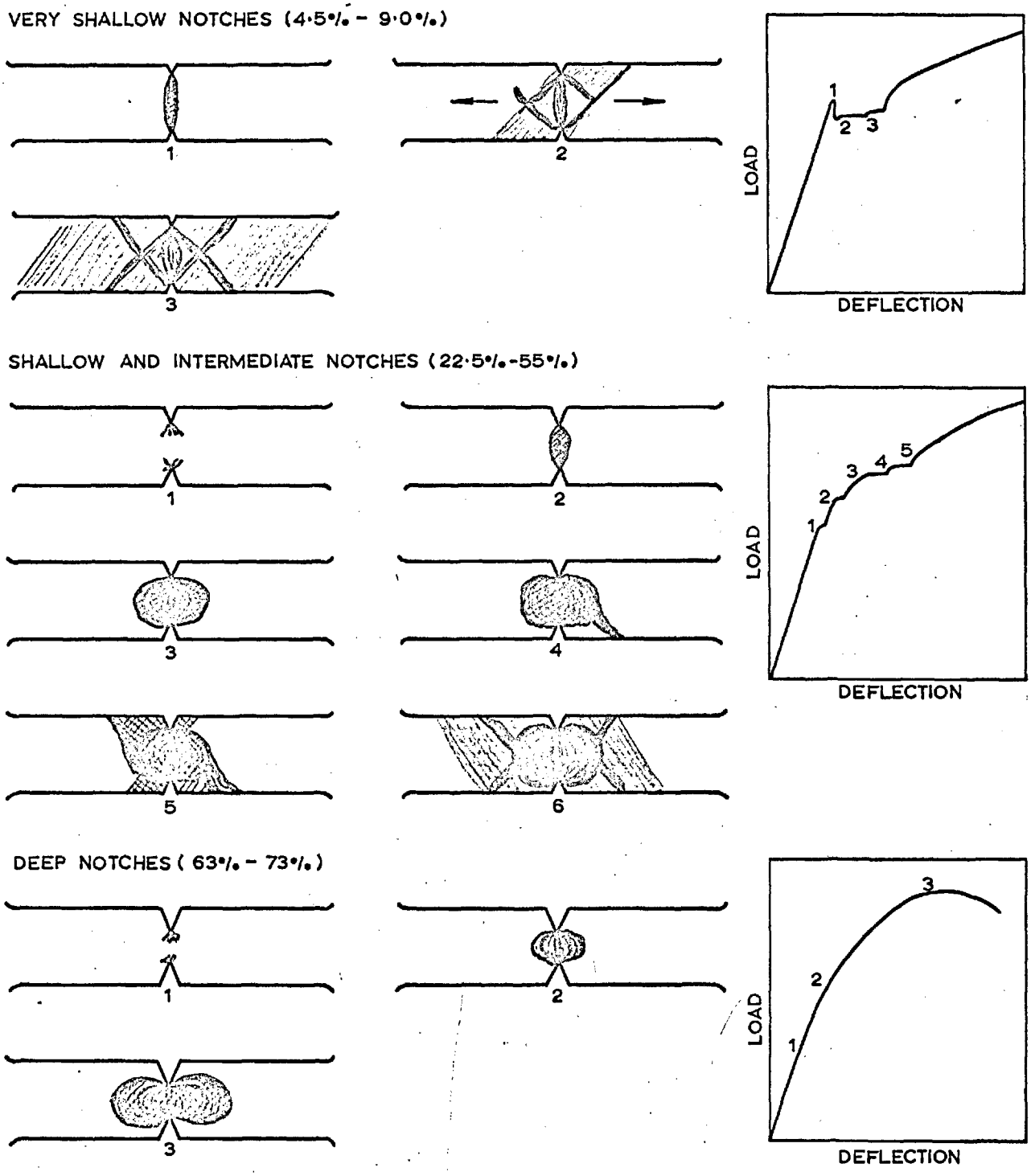

Fig.5.6. SLIP BAND DEVELOPMENT AND THE CORRESPONDING VARIATIONS IN THE LOAD-DEFLECTION CURVES IN MILD STEEL.

5.2.2 Expected Yield Behaviour from Elastic Stress Distribution.

Before discussing the notch strength and ductility values obtained from experiment it is instructive to examine the expected yield behaviour of the notched specimens in the light of the elastic stress state at the point of yielding. The elastic stress distribution can be described in terms of the stress concentration factors and transverse stresses arising from the notches.

NEUBER's (1) analytical solutions presented in the form of nomographs provide a convenient means for calculating stress concentration factors as a function of notch depth and sharpness for a wide range of loading conditions. Elastic stress concentration factors obtained in this way have been presented in Table 5.4 and Fig. 5.7. Fig. 5.7 shows the variation of the elastic stress concentration factor with increasing notch depth for the three root radii investigated.

The transverse stress is expected to increase with increasing notch depth, the distribution being characterized by a maximum which is localized and close to the root of the notch for shallow notches, but which becomes flat and nearer to the centre of the specimen for deep notches (SACHS and LUBAHN (10)).

Notch Depth %	Half Width a(ins)	Notch Depth t(ins)	Root Radius, r = 0.015" a/r	t/r	α_k	Root Radius, r = 0.004" a/r	t/r	α_k	Root Radius, r = 0.0015" a/r	t/r	α_k
4.5	0.105	0.005	2.65	0.62	2.05	5.14	1.11	3.00	8.43	1.73	4.25
9.0	0.100	0.010	2.59	0.85	2.40	5.02	1.60	3.75	8.22	2.57	5.56
22.5	0.085	0.025	2.38	1.32	2.70	4.64	2.56	4.50	7.60	4.05	6.95
36.0	0.070	0.040	2.18	1.64	2.60	4.23	3.10	4.65	6.91	5.14	7.28
45.0	0.060	0.050	2.00	1.84	2.47	3.92	3.50	4.50	6.41	5.71	7.10
54.5	0.050	0.060	1.83	2.01	2.28	3.51	3.92	4.23	5.92	6.28	6.83
63.5	0.040	0.070	1.66	2.16	2.23	3.20	4.19	3.92	5.29	6.79	6.35
73.0	0.030	0.080	1.46	2.30	1.97	2.80	4.47	3.50	4.60	7.27	5.66

TABLE 5.4. Elastic Stress Concentration Factors, α_k, calculated from nomographs of NEUBER (1).

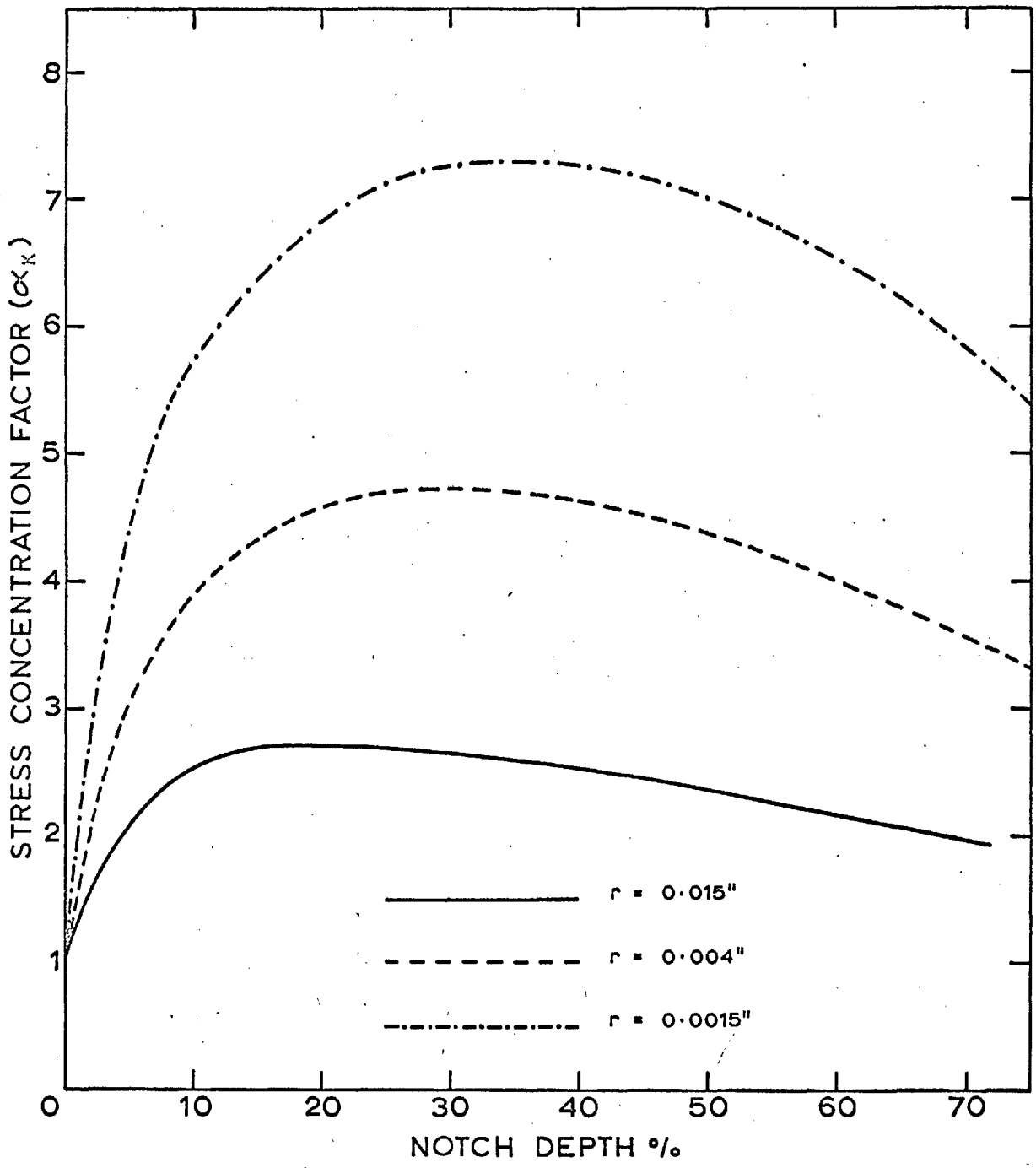

Fig.5.7. PREDICTED VARIATION OF ELASTIC STRESS CONCENTRATION FOR THE RANGE OF NOTCHES INVESTIGATED (from H.NEUBER[1])

From the expected trends of the stress concentration factors and transverse stresses the probable stress distribution for the notches under investigation has been diagrammatically presented in Fig. 5.8. The distinctions in terminology, e.g., shallow, intermediate and deep notches, were made on the basis of notch strengths and the etch-pit observations described in Chapter 6. Notches of 22.5% and 36% depth were included in the shallow range because etch-pit observations show that up to a depth of 36% the mode of yielding is substantially similar to that that occurs in unnotched specimens.

In Fig. 5.8 the line I represents the approximate longitudinal stress in the specimen just before yielding when $(\sigma_x)_{max}$ at the notch root equals σ_{yd}, the yield stress for an unnotched specimen. The nominal applied stress at this point is given by the line V and is equal to $(\sigma_x)_{max}/\alpha_k$ or σ_{yd}/α_k, where α_k is the stress concentration factor for the notch. The transverse tension (line II), once yielding starts, when superimposed on the longitudinal tension raises the average flow stress by that amount above $(\sigma_x)_{max}$ as shown by line (IV).

Since the transverse stress is expected to increase with increasing depth of notch, the yield strength too would be expected to increase as shown in Fig. 5.8.

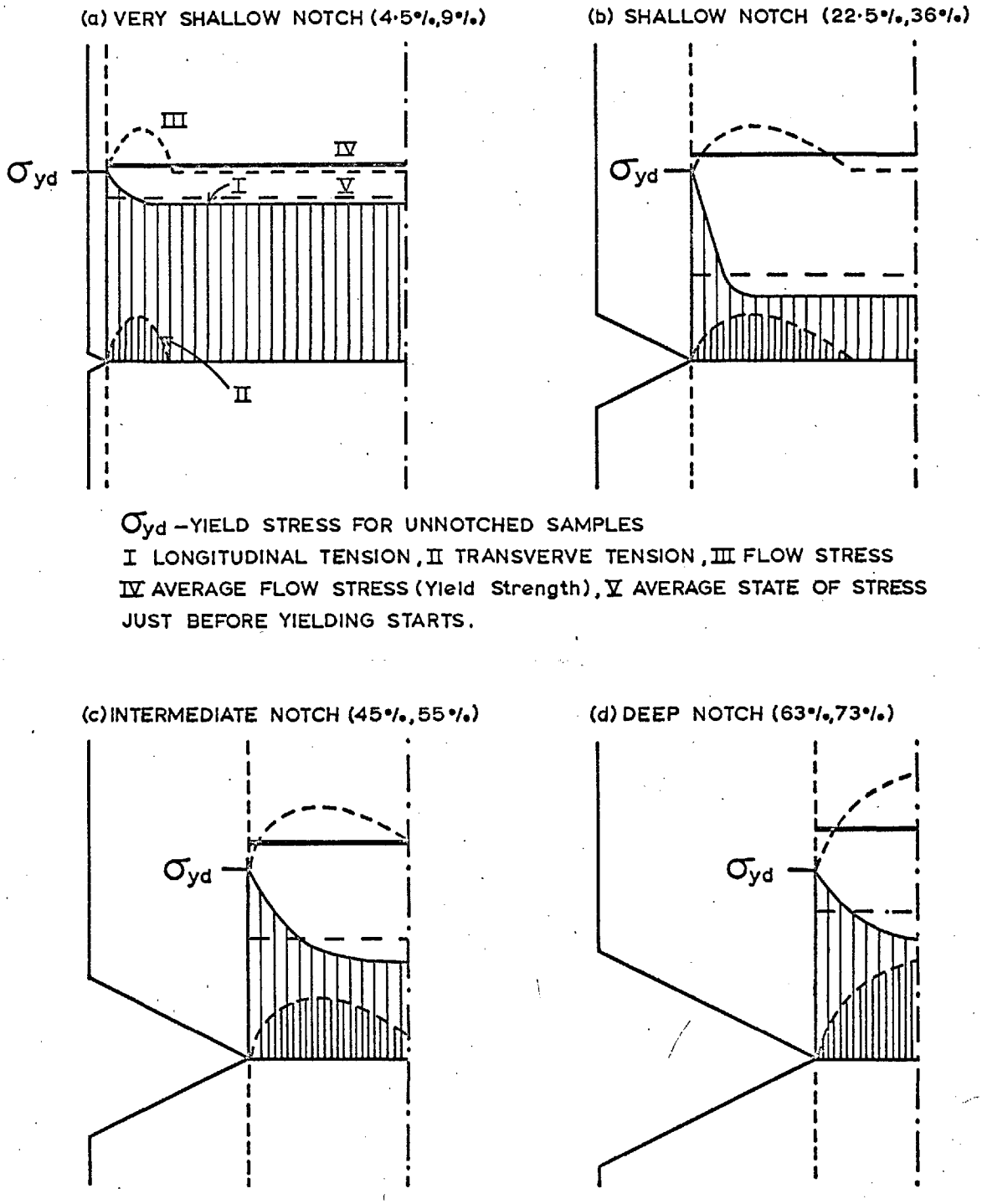

σ_{yd} – YIELD STRESS FOR UNNOTCHED SAMPLES
I LONGITUDINAL TENSION, II TRANSVERVE TENSION, III FLOW STRESS
IV AVERAGE FLOW STRESS (Yield Strength), V AVERAGE STATE OF STRESS JUST BEFORE YIELDING STARTS.

Fig. 5.8. THE EFFECT OF NOTCH DEPTH ON STRESS STATE AND THE YIELD STRENGTH

Experimental values of yield strength could not be determined to a sufficient degree of accuracy to warrant a discussion. From the approximate values presented in Tables 5.1, 5.2 and 5.3, it is most likely that the yield strength of the notched samples shows a similar character to the notch strength curves of Fig. 5.1 - 5.3, rather than the continuous increase with depth to be expected from the average flow stress shown by lines (IV) in Fig. 5.8.

5.2.3 The Yield Mode and the Yield Criterion from a Consideration of Limit Loads.

If a metal has a flat yield region as does mild steel, or is only moderately work-hardening as are some Si-Fe alloys, they can be expected to behave in close approximation to elastic - perfectly plastic materials in which the initial elastic response to increasing load reaches a maximum and then levels out. In this limiting case of zero work-hardening, the load at which the fully plastic behaviour occurs in a perfectly plastic material is called the limit load. DRUCKER and FINDLEY (79) have shown how the magnitude of this limit load, P_{yd}, can give an indication of the closeness to plane stress or to plane strain conditions. They did this simply by comparing yield loads for notched specimens of varying thickness, (t)/width, (2a) ratios with

the predicted values of limit loads for ideally plane stress, i.e., rigid block sliding on planes inclined at 45° to the plane of the specimen and for ideally plane strain, i.e., slip in the plane of the specimen.

For the plane strain condition, DRUCKER and FINDLEY obtained the limit load, P_e, from the slip-line field solution of LEE (78).

$$P_e = 2k(2a.t)\left[1 + (\pi/2) - \alpha\right] \qquad (5.1)$$

where k is the yield shear stress, 2a is the width of the bar between notch roots and α is half the total notch angle.

An upper bound, P_u, on the limit load, P_{yd}, for the plane stress type of deformation, has been found by DRUCKER (90) by equating the work done by P_{yd} to the internal dissipated energy and is given by the relationship

$$P_{yd} \leqslant P_u = 2k(2a.t)\left[1 + (2)^{\frac{1}{2}}t/4(2a)\right] \qquad (5.2)$$

for notched bars of any thickness t. For an extremely thin sheet, $t/2a \rightarrow 0$, the relation 5.2 reduces to the form

$$P_{yd} \leqslant P_u = 2k(2at) \qquad (5.3)$$

which also gives the lower bound of the limit load.

DRUCKER's relation (equation 5.2) has been used here (Fig. 5.9) to obtain an upper bound for the plane stress type of deformation for the thickness/width ratios involved in the range of notches under investigation. Yield loads for the three experimental materials have been plotted as a

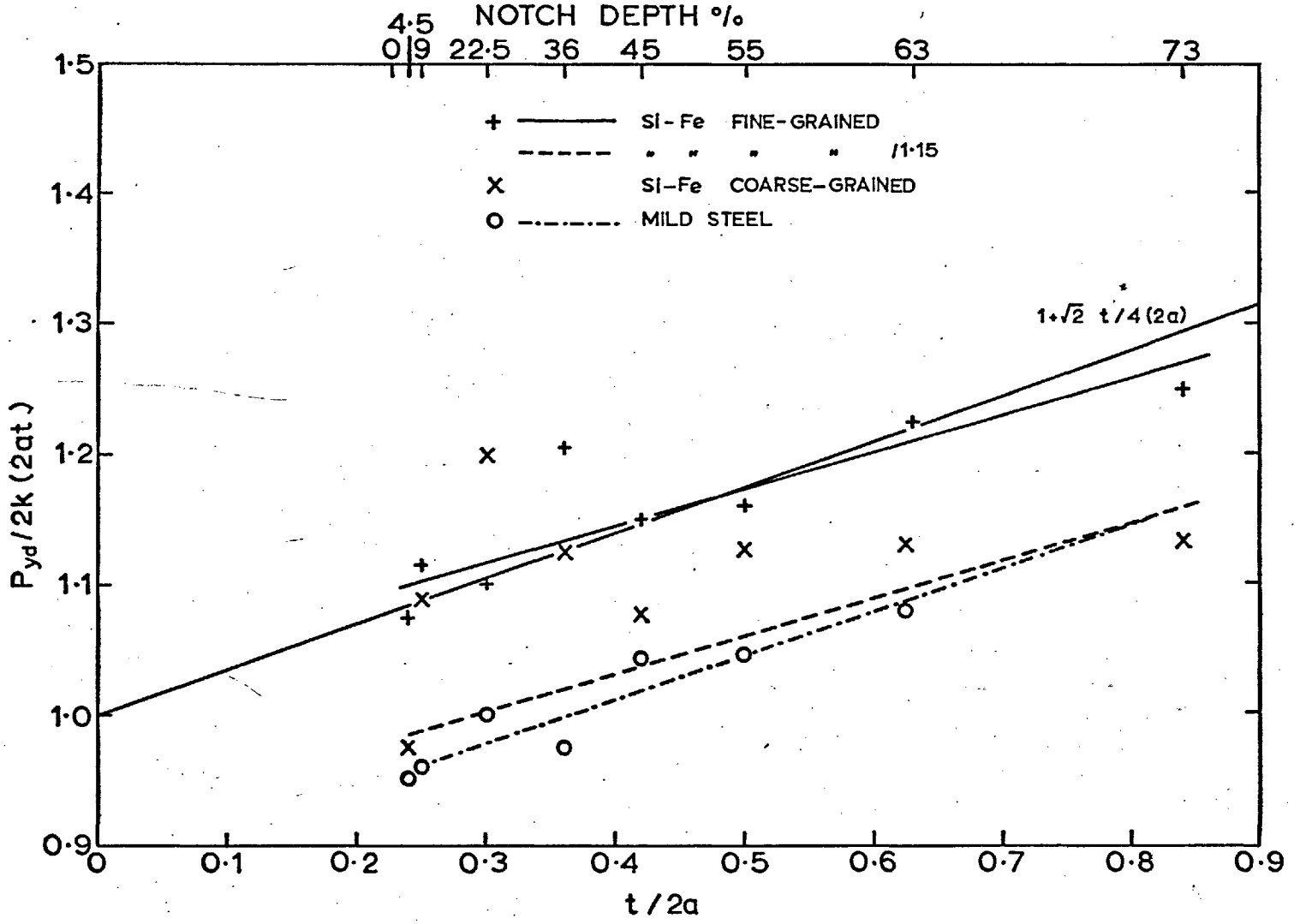

Fig. 5.9. LIMIT LOAD, $P_{yd}/2k(2at)$ versus THICKNESS, t/width, 2a.
(SHARP NOTCHES).

ratio of 2k(2at) using the Tresca criteria of yielding, i.e., $2k = \sigma_{yd}$.

Fig. 5.9 shows that whilst the yield loads for the steel is well below the upper bound, those for the Si-Fe, particularly the fine grained variety, are very close to the bound with a few in the shallow notch region clearly above the upper bound. Bearing in mind that the limit loads plotted actually correspond to the loads at which yielding was first visually observed, and therefore must underestimate the true limit load, it would appear that the limit loads for mild steel are within the predicted bounds, whereas those for the Si-Fe are slightly higher than the upper bound.

There could be two ways of explaining this observation:

(a) that Si-Fe yields in a plane strain manner even for very small thickness/width ratios,

(b) that it follows the von Mises yield criterion rather than the Tresca criterion.

Of these the first possibility seems unlikely especially because limit loads exceeding the upper bound were obtained for the shallow range of notches where plane stress rather than plane strain conditions are expected. The second possibility offers a more attractive and convenient explanation, because if it were assumed that Si-Fe follows the

von Mises yield criterion, then the yield stress of a notched member could be raised by a factor of as much as 1.15 ($2k = 1.15\,\sigma_{yd}$ for von Mises criterion). Lowering the fine grained Si-Fe curve along the ordinate by 1.15 (dashed curve in Fig. 6.9) provides a basis for comparison and this shows comparable notch yield behaviour for the fine-grained Si-Fe and steel specimens.

Results of the coarse grained Si-Fe were inconclusive because of the large scattering in yield load data.

From the preliminary considerations of limit loads it would appear then that the best assumptions as regards yield criteria would be to choose the Tresca criterion for mild steel and the von Mises criterion for Si-Fe.

5.2.4 Notch Strength.

(i) The effect of notch depth.

The increase of tensile strength that is produced by notching has been ascribed to the development of transverse tension which restricts the flow of the metal under the action of the applied longitudinal tension. Previous workers (SACHS and LUBAHN (8, 10)) have suggested that a linear increase in notch strength with notch depth is the general relation for any ductile and homogeneous metal. In the case of a fairly sharp notch such a linear relationship on

extrapolation to a 100% notch depth, has often been found to terminate in a value approximately twice the ultimate strength of the metal.

In this investigation, however, sufficient evidence has been found to show (Fig. 5.1) that the notch strength does not follow this simple linear relationship with notch depth. The fact that a reversal in notch strength was found to occur at a depth of about 36%, reaching a minimum for about a 55% notch must indicate that either -

(a) the magnitude of the transverse tension decreases when the notch depth is between 36% and 55% and subsequently rises again, or

(b) the mode of deformation changes to make the notches weaker.

The first possibility is very unlikely. The stress analysis described in Chapter 7, Figs. 7.14 - 7.16, shows that on the theoretical basis adopted there the average transverse stress should increase with increasing notch depth.

It is suggested that an explanation of the reversal in notch strength lies in the different modes of deformation associated with varying depth and radius of notching and is discussed with respect to etch-pit patterns in Chapter 6. At this stage, however, it is worth attempting to understand the decrease in notch strength for the notches of intermediate

depth in terms of the notch ductility and elongation curves in Figs. 5.1 - 5.4.

The notch ductility curves in Figs. 5.1 - 5.3 refer to reduction in area at fracture as measured on a projection microscope. Transverse strain was not measured during the deformation routine because of the difficulties of designing and using a suitable strain gauge which would not at the same time affect the existing stress state. The curves show a character opposite to that of the notch strength curves. The ductility falls with increasing notch depth reaching a minimum at a depth of about 20% and then rises to a maximum at a depth of about 55%, again decreasing for the deep notches. This behaviour can be understood by considering the nature of the elongation curves in Fig. 5.4. Since plastic deformation in a notched specimen is confined to some area around the notch, the elongation measured is due only to that length along the longitudinal axis over which the deformation extends. The elongation curves then show, in effect, the extent of deformation around the notch in the tensile direction. Fig. 5.4 shows that with increasing notch depth the elongation becomes very small. This means that the spread of deformation is increasingly restricted to the notched section. The strain at the root in the deeper notches has thus to be accommodated by deformation within a

much reduced area which could account for the weakening of the notches of intermediate depth and a consequent increase in reduction in area. The notch strength values were calculated on the original notched area and the increased reduction in area could account for the first reversal in notch strength.

In the region of the deep notches, i.e., 63% and 73%, the elongation curves tend to flatten off to a minimum indicating that the spread of deformation around the notch is approaching some minimum size. This could lead to a halt in the rise in the reduction in area or notch strengthening through rapid work hardening. It is also expected that triaxiality is high. All these factors could contribute to the second reversal and the subsequent fall in ductility and increase in notch strength.

The effect of increasing notch depth on the tensile strength can then be summarized as:-

(a) As long as the general or unnotched mode of deformation is not disturbed, the strain at the notch root is eventually obliterated by far-reaching yield, and the only effect is that the local transverse stress increases the strength. This occurred up to a notch depth of 9%.

(b) Increasing longitudinal stress, σ_x, and the occurrence of a peak in the transverse stress, σ_y, nearer to the

centre of the specimen, brings about yielding in the central notched section in preference to far-reaching yield. Consequently, the elongation falls and the reduction in notched area increases (when notch depth is 20% or more - Figs. 5.1 - 5.3). Because of this, the increase in notch strength due to increasing transverse stress is less marked, until at a depth of about 36% the effect of the transverse stress is entirely lost and the notch strength decreases.

(c) The fall, however, is temporary and as the restricted flow starts to flatten off to a minimum from about a 45% notch depth upwards (elongation curves - Fig. 5.4), the strength reducing effect ceases and the effect of the transverse stress in increasing the notch strength is able to take over again.

Subsequently, the reduction in area falls (from about a 54% notch - Figs. 5.1-5.3) and the notch strength continues to increase.

(ii) The effect of root radius.

It can be noted from the notch strength and notch ductility curves of fine grained Si-Fe (Fig. 5.1) and steel (Fig. 5.2) that the curves for the sharper notches are close together while those for the large radius (r = 0.015") are distinctly separate and show a reduced effect due to increasing notch depth.

Similar root radius dependence of notch ductility has been reported by SACHS et al (4) in cylindrical specimens. They found that the ductility was not affected much by root radius up to a radius of about 0.030", after which increasing the radius brought about a corresponding increase in ductility. From this they concluded that the transverse stress must be independent of the root radius up to a critical radius. Whether this is a valid reason for the observed ductility and strength properties is doubtful. The theoretical plane stress solution presented in Chapter 7 shows that the distribution of the transverse stress, σ_y, is practically unaffected by the root radius (Figs. 7.14 - 7.16) yet a distinct deviation towards higher ductility is observed for the largest radius (r = 0.015"). It is anticipated that this effect is due to a difference in the deformation mode associated with a large root radius. This is discussed in Chapter 6 together with the influence of the thickness of the specimen with respect to observed yield zones.

In the coarse grained Si-Fe, the notch ductility values showed a very high sensitivity to notch depth but hardly any to the root radius (Fig. 5.2). This is probably due to the anisotropy associated with a large grain size and the relative unimportance of even the largest radius investigated when compared with the grain diameter.

CHAPTER 6

YIELD ZONES

6.1 YIELDING IN UNNOTCHED SPECIMENS

Recently an increasing emphasis has been given to the importance of dislocation velocity as a deciding factor in the yield phenomenon (91, 92, 30, 37, 38). In explaining the stress-strain curves of some b.c.c. metals with the use of the Johnston-Gilman model, HAHN (41) found it convenient to differentiate between two types of yielding -

"The steady-state nonuniform yielding usually envisioned, involving a constant lower yield stress, σ_{LY}, and fixed Lüders band strain profile and band-front velocity, is stable if the deformation contributed by the material outside the band remains small compared with the contribution of the growing band. If, on the other hand, the material outside the band deforms rapidly at σ_{LY} the stress-strain curve will approach the form of uniform yielding."

Present observations in steel (Fig. 6.1 (a)) and silicon iron (Fig. 6.1 (b)) are in accord with the model proposed by HAHN, in which nonuniform yielding and the uniform mode are possible alternative forms of deformation after an abrupt yield drop.

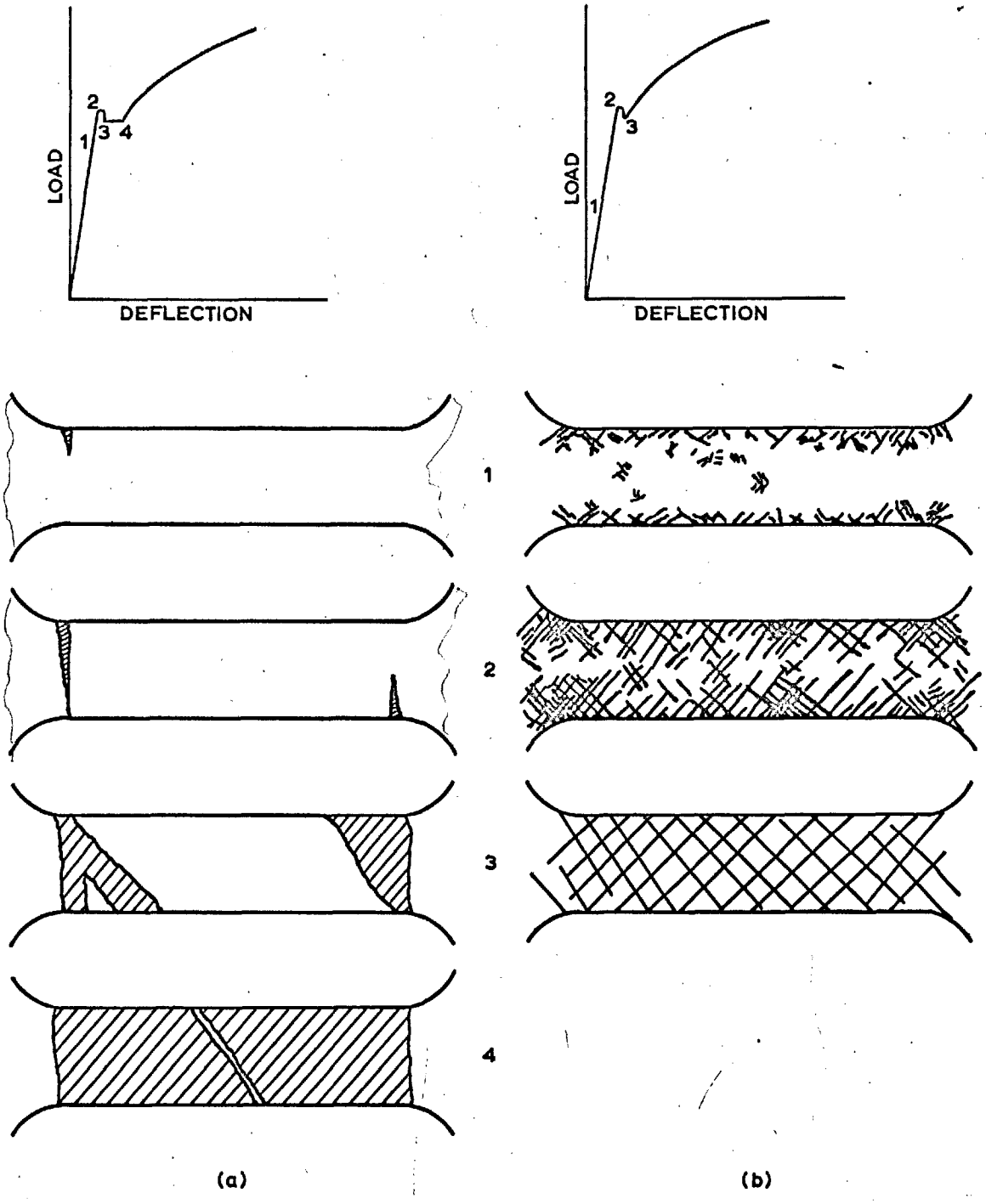

Fig.6.1. STAGES OF SLIP BAND DEVELOPEMENT IN (a) STEEL AND (b) Si - IRON AND THEIR CORRESPONDING POSITIONS ON THE LOAD-DEFLECTION DIAGRAM

Several b.c.c. metals when tested in two distinct ranges of temperature, e.g., Nb at -78°C and 20°C, Mo at -34°C and 100°C, 0.2%C steel at -150°C and 25°C, have been shown to exhibit these two types of yielding. Uniform yield is found at the lower temperatures whilst it is nonuniform at the higher temperatures (66-70).

It is significant that at lower temperatures, the non-uniform deformation at σ_{LY} can be eliminated. It is quite likely that by testing the Si-Fe specimens at a higher temperature the nonuniform mode of yield propagation at the σ_{LY} can be brought about - and this has indeed been found to occur in polycrystalline Si-Fe (STEIN and LOW (65)) at a temperature of 100°C.

6.1.1 Yielding in Mild Steel.

Yielding in mild steel was characterized by heterogeneity, some parts of the sample being deformed by the development of Lüders bands while others were practically undeformed.

Usually, yielding was initiated by the formation of pre-yield "cross-bands" whose fronts were perpendicular to the tensile axis (Fig. 6.2). This sort of slip is nucleated at stress concentrators such as the shoulder or fillet of the specimen and grows mainly by the movement of screw

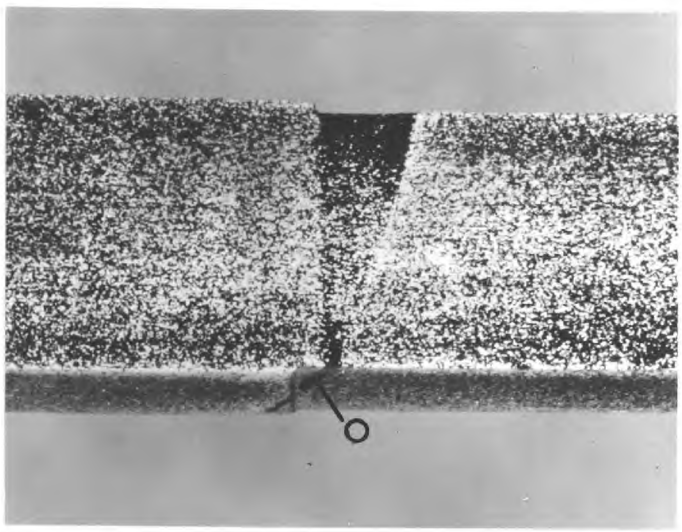

Sample S2, unnotched, σ_n/σ_{yd} = 0.9. x 6

Fig. 6.2. Pre-yield "cross band" formation at a fillet in an unnotched sample of mild steel. "O" indicates out-of-plane shear.

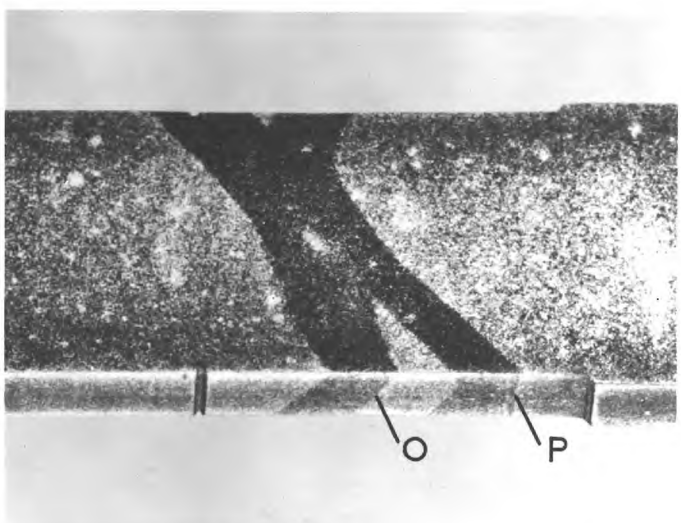

Sample 1"S2 (d = 4.5%, σ_n/σ_{yd} = 1.1). x 6

Fig. 6.3. "Oblique bands" at a very shallow notch showing shear in the plane of the specimen; indicated by "P", and out-of-plane shear; indicated by "O".

dislocation with the direction of shear oblique to the plane of the specimen (CRUSSARD (64)). This type of progression is slow and continues up to the upper yield stress where there is a yield drop due to the formation of one or several "oblique bands" (Fig. 6.3). The deformation in these oblique bands is mainly a shear in the plane of the specimen and the fronts make an angle of approximately 50° with the tensile axis (JAOUL (14)). This type of band progresses very rapidly through edge dislocations crowded at the tip. The two types of deformation bands observed have been illustrated by employing several techniques - surface etching (CRUSSARD (64)), surface coating with photo-elastic varnish (POMEY and GRUMBACH (94)), acoustic recording of noise emitted by test piece during loading (LEAN, PLATEAU et al (95)).

While the deformation in the cross bands consisted solely of "out-of-plane" shear, i.e., in planes inclined at about 45° to the plane of the specimen, shear in oblique bands was both in the plane of the specimen as well as in planes inclined to the specimen plane. Some of the very shallow notched specimens, which yielded in a manner similar to the unnotched ones, brought this out clearly (Fig. 6.3), where the plane of shear in the oblique bands can be seen to make traces of approximately 45° to both the top and

edge surfaces of the specimen. This involves a larger shear surface than the first two modes. The fact that all three forms of shear are observed shows that easy glide is possible on a number of planes at the same time in this material under the applied tensile load.

In this case a very high σ_{UY} (almost twice the σ_{LY}) can be attained and deformation starts by an oblique band causing a big drop in load. It has been suggested that there exists a critical stress for the formation of oblique bands (CRUSSARD (64)), which is generally not reached in the presence of stress concentrators prior to the formation of cross bands.

In the pre-yield region, the Fry's etchant used here could only show the cross band development in a macroscopically undeformed matrix. That the matrix itself is in a state of plastic microstrain (of the order of 10^{-3}) is borne out by many investigators. In fact, non-elastic strains as small as 10^{-5} have been recorded even in the centre of a specimen (BROWN and LUKENS (55), BROWN and EKVALL (23)).

The yield behaviour of this material, therefore, indicates that dislocation unlocking at σ_{UY} is the determining mechanism of yielding at room temperature. The basis of this statement is that there is no evidence to show any stress relaxation (in the absence of concentrators) prior to σ_{UY}, so that the whole matrix is under a high stress

approaching σ_{UY} when a yield nucleus is formed. Under the applied shear, therefore, the band can spread across the specimen with a minimum amount of work, very rapidly.

6.1.2 Yielding in Silicon Iron

All the Si-Fe specimens showed a yield drop, and none displayed any appreciable non-uniform deformation.

The start of microyielding occurred appreciably before σ_{UY} with grains along the specimen edges yielding first (due to stress concentrators along the edge). Yielding at isolated grains all along the gauge length and also in the centre of the specimen then followed without the formation at this stage of any clusters of yielded grains. The progress of heavier deformation from the edges towards the centre and an increase in the number of lightly deformed grains (mainly around the isolated grains which already showed slip nuclei) all over the specimen took place simultaneously. At the σ_{UY} the growing regions of fairly heavy slip, almost all along the edges of the specimen, met along the central longitudinal axis bringing about a yield drop. At this stage almost all the grains have lost their mobile dislocations and show slip traces (Fig. 6.4). Further slip takes place in intersecting directions, at 45° to the tensile axis and presumably shearing in the plane of the specimen.(Fig. 6.1), with

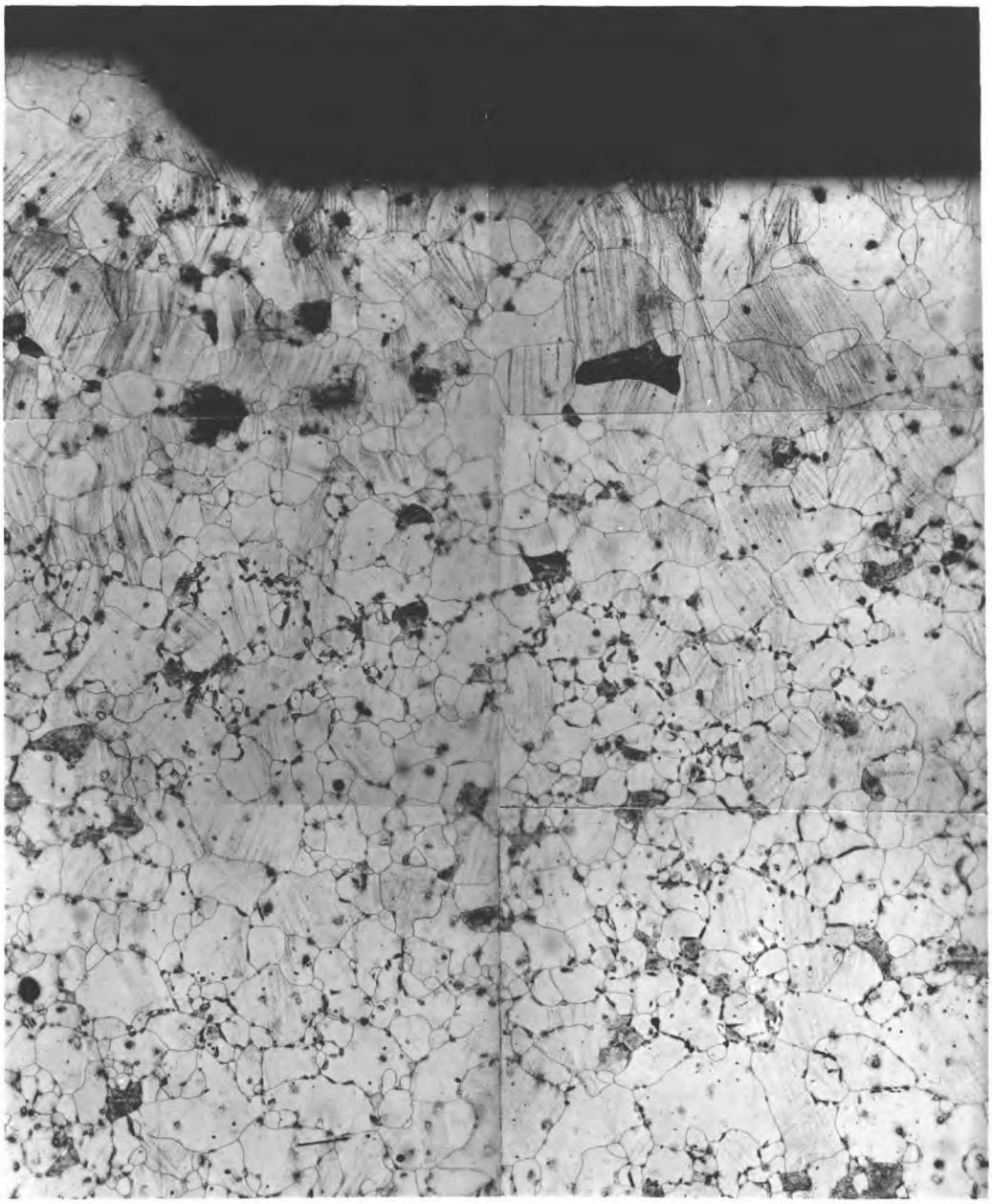

Sample M1, unnotched, $\sigma n/\sigma yd = 0.90$. x 60

Fig. 6.4. Pre-yield microstrain revealed by etching the surface of an unnotched specimen of 3% Si-Fe. Distribution from one edge to the central axis in the fillet region and part of the gauge length.

resulting work-hardening. Although slip is heaviest at the fillets it is still restricted from spreading across the specimen until the rest of the material has also had a chance to deform (Fig. 6.4).

By avoiding stress concentrators along the edges of the specimens, a much more uniform deformation could presumably have been obtained by the bowing out of mobile grow-in dislocations in grains randomly distributed throughout the matrix. These could then act as nucleating sites for further slip in adjoining grains until all "soft" dislocations which could move without upsetting local equilibrium between elastic and non-elastic grains, have bowed out. Increasing stress would then bring about new nucleating sites which would grow along with heavier deformation within the first sites. When a certain critical stress is attained, the "contained" deformation cannot go any further (due to tangles and constraint in the first sites), and slip progresses rapidly in the direction of maximum shear by the failure of grain boundary resistance.

It seems, therefore, that the main barrier to yielding in silicon iron is the lack of mobility of unpinned dislocations rather than the impurity locking of dislocations as in steel. This means, as has been suggested by JOHNSTON and GILMAN (37), STEIN and LOW (38), TETELMAN (84) that the

macroscopic yield stress is determined by the ability of dislocations to attain a particular velocity (10^{-3} cm/sec).

6.1.3 Effect of Material on the Mode of Yielding.

Since plastic deformation must take place by the passage of dislocations through the matrix, the different modes of yielding must depend on the nature of the matrix. An understanding of the yield behaviour must take into account a large number of interdependent factors such as impurities, directional bonds, Peierls-Nabarro force, grain size and temperature, all of which combine in a complex way to determine the path and the velocity of dislocations through the matrix metal.

Under the conditions of the present investigation, it is most likely that differences in the density and mobility of grown-in dislocations are the underlying cause for the observed effects.

In mild steel, a low initial density of mobile sources (due to strong pinning - COTTRELL (44)) could explain the near absence of plastic deformation until some critical stress level, σ_{UY}, when an avalanche of dislocations is released at some point. The sharp development of the slip band is perhaps because dislocations are wide, whereby high velocities can be attained.

In silicon-iron on the other hand, a high density of grown-in dislocations (GRIFFITHS and RILEY (96), CARRINGTON et al (63), LOUAT (97)) permits non-elastic deformation to start much before σ_{UY}. The resulting slip bands are, therefore, ill-defined with wide-spread relaxation around them. A low mobility of the dislocations (narrow dislocations) prevents them from traversing the specimen at high velocities and allows more time for blunting of the bands through relaxation of neighbouring grains.

It is expected that multiplication rates would be different in the two materials because while available slip planes in iron are $\{110\}$, $\{112\}$ and $\{123\}$ (BARRETT, ANSEL and MEHL (85)), addition of silicon tends to restrict slip on the $\{110\}$ planes (GRIFFITHS and RILEY (96)) and this property is further enhanced by high strain rates, high yield stresses and low temperatures (SESTAK and LIBOVICKY (98, 99, 100)). Thus while multiple cross-slip is easy in mild steel, the Frank-Read mechanism is more favoured, at least in the initial stages, in silicon iron. However, the large amount of relaxation ahead of a band front cannot be adequately accounted for by a difference in multiplication rates, because many narrow slip bands occur in silicon iron while only a few, but very broad, bands exist in mild steel. This should suggest that the density of active sources (Frank-Read

or otherwise) is much lower in mild steel.

From a consideration of the yield characteristics of the two materials one would expect that the effect of a notch would be

(i) to bring about earlier and more far reaching yield in silicon iron - because lower stresses at a distance from the notch would be capable of moving dislocations which are not strongly pinned as in steel;

(ii) once yielding starts at the notch in steel its propagation would be much more rapid than in silicon iron;

(iii) because of the slow development of the bands in silicon iron, the stresses and strains get a chance to equilibrate so that each stage of the band development is determined by the previous one. Different notch geometries should be expected to affect the yield modes quite strongly. By contrast, in steel, once slip is activated it would progress too rapidly for the mode to be altered by a change of the stress state or the notch geometry.

6.2 RESULTS : YIELDING IN NOTCHED SPECIMENS

The deformation patterns included in this chapter were obtained from the etch-pitting technique described in Chapter 4. All the patterns illustrate deformation zones in specimens in the unloaded state.

A few interference patterns are also included to illustrate the surface relief due to local yield at the notch.

6.2.1 The Deformation Sequence.

In order to demonstrate some of the trends exhibited by the deformation patterns it is convenient to give some indication of the deformation sequence as observed during the tension routine. While it is difficult to elicit a general picture of the sequence for all the notch depths and root radii investigated due to the large amount of relaxation associated with the propagating band, some of the basic trends persist and these have been presented in Fig. 6.5.

Yield first starts at W followed immediately by two arcs from R and R'. Because of their appearance they have been called "hinges of rotation" or "R-hinges". These two arcs enclose the local strain, and the growth of this local strain

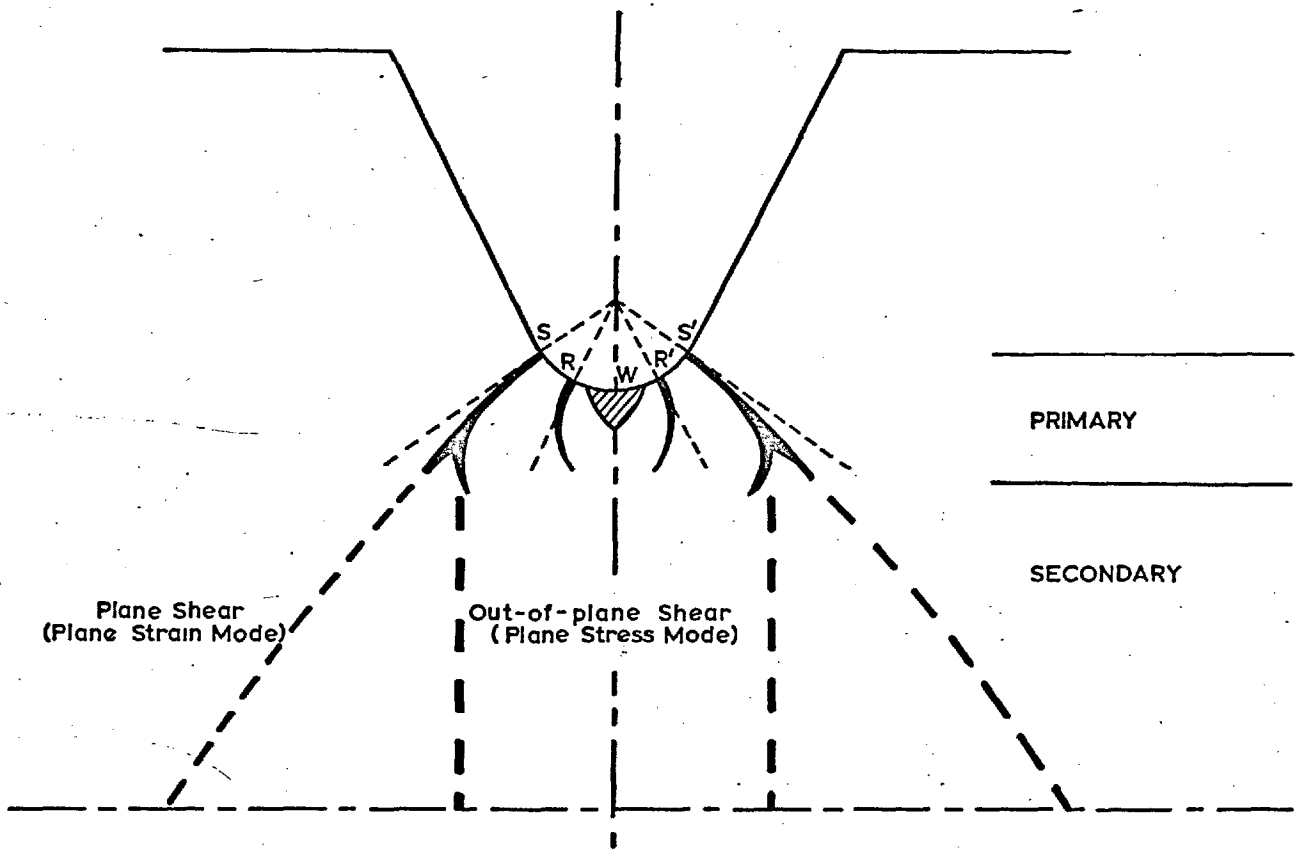

Fig. 6.5. DEFORMATION SEQUENCE AROUND A NOTCH WITH ARBITRARY DEPTH AND ROOT RADIUS.

is described by the primary mode. The rapid and general mode of deformation by plane or out-of-plane shear or a combination of both takes place later, along lines that have been referred to here as "lines of secondary shear". They are represented in Fig. 6.5 by the dashed lines. The secondary shear is initiated either by the "R-hinges" opening out to some position S-S' or by the development of two hinges from S and S'. Because of their association with the secondary shear lines they have been called here "secondary hinges" or "S-hinges."

6.2.2 Yield Development in Silicon Iron.

The photographs included here show the development of yielding from the notch root, the slip traces being brought out as arrays of individual pits on a general background of dislocation fog. Wherever possible, the positions W, R, R' etc., have been scribed on the illustrations to indicate the relative position of the yield zones.

(i) Start of Yield

Slip was initiated at a stress of $\sigma_n/\sigma_y = 0.4$ or below, in one or two grains in the region of stress concentration, W, at the root of the notch. At this stage the distribution of slip was determined by the sharpness of the notch rather than the depth; the blunt notches show bands in separated

groups, while in the sharp notches the grouping is close together.

Typical examples of slip initiation in blunt notches is shown in Fig.6.6. Fig. 6.6 (a) shows the first detection of slip in the region W; (b) and (c) show the growth and link-up of the isolated bands at a very short distance along the root of the notch.

Fig. 6.7 (a) and (b) shows slip initiation in sharp notches. The region of stress concentration is confined to a much smaller area around the tip of the notch and slip occurs over the entire region W of the root surface.

The penetration of the bands at these low stresses was determined by the incidence of grain boundaries below the root. In the sharp notches the stress developed at the root was sufficient to traverse the first grain below the root (Fig. 6.7 (a) and (b)). In the blunt notches, however, stress concentrations being low, a stage could be recorded where slip did not traverse a grain (Fig. 6.6 (a)).

(ii) Development of the Plastic Zones.

Localized deformation progressed by the joining up of separated groups of bands within the region R-R', giving the wedge more definite shape. The growth of the wedge up to this stage, is more pronounced in the sharper and deeper notches. This is followed by the development of the R-hinges

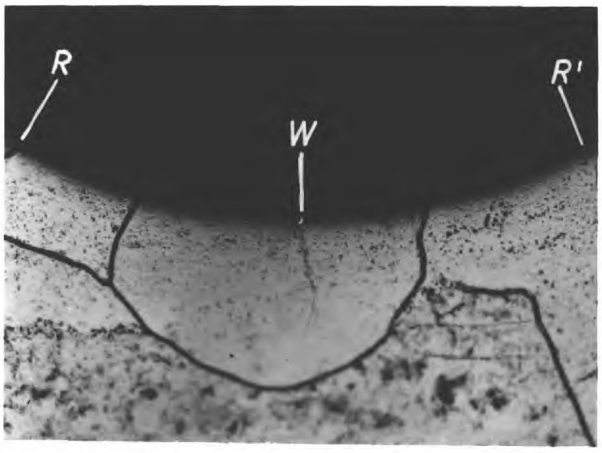

(a) Sample 6M2 (notch depth, d = 55%, σ_n/σ_{yd} = 0.40) x 210

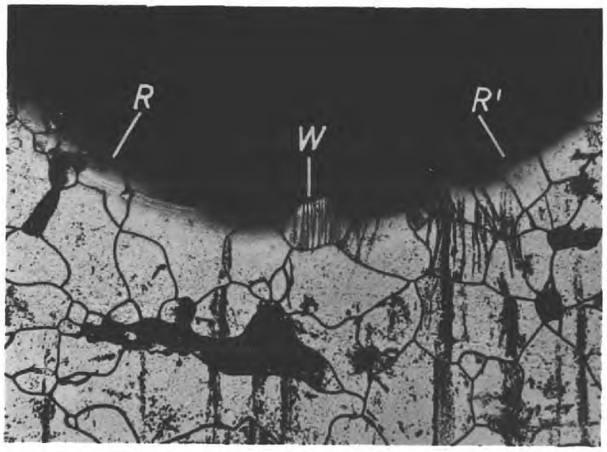

(b) Sample 5M2 (d = 45%, σ_n/σ_{yd} = 0.40) x 90

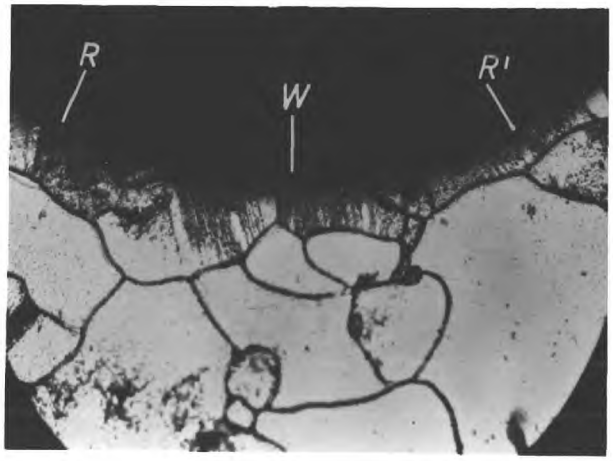

(c) Sample 8M1 (d = 73%, σ_n/σ_{yd} = 0.49) x 160

Fig. 6.6. Initiation of slip at the root of a blunt notch. (Root radius, r = 0.015").

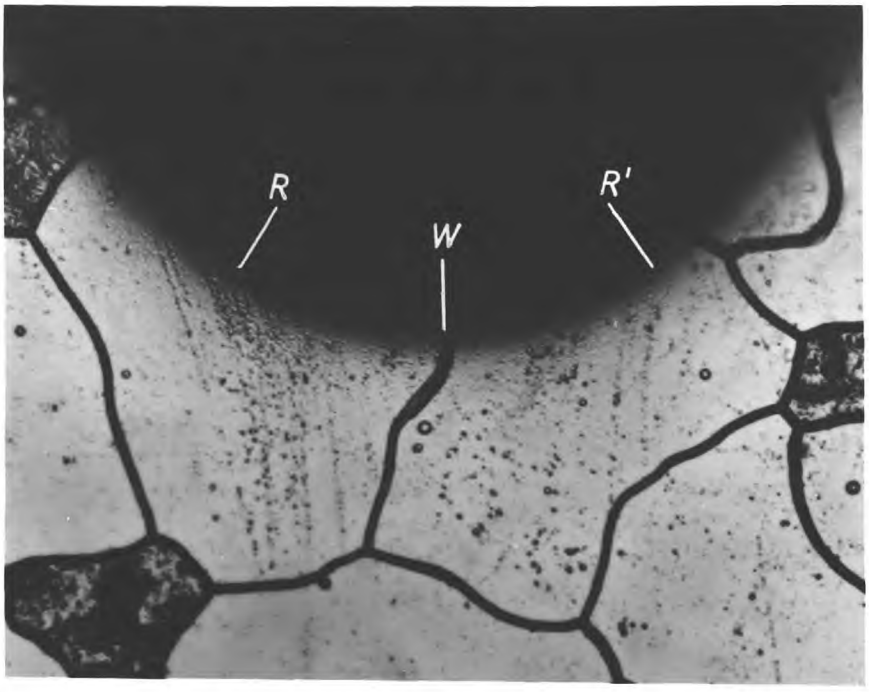

(a) Sample 7"M1 (d = 63%, σ_n/σ_{yd} = 0.25). x 510

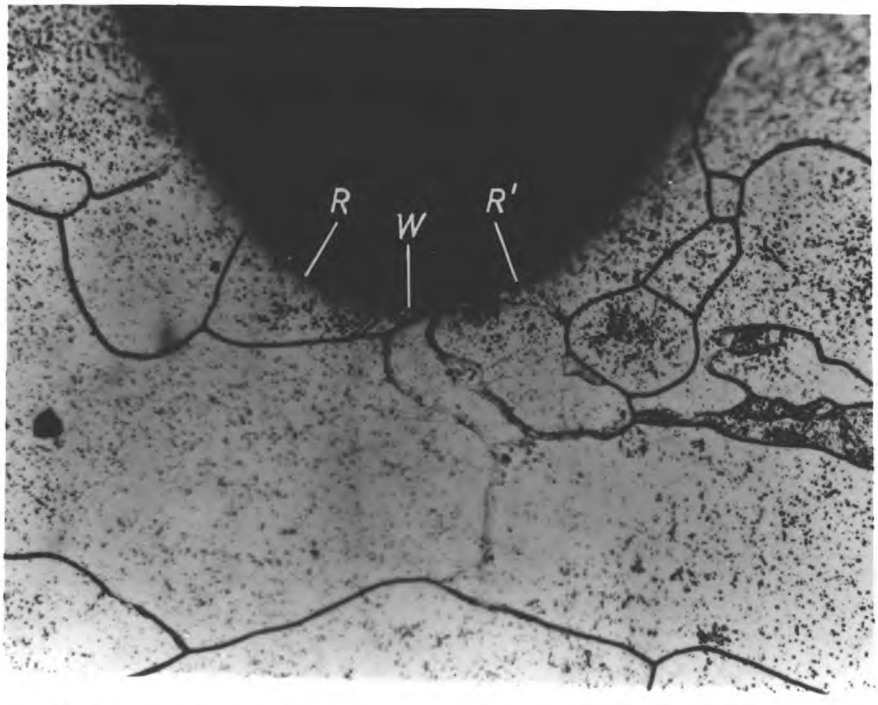

(b) Sample 8"M1 (d = 73%, σ_n/σ_{yd} = 0.40). x 300

Fig. 6.7. Initiation of slip at the root of a sharp notch. (r = 0.0015").

from R and R' at the outer edges of the wedge (Figs. 6.8 (a), 6.9), and these curve in to form a localized region of yield under the notch. The relaxation of stresses caused by the R-hinges retards the growth of the wedge so that deformation proceeds predominantly by growth of the R-hinges. This is brought out quite clearly by comparing Fig. 6.14 (a) with (b) in the case of a notch of intermediate sharpness.

At a further increase in stress the S-hinges appear and start off deformation by the secondary mode. Except in some of the deeper and blunt notches the secondary mode was mainly by plane-strain shear.

The three types of zones were found to occur in all specimens, in varying degrees, depending on the notch profile and the depth. In order to assess the effect of notch geometry on the propagation of these zones effectively, it was found most convenient to present the deformation patterns of increasing notch depth grouped under the three notch radii investigated, that is -

I Blunt Notches (r = 0.015")

II Intermediate Sharp Notches (r = 0.004")

III Sharp Notches (r = 0.0015")

(iii) Effect of Notch Depth on Yield Zones.

I Blunt Notches

(a) Notch Depth - 22% and 36%

After the initial wedge formation (Fig. 6.8 (a)), the deformation spreads mainly by wide (order of root radius) R-hinges (Fig. 6.8 (b)). When the notch depth is 22%, this is followed by the spread of S-hinges from the notch, whereas at the 36% depth the secondary mode starts later on by the forking out of well developed R-hinges. This is brought out clearly in Fig. 6.8 (c), where the R-hinge, on the left side of the notch, has initiated the secondary by forking out both in the plane-stress and plane-strain directions.

(b) Notch Depth - 45% and 55%

In these specimens the wedge formation is more pronounced than in the lower notch depths. Fig. 6.9 shows an early stage of this in a 45% notch.

R-hinges start within R-R' but with increasing penetration they also spread along the surface of the root up to S-S'. They can, however, be identified as R-hinges, because of their characteristic tendency of curving in towards the central notch axis. As in the 36% depth, the secondary mode is initiated by forking out from the R-hinge. With increasing depth the primary hinges were found to

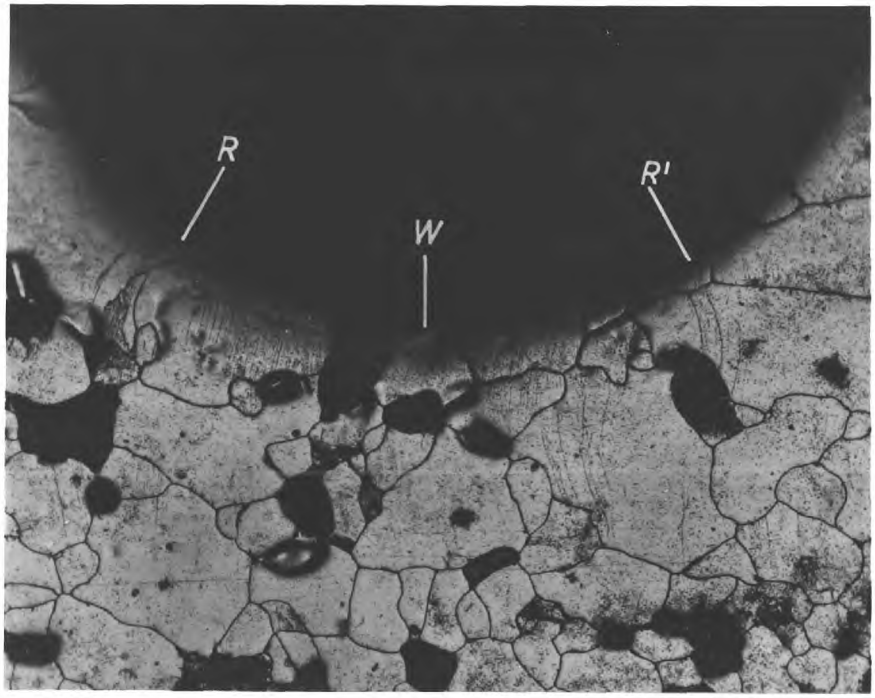

(a) Sample 4M1 (d = 36%, σ_n/σ_{yd} = 0.50) x 130

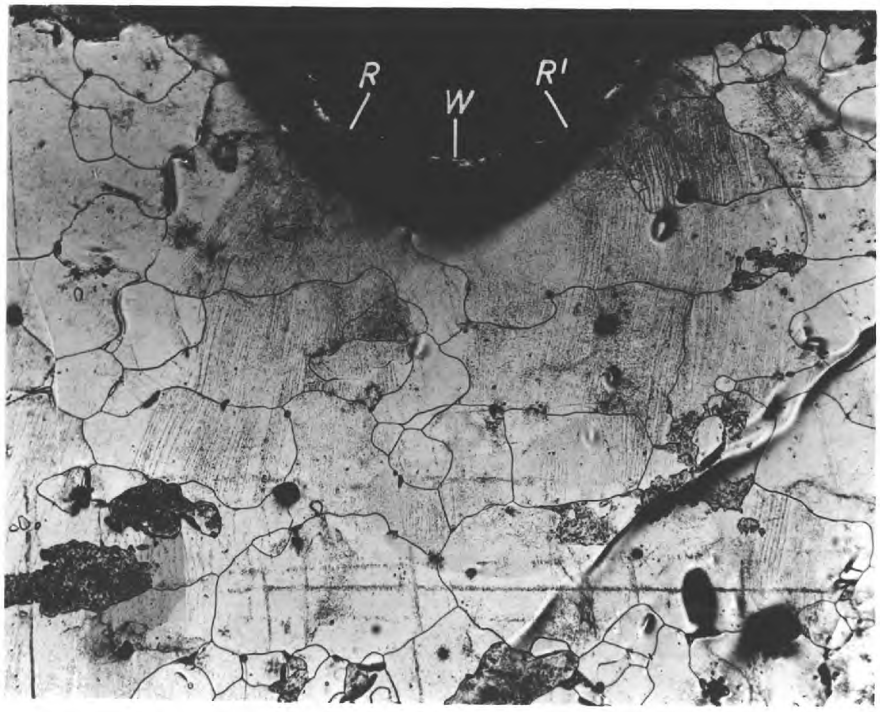

(b) Sample 4M3 (d = 36%, σ_n/σ_{yd} = 0.74) x 95

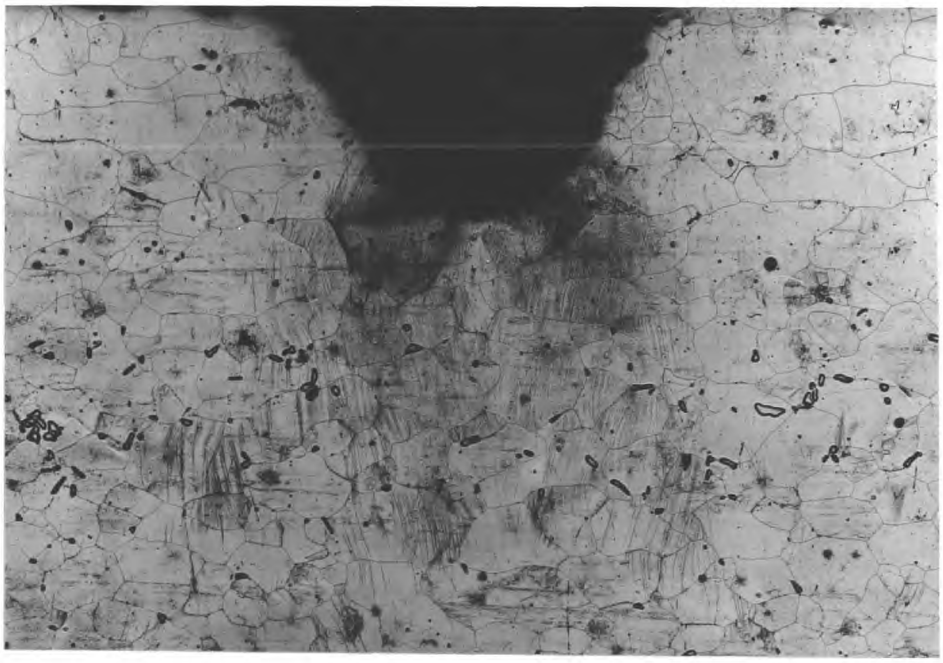

(c) Sample 4M4 (d = 36%, σ_n/σ_{yd} = 0.75). x 45

Fig. 6.8. Stages of plastic zone development in shallow, blunt notched samples. (r = 0.015")

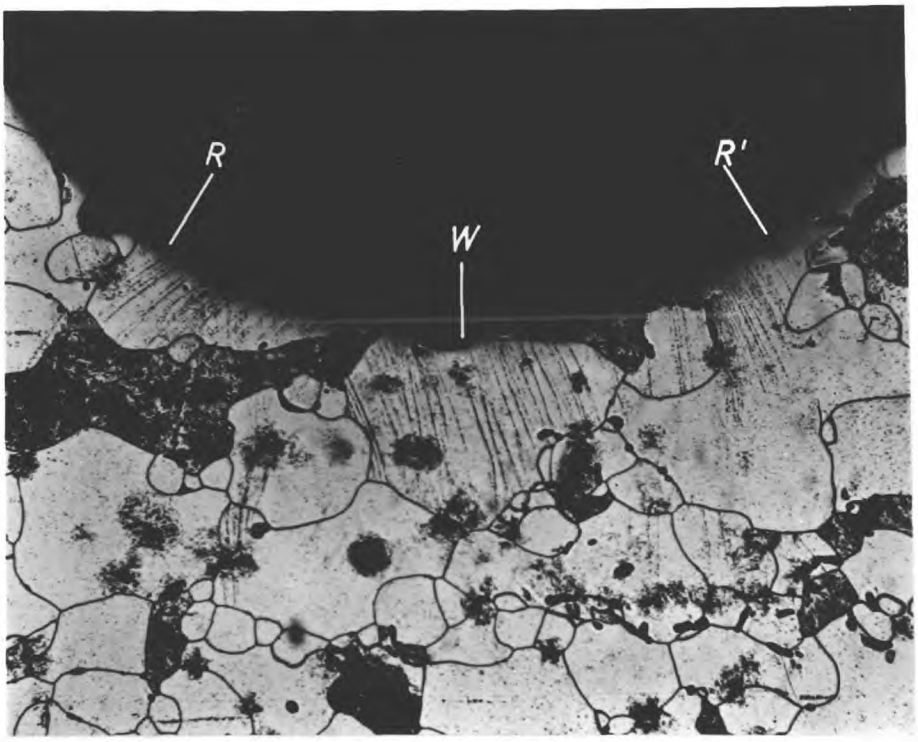

Sample 5M3 (d = 45%, σ_n/σ_{yd} = 0.60). x 150

Fig. 6.9. Deformation pattern under a blunt notch showing slip developing from R, W, R'.

develop more before the secondary mode was initiated. This makes for the deformation to be contained within a smaller boundary enclosing the notched area, with consequent annexations of the large elastic core that is usually found between shallow notches.

(c) Notch Depth - 63% and 73%

In these deeply notched specimens growth of wedge deformation occurs very easily. It joins with the hinges at an early stage and grows inwards with a large flat band front (Fig. 6.10). Although the hinges are fairly wide-angled to start with, like the S-hinges, they do not continue in the plane-shear mode at 45° to the tensile axis. In those specimens with a 73% notch, a distinction as to the type of yield zone can hardly be made at all.

II Intermediate Sharp Notches

(a) Notch Depth 22% and 36%

The hinges begin to grow from about S-S' as shown in Figs. 6.11 (a) and 6.12 (a). Notably there is less sign of any wedge in the 22% notch and the included angle between the shear directions is larger than in the 36% notch.

Progress of yielding is by S-hinges right from the start in the 22% notch with very little sign of R-hinges (Fig. 6.11 (b)). In the 36% notch the R-hinges get more chance to develop into the specimen, as indicated by "R" in

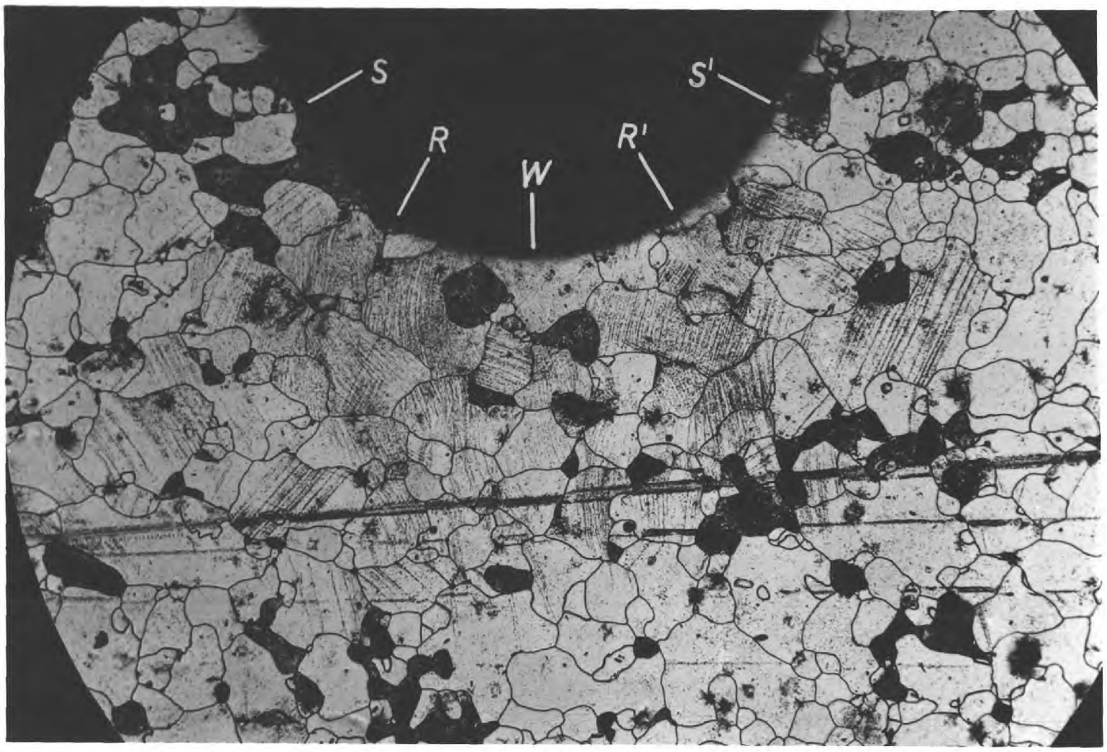

Sample 7M3 (d = 63%, σ_n/σ_{yd} = 0.60). x 80

Fig. 6.10. Pattern showing development of a wide band front under a deep blunt notch.

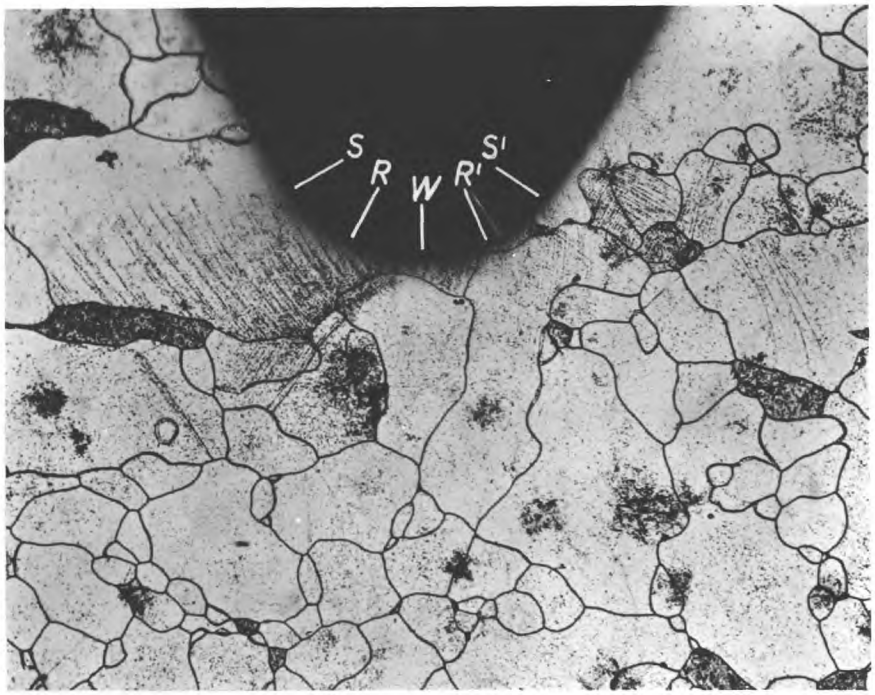

(a) Sample 3'M3 (d = 22.5%, $\sigma n/\sigma yd$ = 0.60). x 150

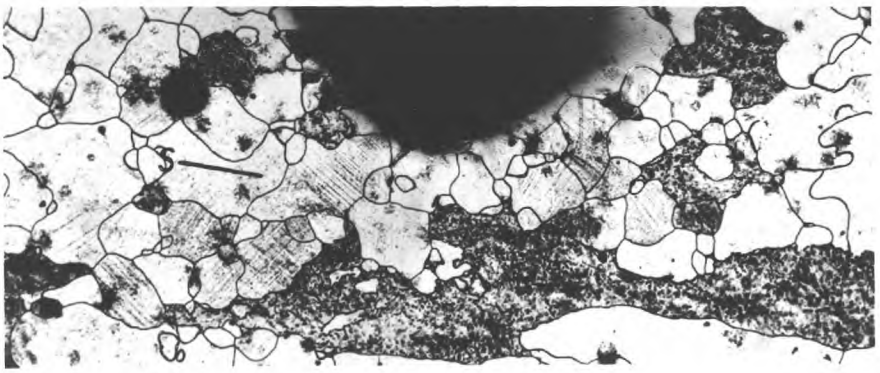

(b) Sample 3'M4 (d = 22.5%, $\sigma n/\sigma yd$ = 0.80). x 80

Fig. 6.11. Pattern illustrating (a) the development of S-type hinges from a notch of intermediate sharpness and (b) its progress in a direction at approximately 45° to the tensile axis. (r = 0.004")

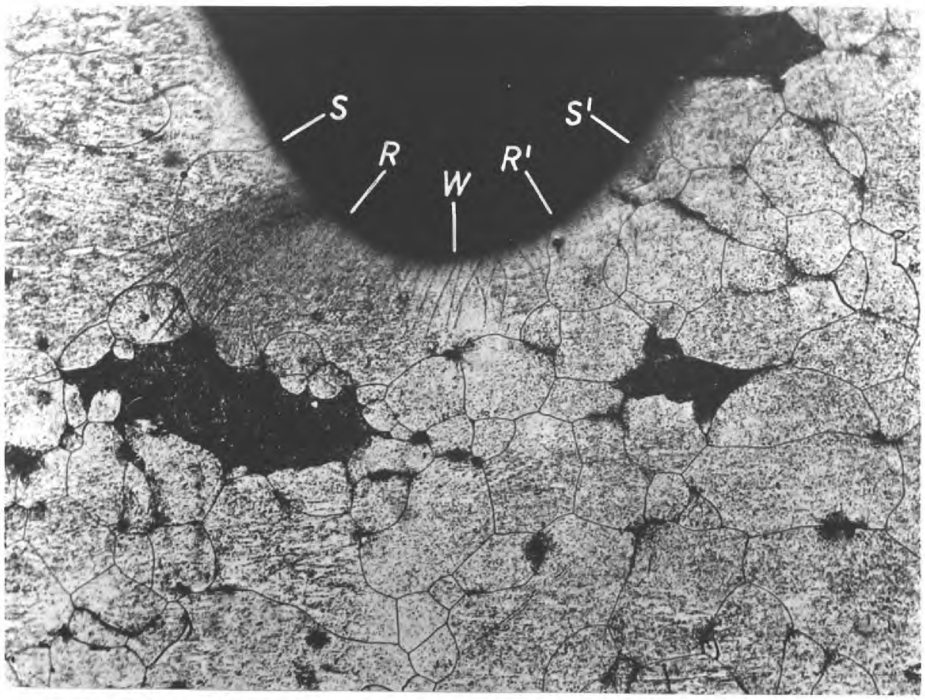

(a) 4'M2 (d = 36%, σ_n/σ_{yd} = 0.40). x 160

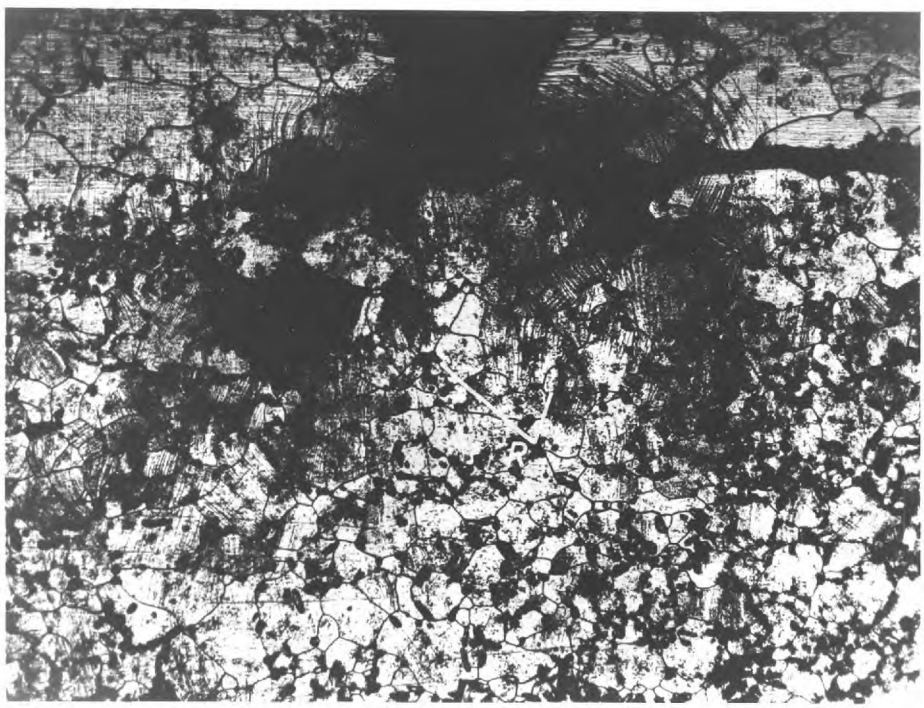

(b) Sample 4'M3 (d = 36%, σ_n/σ_{yd} = 0.90). x 45

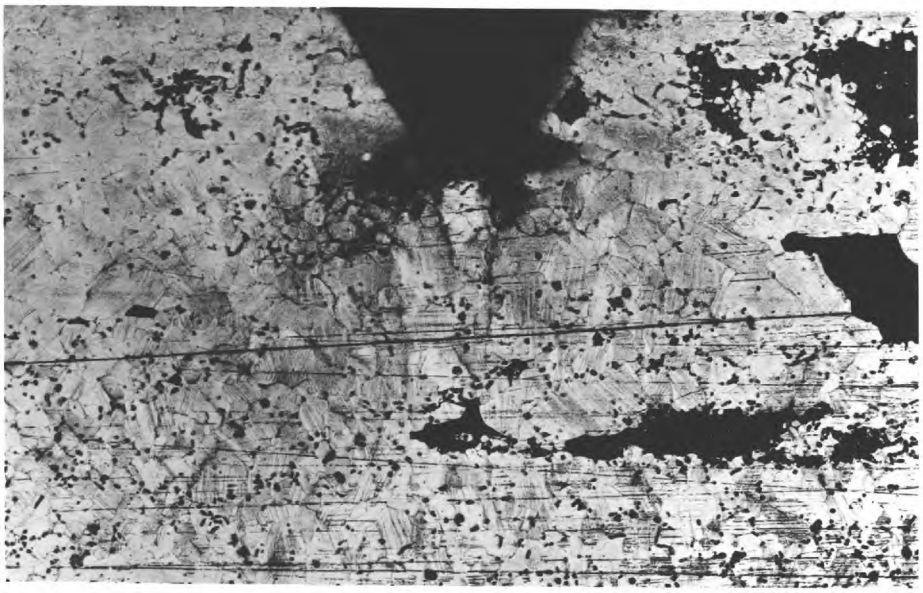

(c) Sample 4'M4 (d = 36%, σ_n/σ_{yd} = 0.95). x 30

Fig. 6.12. Stages of plastic zone development in samples with shallow notches of intermediate sharpness. (r = 0.004").

Fig. 6.12 (b), before showing any signs of forking out in a direction at about 45° to the tensile axis. The R-hinges in Fig. 6.12 (b) have the appearance of the plane-stress type zones reported by DUGDALE (9).

Fig. 6.12 (c) shows the stage where general yielding has taken place by the secondary mode which was initiated by R-hinges after a certain amount of penetration. The inner and outer edges of the secondary zone can roughly be defined by the "plane shear" and "out-of-plane shear" as shown in Fig. 6.5.

(b) Notch Depth - 45% and 55%

As in blunt notches, increasing notch depth makes the wedge-type deformation easier. This can be seen by comparing Figs. 6.13 (a) and 6.14 (a) with Figs. 6.11 (a) and 6.12 (a).

Since the root radius of these specimens was quite small, stresses do not vary much in the vicinity of the notch; as a result the R-hinge merges with the wedge inside at lower stresses and with the S-hinge outside at higher stresses. The distinction between the hinges , made before (Fig. 6.5) becomes more difficult to observe as the zone covers most of the area under the notch. Fig. 6.13 (b) when compared to (a) shows that on increasing stress the wedge stops growing, or grows more slowly. The R-hinges open out more to merge with S-hinges, which, however, show little

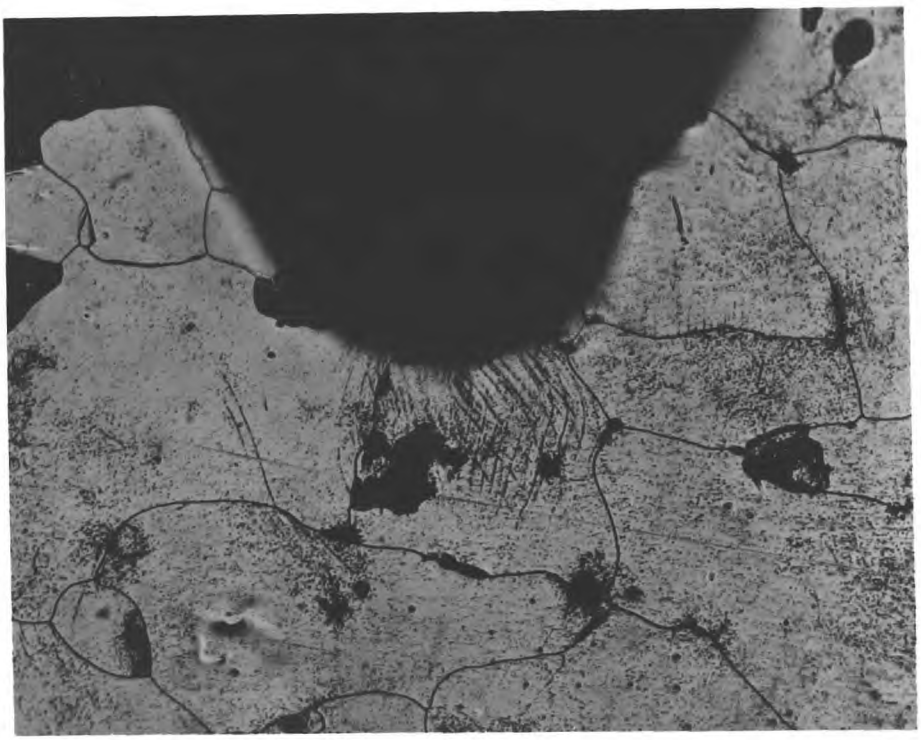

(a) Sample 5'M2 (d = 45%, σ_n/σ_{yd} = 0.59). x 200

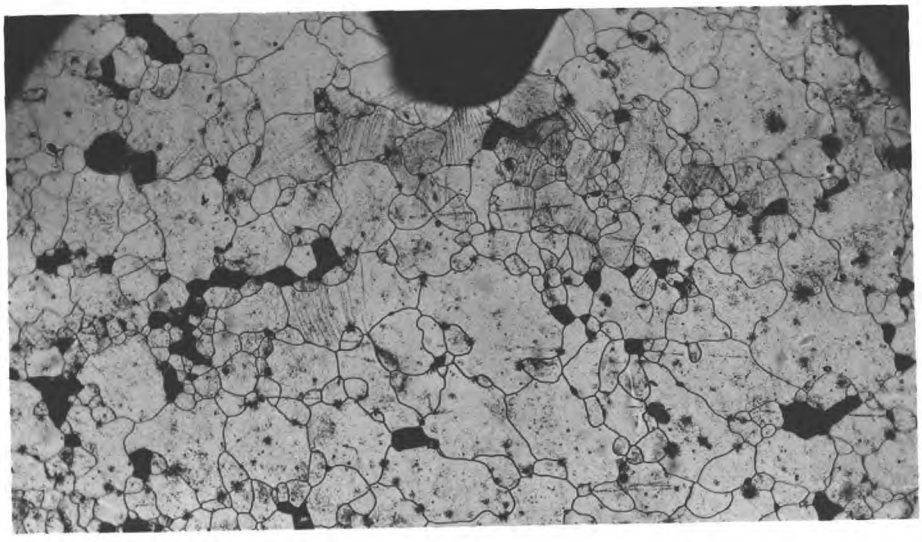

(b) Sample 5'M3 (d = 45%, σ_n/σ_{yd} = 0.77). x 65

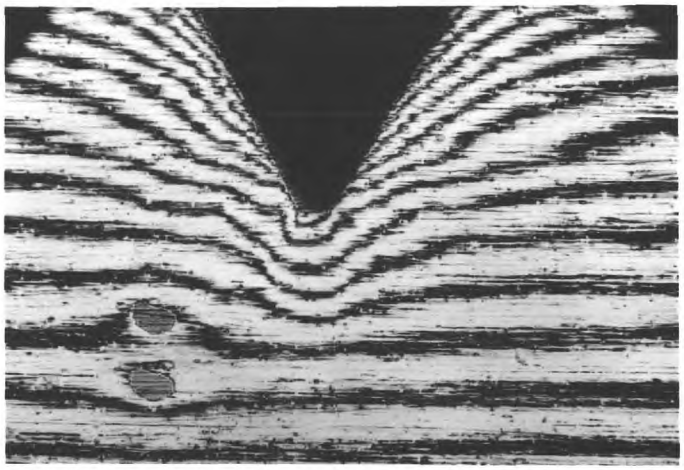

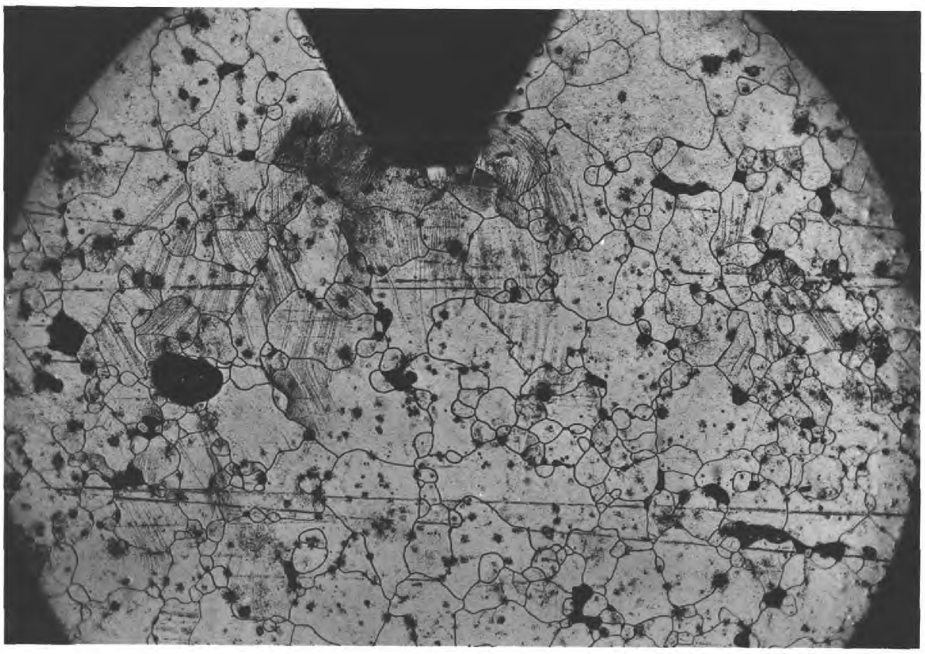

(c) Sample 5'M4 (d = 45%, σ_n/σ_{yd} = 0.85). x 65

Fig. 6.13. Stages of plastic zone development under notches of intermediate depth and sharpness. Interferogram shows surface relief before etching sample 5'M4.

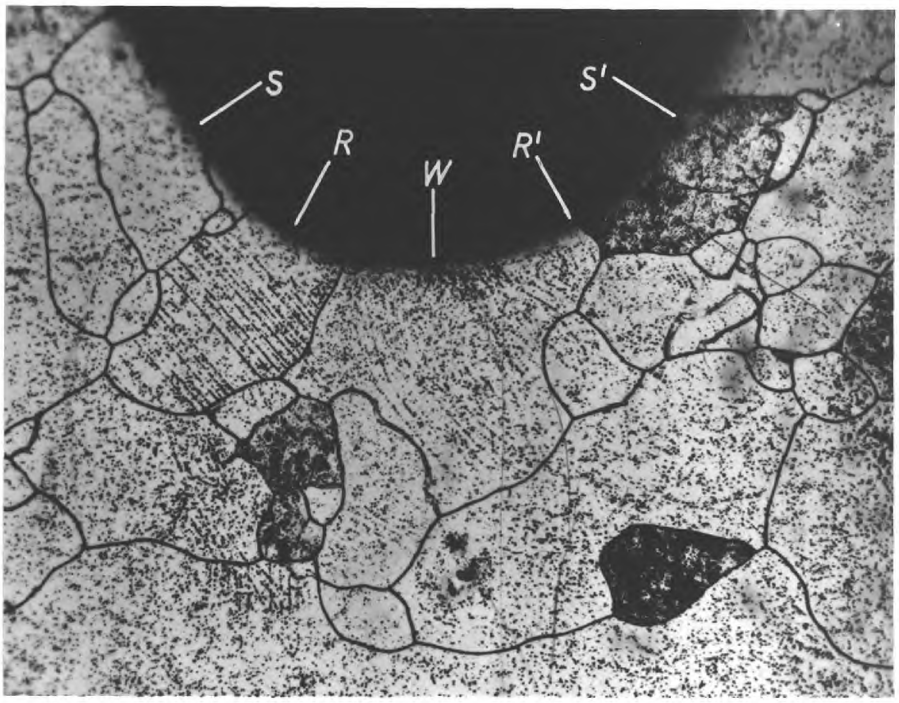

(a) Sample 6'M2 (d = 55%, σ_n/σ_{yd} = 0.40). x 255

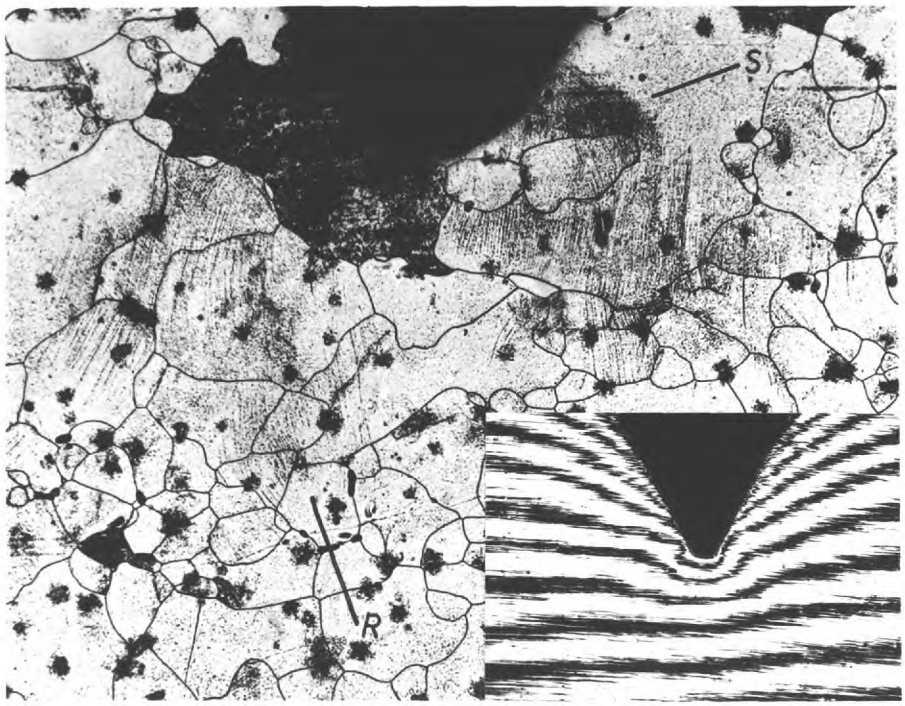

(b) Sample 6'M3 (d = 55%, σ_n/σ_{yd} = 0.72). x 100

Fig. 6.14. Patterns showing stages of zone development in samples having intermediate sharp notches. R and S refer to types of hinges. The interferogram illustrates the surface relief associated with the hinges. (r = 0.004").

or no lateral spread. The next notch (55% deep) shows this even better (Fig. 6.14 (b)), where deformation at the left hand edge is like the S-hinge, while the inside edge resembles an R-hinge which has opened out.

Fig. 6.13 (c) shows a deformation pattern much the same as in Fig. 6.13 (b), but with a larger area of yield. Although considerable deformation has taken place there is hardly any sign of the secondary plane-shear mode - except perhaps at the right side of the notch, where a few yielded grains can be seen set apart from the main body of the zones at the notch, and in the path of the hypothetical secondary plane-shear mode. An interference pattern of the sample was included in Fig. 6.13 (c) to show that the R-hinge and the S-hinge to a certain extent, are associated with steps on the surface, but not the wedge to any appreciable extent. This seems to indicate that the R-hinge, at least for this particular geometry, might be associated with a plane stress mode. This seems to be confirmed by the shape of the zones in Figs. 6.13 (c) and 6.14 (b) which bear a marked resemblance to that found in the plane stress DUGDALE (9) model and shown to occur in Si-Fe by HAHN (74).

III Sharp Notches

Deformation patterns are much the same as those found with notches of intermediate sharpness, except that the

notch being sharper the effect of variations in stress is even less evident in the immediate vicinity of the notch root. A relatively larger area of the root is under high stress and yields; the deformation zones are, therefore, not confined to the region S-S' except at very low stresses.

(a) Notch Depth - 22% and 36%

At low stresses all three types of zones, i.e., the wedge, R-hinge and S-hinge can be seen, but increasing stress brings about deformation by band fronts travelling along a plane-shear direction, approximately at 45° to the tensile axis (Fig. 6.15). A noteworthy feature is that the deformation zone has much more lateral spread and encloses a much larger elastic core than the notches with larger root radii of comparable depth (Figs. 6.8 (c), 6.12 (b, c)). The effect of reducing the root radius was to change the mode of deformation from "out-of-plane shear" to "plane-shear" type as is seen on comparing Figs. 6.8, 6.12 and 6.15.

(b) Notch Depth - 45% and 55%

As in the intermediate sharp notches, and the blunt notches to a certain extent, a sharp change in the deformation mode is observed from a notch depth of 45% onwards (Fig. 6.16 (a)). Much more wedge-type deformation is seen, the hinge arms have a lower included angle and they grow

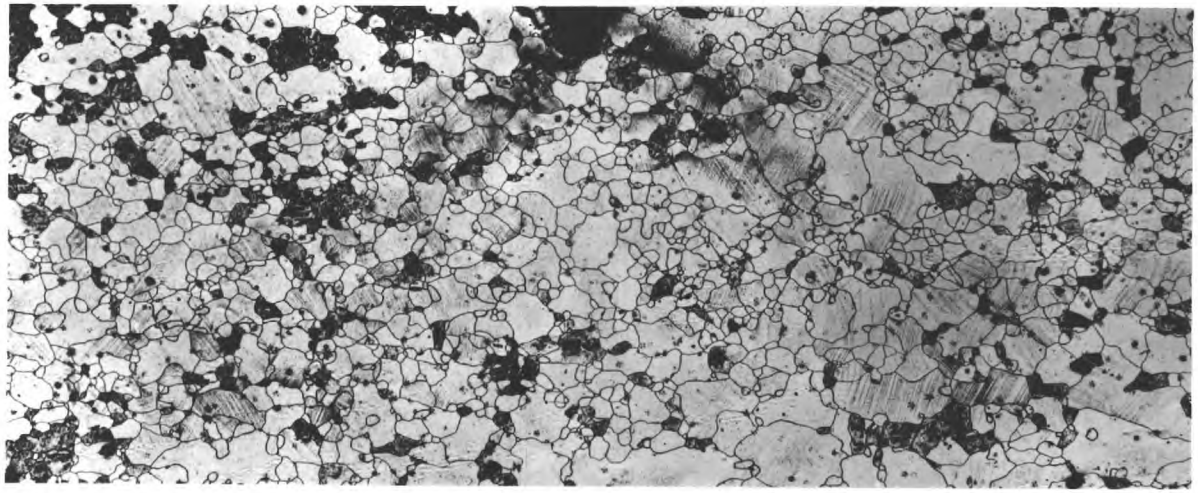

Sample 4"M4 (d = 36%, σ_n/σ_{yd} = 1.10). x 30

Fig. 6.15. Deformation pattern under a sharp, shallow notch. (r = 0.0015").

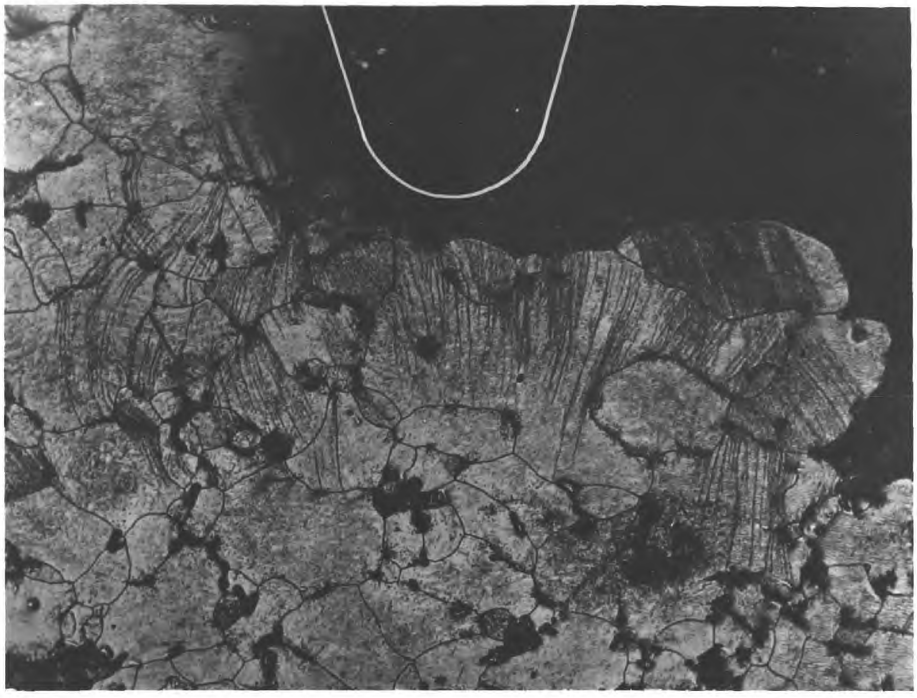

(a) Sample 5"M3 (d = 45%, σ_n/σ_{yd} = 0.61). x 105

(b) Sample 5"M4 (d = 45%, σ_n/σ_{yd} = 0.97). x 30

Fig. 6.16. Patterns showing (a) primary zones of wedge and R-hinge type, and (b) further development by the secondary mode (II) under a sharp notch of intermediate depth.

further inwards along the y-axis before the secondary shear mode takes over - indicated by II in Fig. 6.16 (b). It is interesting to note that this has a similar appearance as the pattern at a more blunt but shallower notch (Fig. 6.12 (b)). It seems that the "general" or secondary mode of deformation is allowed to continue to larger depth of notching in sharp notches, while at larger roots the primary mode is initiated at smaller depths. A comparison of Figs. 6.15 and 6.16 (b) shows how larger primary development with increasing notch depth reduces the elastic core between the notches.

Fig. 6.17 (a), (b) shows deformation patterns for a 55% notch. They are similar in appearance to those in Fig. 6.16. As expected with deeper notches, x-axial spread of deformation is even less in these.

(c) Notch Depths - 63% and 73%

The secondary plane-shear mode is practically non-existent except at a very late stage, just before general yield, when the zones have nearly spread to the x-axis (Fig. 6.18 (b)). Primary zones consisting of wedge and R-hinges penetrate into the specimen readily at comparatively low stress levels ($\sigma_n/\sigma_{yd} = 0.2$) but are arrested after a certain stage ($\sigma_n/\sigma_{yd} = 0.4$ in Fig. 6.18 (a)). Further deformation takes place by the broadening of the zone within

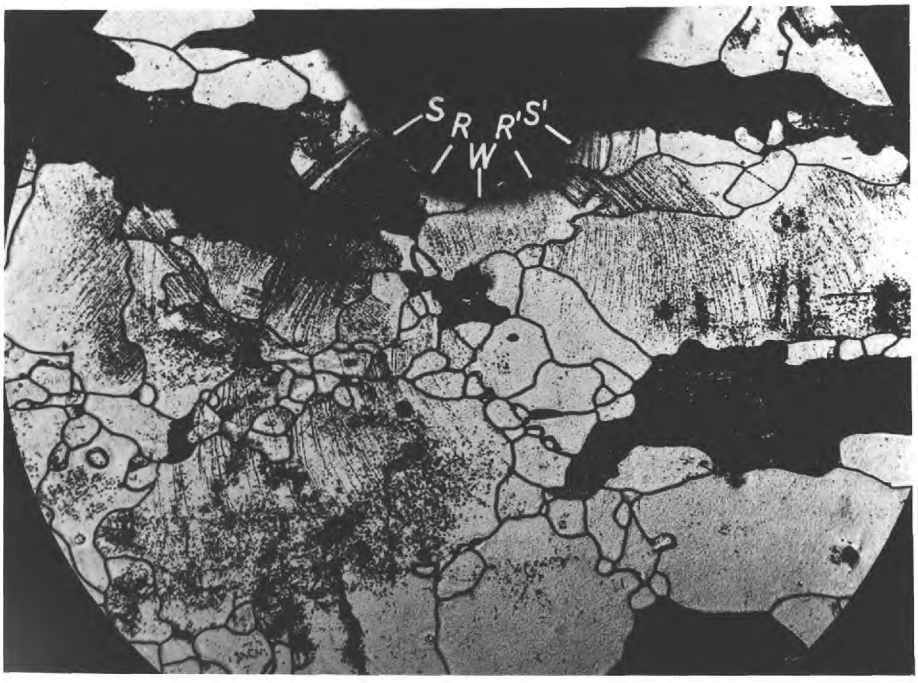

(a) Sample 6"M2 (d = 55%, $\sigma n/\sigma yd$ = 0.77). x 115

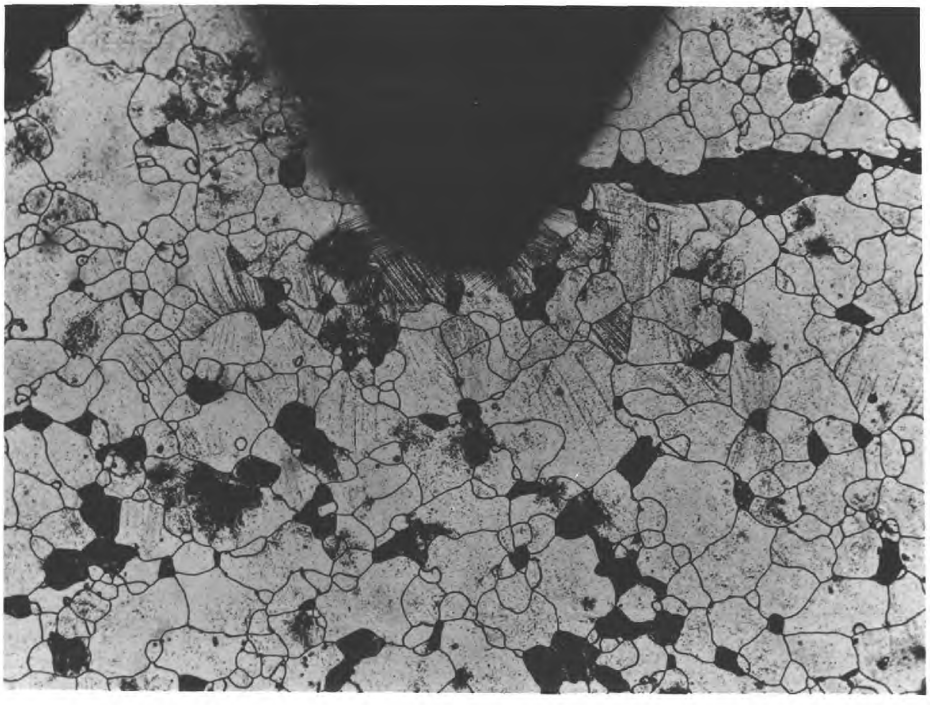

(b) Sample 6"M3 (d = 55%, $\sigma n/\sigma yd$ = 0.85). x 70

Fig. 6.17. Deformation patterns below a sharp notch. (a) R-hinges develop from S, S'; wedge formation is between R, R'. (b) Yield spread by R-hinges developing from above S,S'.

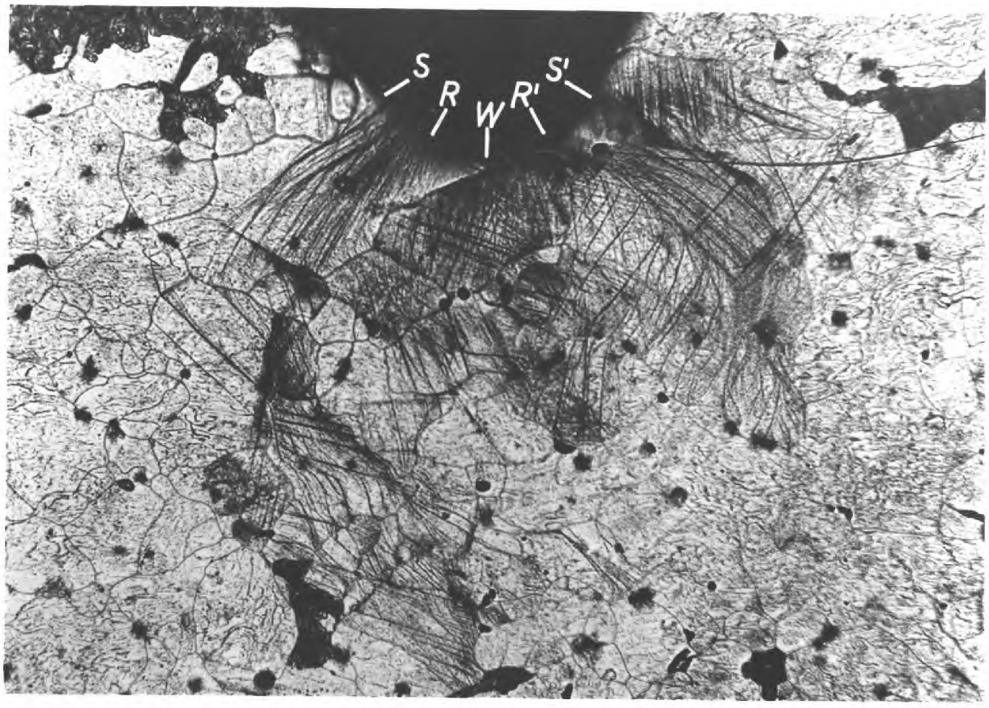

(a) Sample 7"M2 (d = 63%, σ_n/σ_{yd} = 0.40). x 100

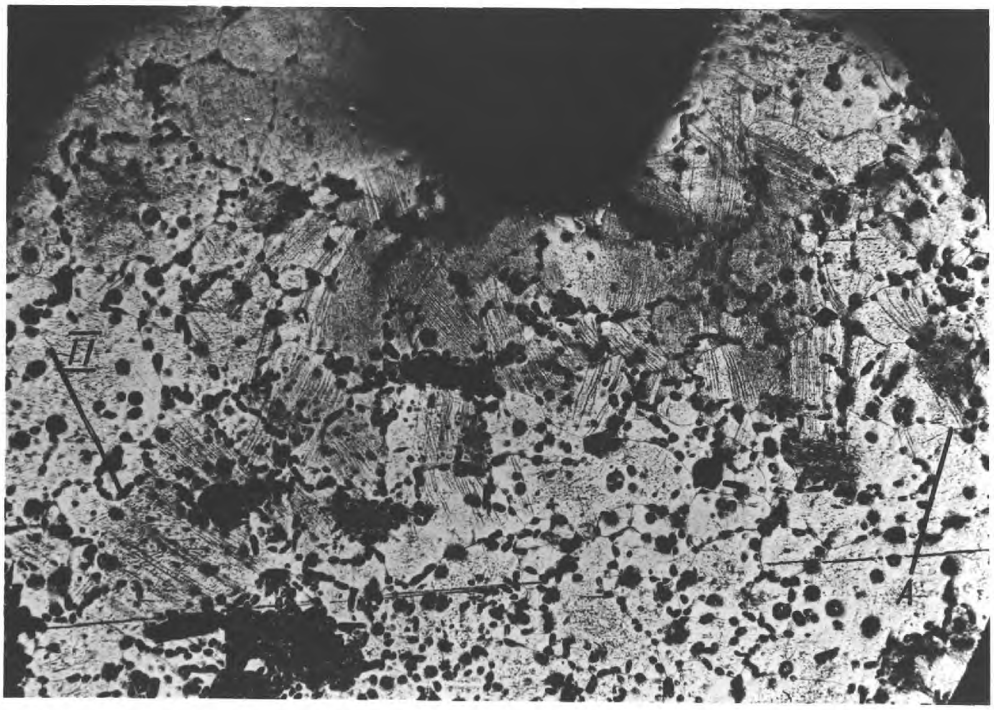

(b) Sample 7"M3 (d = 63%, σ_n/σ_{yd} = 0.68). x 90

Fig. 6.18. Deformation patterns below a sharp notch. (a) R-hinges develop from S, S'; wedge is between R, R'. (b) Bands develop in direction of notch axis, but are broadened by joining of other yielded areas like "A"; "II" is start of secondary shear

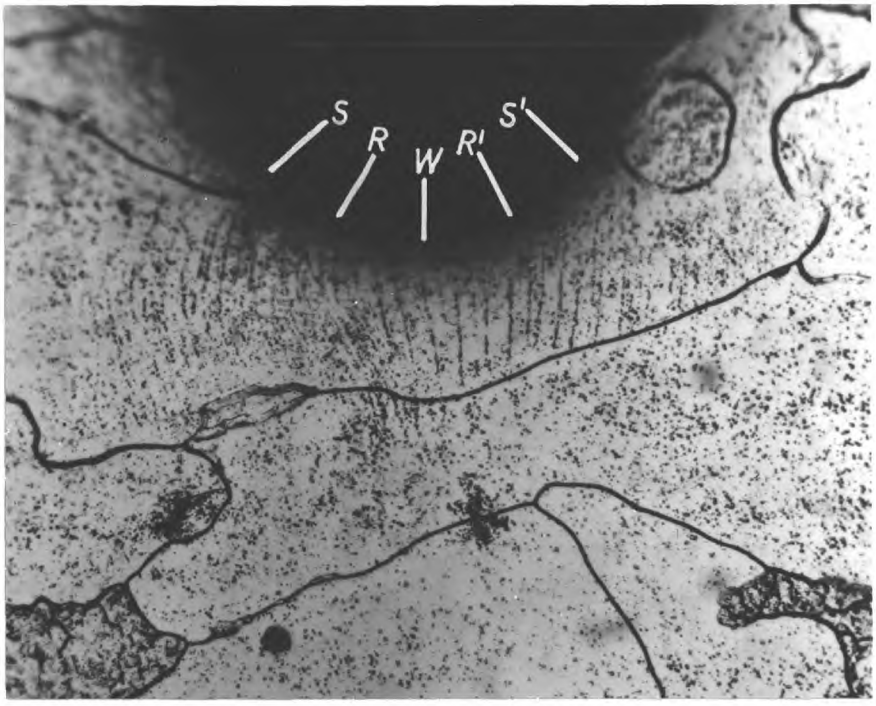

(a) Sample 8" M3 (d = 73%, σ_n/σ_{yd} = 0.45) x 295

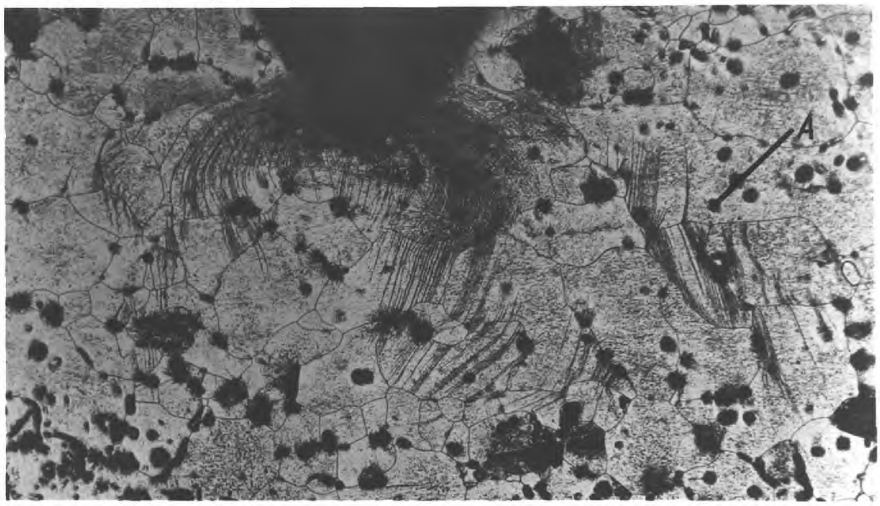

(b) Sample 8" M4 (d = 73%, σ_n/σ_{yd} = 1.0) x 100

Fig. 6.19. Deformation patterns below a deep sharp notch. (a) Slip is in the entire region between S, S', in the form of a blunt wedge. (b) Yield spread by R hinges developing from above S, S' and joining of regions like "A".

the highly stressed area under the notch without much penetration. This results in very blunt band fronts, which probably explains the high stress increment (70% from Fig. 6.18 (a) to (b)) needed to initiate a secondary shear mode.

Fig. 6.19 (a) shows a stage in the 73% notch where the R-hinges have not developed.

Fig. 6.19 (b) shows a stage equivalent to that in Fig. 6.18 (b) for the shallower notch, where the plastic zone under the notch is getting broadened by annexations of other areas within the high-stressed region. One such area which has not yet joined with the main body of the zone is indicated by 'A' in Figs. 6.19 (b) and 6.18 (b).

6.2.3 Yield Development in Mild Steel.

It was characteristic of mild steel that zones spread across the specimen much more rapidly than in Si-Fe.

All notch depths and root radii, except in the very shallow range, showed primary zones, i.e., wedge and R-hinges, before the development of the secondary mode.

(i) Very shallow notches.

Yielding in these was similar to that at fillets in unnotched samples.

Usually, a cross band developed from one side of a notch and progressed to the opposite notch in a plane stress

manner, and this was followed immediately by general yielding with the development of oblique bands extending to the opposite edge of the specimen.

In the blunt notched specimens bands were very thick (Fig. 6.20 (a)), because constraining effects being low, stresses are uniformly distributed over larger areas and consequently a larger area is able to yield when a critical stress level is reached.

At the sharp notches where non-uniformity was higher, bands were much thinner and development was less rapid. Yielding in these shows characteristics of both unnotched and deeper notched samples. Fig. 6.20 (b) shows a typical example of this type, where the portion of the cross band near the notch can be likened to unresolved wedge and R-hinges and the oblique bands to the secondary plane shear type zones as seen in sharp-notched specimens of Si-Fe, up to a depth of 36%.

Increasing notch depth intensifies the non-uniformity, the effect of which is felt over larger distances. This extends the primary formation and increases the differential between the occurrence of the primary and secondary modes.

(ii) Primary zones.

Local deformation, as in Si-Fe, starts with the formation of both wedges and R-hinges.

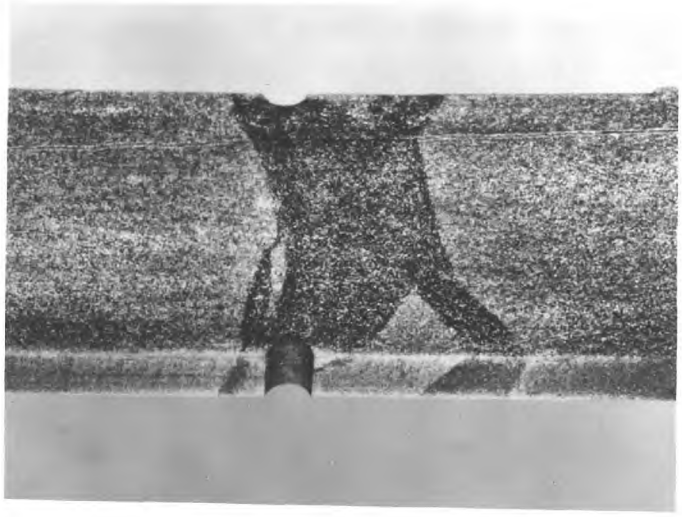

(a) Sample 2S2 x 6
(d = 9%, σ_n/σ_{yd} = 1.1)

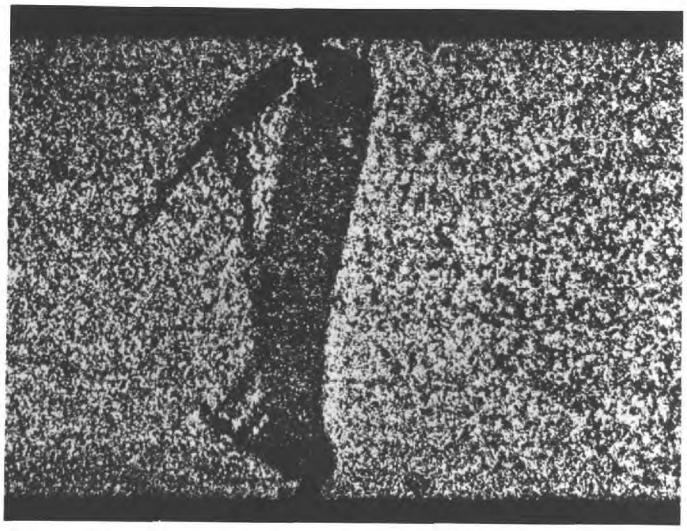

(b) Sample 2"S3 x 10
(d = 9%, σ_n/σ_{yd} = 1.0)

Fig. 6.20. Slip band development at a very shallow, (a) blunt and (b) sharp notch in mild steel.

Figs. (a) and (c), 6.21 - 6.23 illustrate the primary zones in the blunt and sharp notches, respectively. A comparison of the zone shapes shows that R-hinges in the blunt notches are considerably straighter and they develop farther into the specimen along the notch axis.

(iii) Secondary zones.

The general mode of yielding in all but the very shallow notches was by the plane stress (out-of-plane shear) mode - slip traces on the opposite face of specimens show this quite conclusively.

Initiation of general yield by S-hinges was more marked in the shallower and sharper notches. This is because the primary zones are more localized for these notches. Fig. 6.21 (b), (d) shows the general yield mode by the development of an S-hinge from one side of both the blunt and sharp notches.

The sharp notches show the same tendency, although to a lesser extent, up to larger depths (55%) of notch as shown in Fig. 6.22 (d). In blunt-notched specimens, R-hinges develop at positions from which progress in a plane-stress manner is easy; these carry the zone too far into the specimen for S-hinges to occur for depths greater than 36% (Fig. 6.22 (b)).

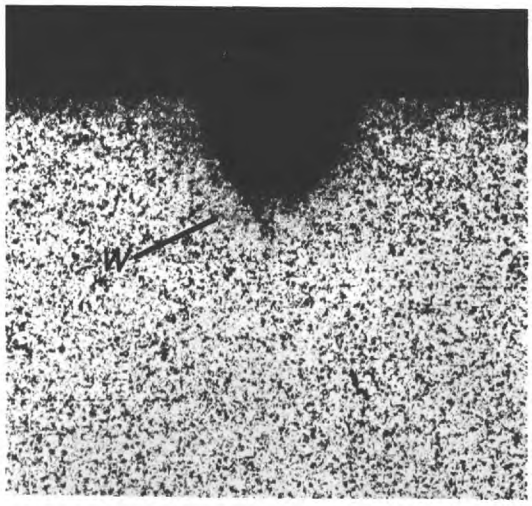

(a) Sample 3S1, x 25
d = 22.5%
σ_n/σ_{yd} = 0.50

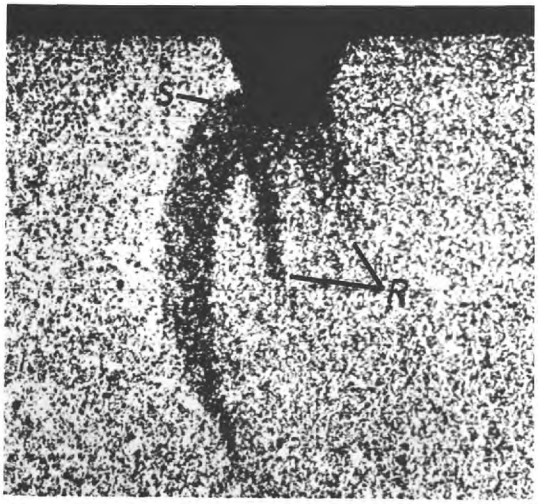

(b) Sample 3S3 x 20
d = 22.5%
σ_n/σ_{yd} = 0.60

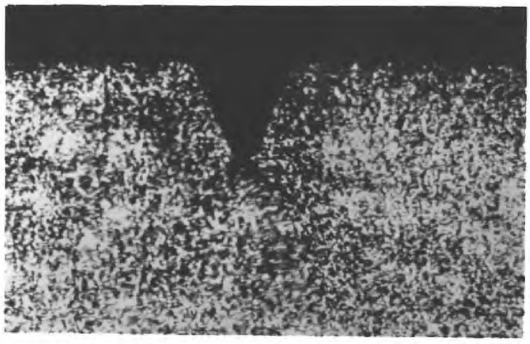

(c) Sample 3"S1 x 20
d = 22.5%
σ_n/σ_{yd} = 0.59

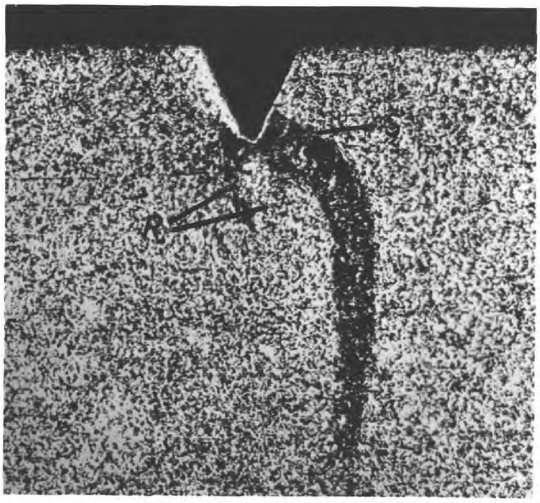

(d) Sample 3"S2 x 20
d = 22.5%
σ_n/σ_{yd} = 0.67

Fig. 6.21. Plastic zone development in shallow-notched samples of mild steel: (a) and (b) blunt notches, (c) and (d) sharp notches.

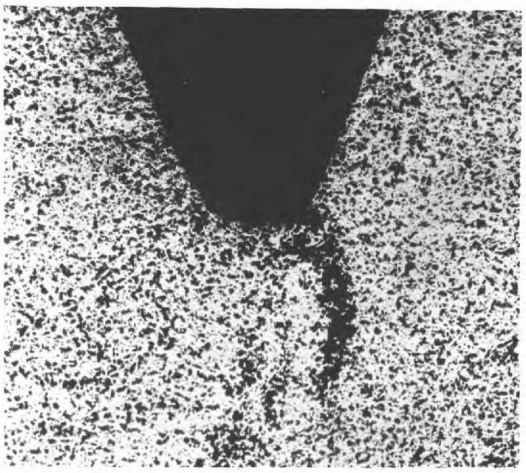

(a) Sample 6S1 x 25
d = 55%
σ_n/σ_{yd} = 0.54

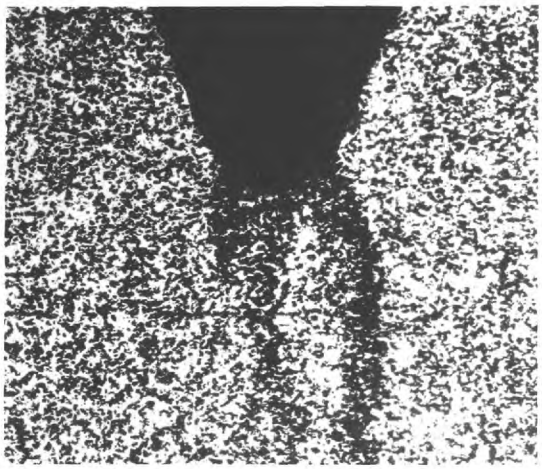

(b) Sample 5S2 x 25
d = 45%
σ_n/σ_{yd} = 0.60

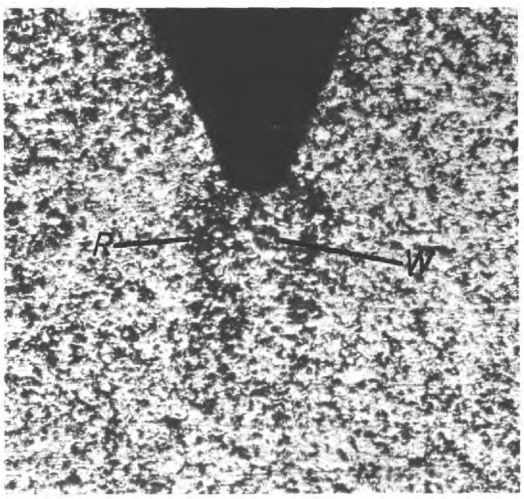

(c) Sample 5'S1 x 40
d = 45%
σ_n/σ_{yd} = 0.60

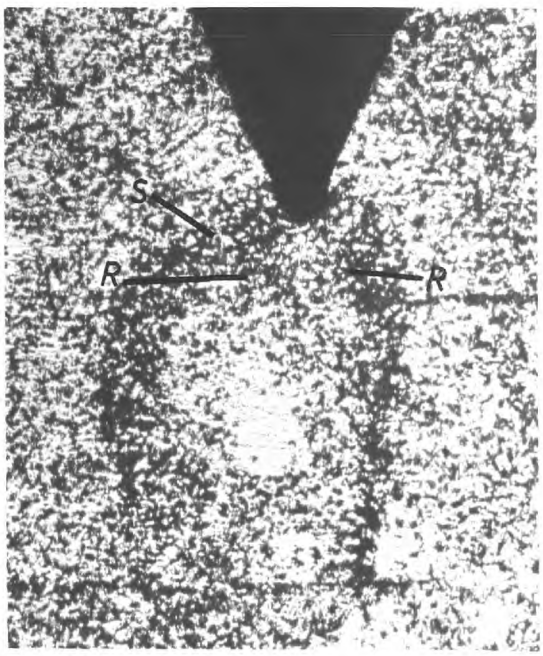

(d) Sample 6"S2 x 40
d = 55%
σ_n/σ_{yd} = 0.67

Fig. 6.22. Plastic zone development in blunt (a and b) and sharp (c and d) notches of intermediate depth in mild steel.

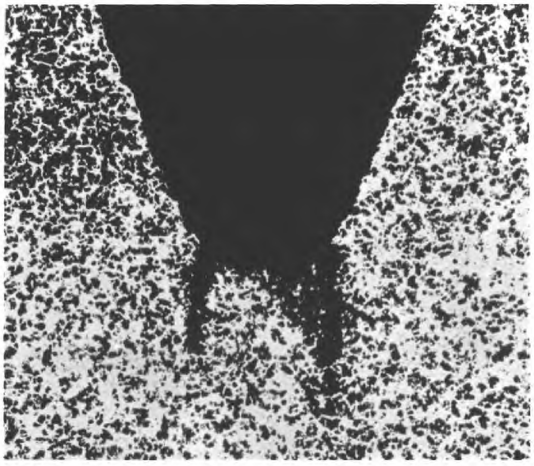

(a) Sample 7S2 x 25
d = 63%
σ_n/σ_{yd} = 0.69

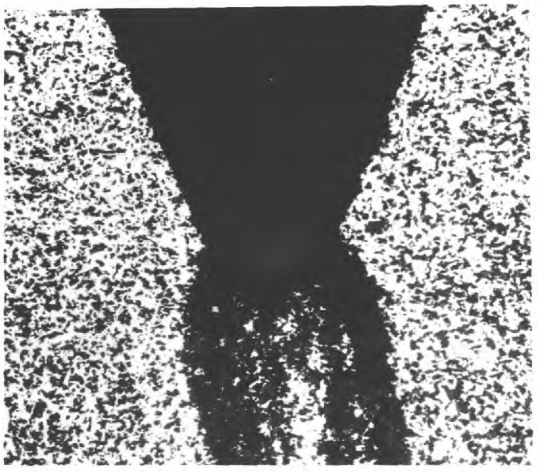

(b) Sample 7S3 x 25
d = 63%
σ_n/σ_{yd} = 0.71

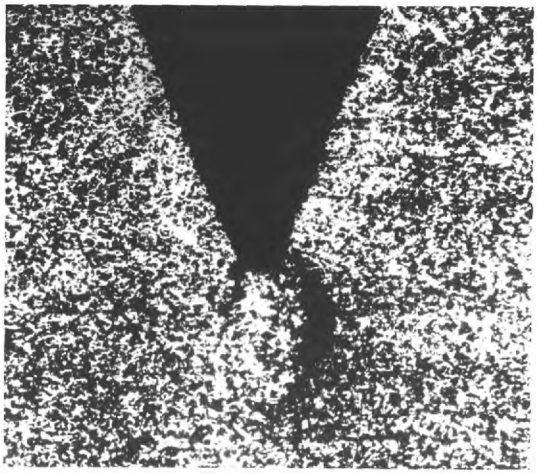

(c) Sample 7'S2 x 25
d = 63%
σ_n/σ_{yd} = 0.67

(d) Sample 8"S3 x 30
d = 73%
σ_n/σ_{yd} = 0.71

Fig. 6.23. Plastic zone development in deep-notched samples of mild steel: (a) and (b) blunt notches, (c) and (d) sharp notches.

This trend is carried into the deep (63% and 73%) notches where the plane stress mode is initiated from hinges, which are too broad to be classified (Fig. 6.23 (b), (d)).

6.3 DISCUSSION OF RESULTS

From a study of slip bands and dislocations etched on the surface of specimens, only the macroscopic shape of the slip surfaces can be determined. The planes on which the dislocations causing slip move cannot be directly understood from this, and it is, therefore, pointless to discuss the crystallographic aspects of slip. Curved slip bands observed in single grains near the notch (Figs. 6.16 (a), 6.17 (a)), however, support the idea of non-crystallographic slip proposed by TAYLOR and ELAM (101) and found by other investigators, e.g., STEIJN and BRICK (102), JAOUL and GONZALEZ (103), SESTAK and LIBOVICKY (104), whereby any arbitrary plane of the slip direction with a maximum resolved shear stress can be a slip plane.

Distinct yield surfaces were observed in steel, but not in silicon iron because slip bands in the latter progress slowly with band fronts blunted by wide spread relaxation in neighbouring grains. The common feature in the two materials was the general similarity of yielding close to the notch in the highly and non-uniformly, stressed region.

Further progress of yield across the width followed different modes. Observations of the rate of zone development with increasing stress seem to suggest that yielding passes from one mode to another. It has been attempted, therefore, to discuss deformation in notched specimens as occurring in two stages:

(i) Primary - the development of a local deformation consisting of a wedge and two thin arcs ("R-hinges").

(ii) Secondary - a general mode of deformation which progresses either by a substantially plane strain (silicon iron) or by a substantially plane stress mode (steel).

The secondary or general mode of deformation was relatively simple and can be understood from the discussion in section 6.1. It is more difficult to visualize a physical mechanism by which the primary yielding takes place, especially in silicon iron where band fronts progress with attending relaxation.

A mechanism of yielding is presented in the following section and the effect of notch depth and profile on yield patterns in Si-Fe is discussed with respect to the mechanism. The effect of notch geometry in steel is discussed in section 6.3.7.

6.3.1 A Mechanism of Deformation.

The effect of the high $(\sigma_x)_{max}$ attained at the root of the notch is to extend the notch, after the manner envisaged by DUGDALE (9) and HAHN (83) in their crack models, through the development of the small wedge WW_1 (Fig. 6.24). Subsequently, due to the action of the transverse tension and the movement of the flank ABRWR'CD to $A_1B_1RWR'C_1D_1$ two plastic arcs extend from R and R' following a roughly circular path RR_1 and $R'R_1'$ with its centre at the tip of the wedge W_1. The extent of the arcs in the x and y direction would then depend on the penetration of the wedge, the magnitude and the position of the σ_y peak under the notch and the geometry of the notch - i.e., the length of the flanks BR and CR', the included angle, α, and the root radius, r. The severe stress state existing at the tip of the wedge (σ_y attains a maximum near about W_1) is relaxed by the formation of these plastic arcs, which in effect break down the constraining influence of the surrounding material. The maximum stress is thus lowered bringing about a halt in the growth of the wedge. If, however, the maximum stress $(\sigma_x)_{max}$, is not lowered sufficiently, the wedge penetrates more deeply into the specimen to W_2 and this again is relaxed by another set of plastic arcs RR_2 and $R'R_2'$ with their pivot now at W_2. This

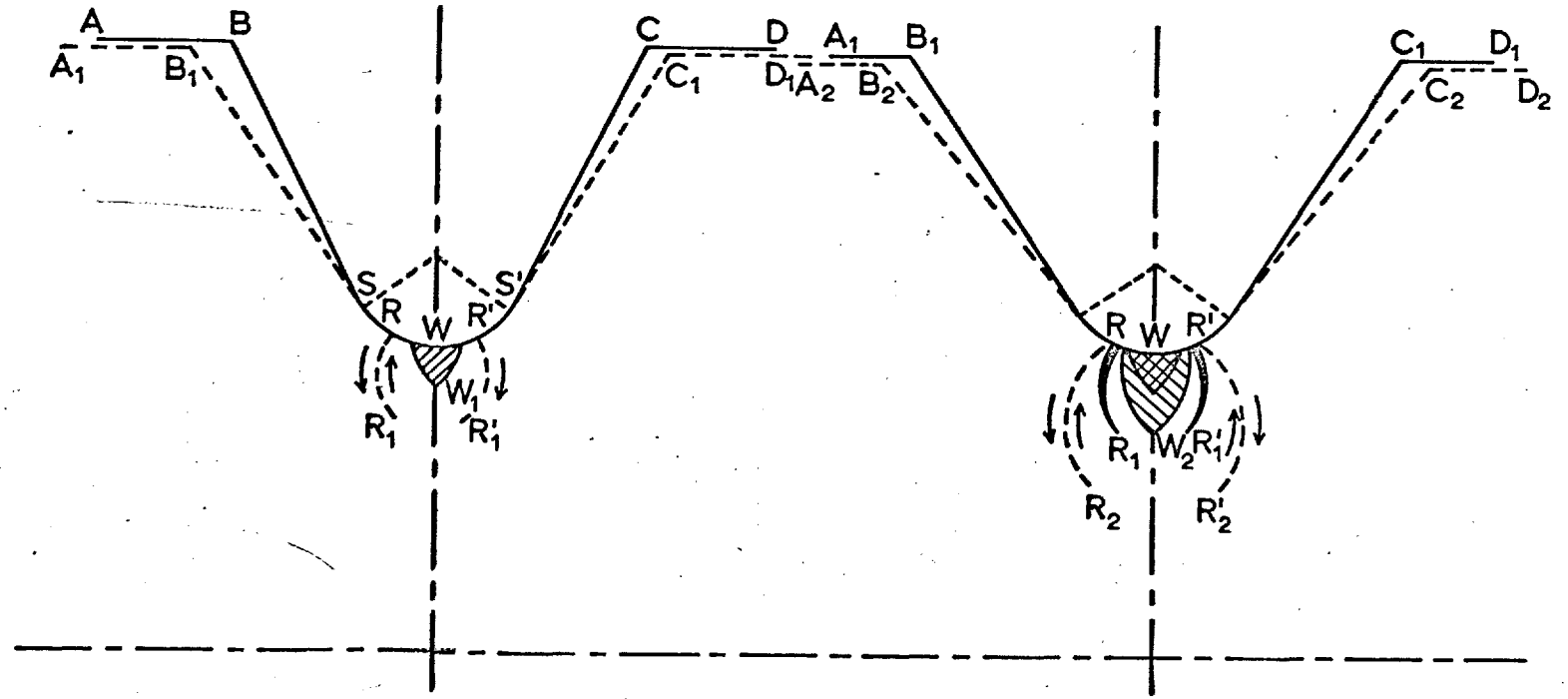

Fig.6.24. A MECHANISM OF YIELDING LOCAL TO A NOTCH.

process has been referred to as the primary mode and this continues with successively deeper penetrations of the wedge accompanied by successively wider R-hinges until the rest of the material between the notches reaches a stress level where a general mode of yielding - i.e. along lines at 45^{o} to the tensile axis - is possible. This is the secondary mode and resultant zones have been referred to by COTTRELL (76) as "accommodation zones" by which the local plastic strain at the root is accommodated.

The R-hinges, while also being accommodation zones, accommodate a hinge-like displacement of the arms of the notch about the root and not a displacement of the notch itself.

6.3.2 Measurement of Plastic Zones

(a) Experimental curves for fine-grained Si-Fe: σ_n/σ_{yd} vs ρ .

The plastic zone development in the transverse direction has been plotted against the nominal stress level in Figs. 6.25, 6.26 and 6.27 for all notch depths and root radii. It becomes quite clear from the slopes of these curves that there are in fact two distinct stages of yield development.

Upto a depth of approximately 36% the transverse stress and the local deformation are both small. This is indicated

Notch Depth %		Blunt (r = 0.015")				Inter. Sharp (r = 0.004")				Sharp (r = 0.0015")			
22.5	σ_n/σ_{yd}	0.4	0.6	0.72	0.78	0.4	0.6	0.7	0.78	0.4	0.55	0.7	0.83
	Pntrn. of Zone, %	0	5	16	96	0	4	9.5	30	2	4	8.6	100
36	σ_n/σ_{yd}	0.4	0.5	-	0.78	0.4	0.5	-	0.85	0.4	0.6	0.7	-
	Pntrn. of Zone, %	1	3	-	100	4.5	5.5	-	97	0.6	2	10.8	-
45	σ_n/σ_{yd}	0.4	0.6	0.8	0.9	0.4	0.6	0.79	0.91	0.4	0.6	0.7	0.95
	Pntrn. of Zone, %	1.5	6	12.5	25	6.5	12.5	20	100	0	8.5	11.7	100
55	σ_n/σ_{yd}	0.4	0.6	0.7	0.85	0.3	0.4	-	0.82	0.4	0.6	0.85	-
	Pntrn. of Zone, %	1.5	8	17.5	79	3	7.5	-	21.5	5	10.5	27.5	-
63	σ_n/σ_{yd}	0.4	0.6	0.7	-	0.3	0.4	0.6	-	0.2	0.4	0.68	--
	Pntrn. of Zone, %	2	27	43.5	-	4	15.4	38	-	5	35	45.5	-
73	σ_n/σ_{yd}	0.4	0.5	-	1.0	0.4	0.6	-	-	0.4	0.5	-	1.1
	Pntrn. of Zone, %	2.5	16	-	100	12.5	30	-	-	5	25	-	45.5

TABLE 6.1. Plastic Zone Penetration with increasing applied stress (3% Si-Fe, fine-grained).

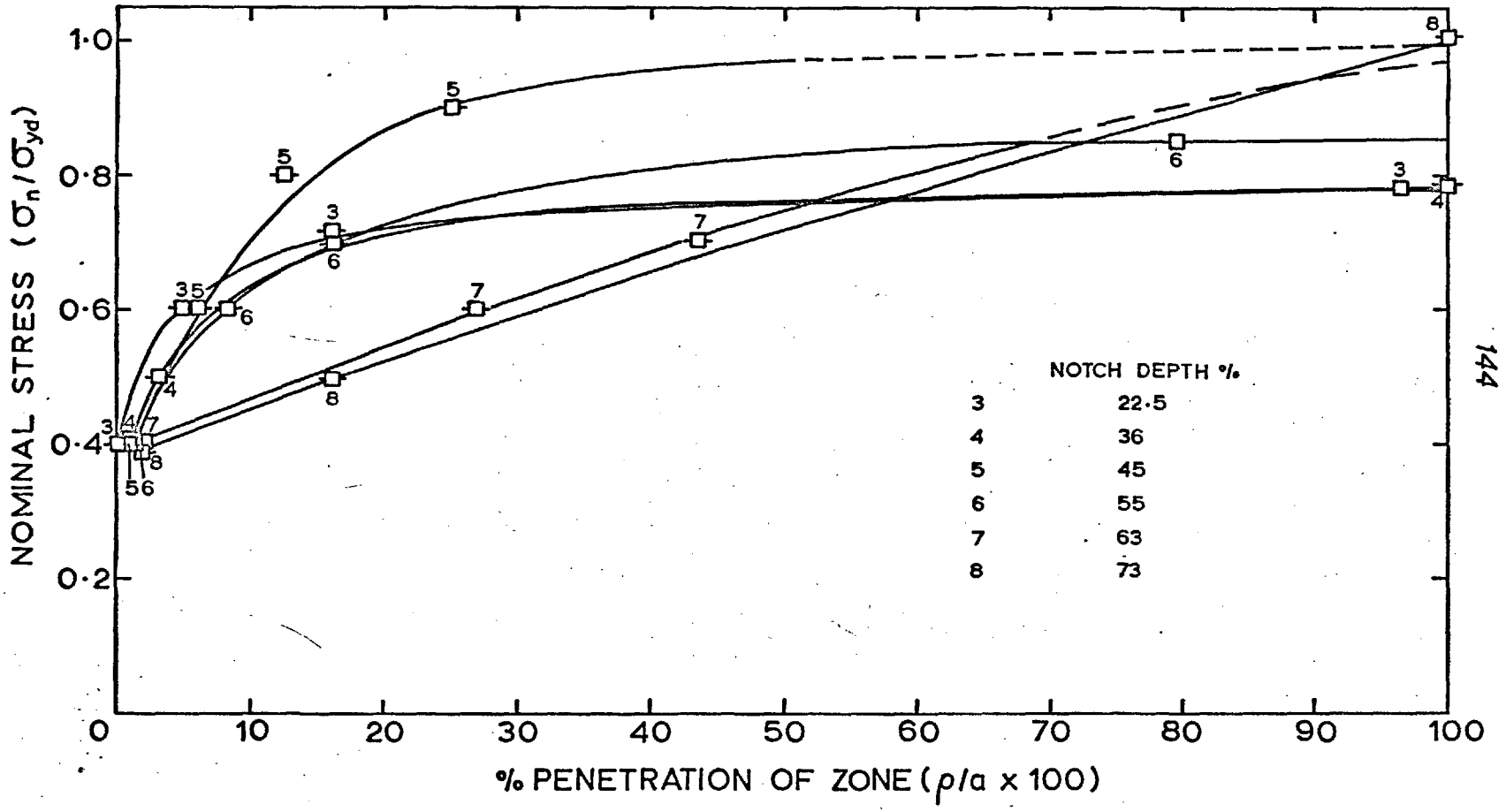

Fig.6.25. THE EFFECT OF NOTCH DEPTH ON PLASTIC ZONE DEVELOPMENT IN SPECIMENS WITH BLUNT NOTCHES (3% Si -Fe, fine grained)

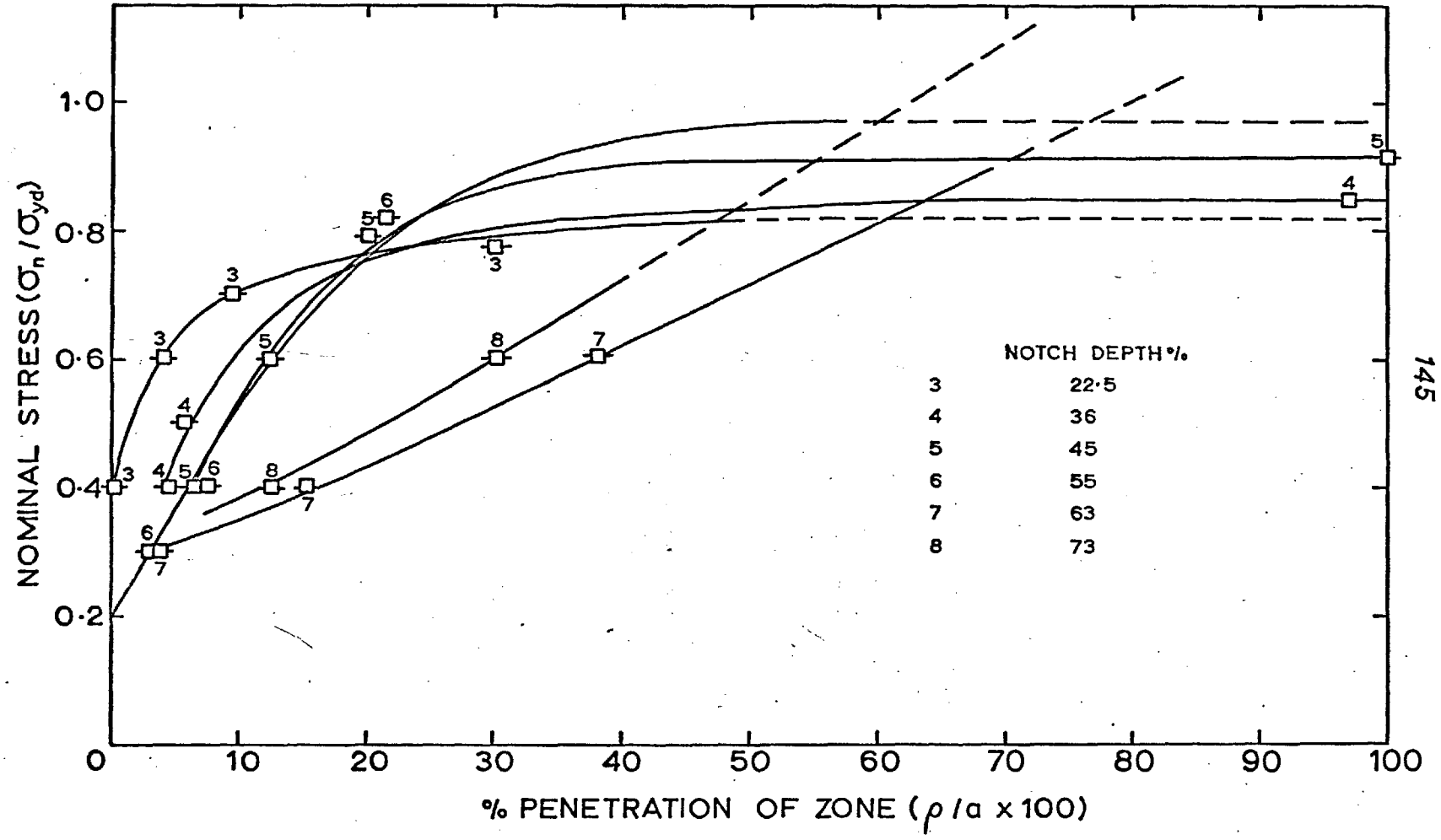

Fig. 6.26. THE EFFECT OF NOTCH DEPTH ON PLASTIC ZONE DEVELOPMENT IN SPECIMENS WITH INTERMEDIATE SHARP NOTCHES (3% Si - Fe, fine grained)

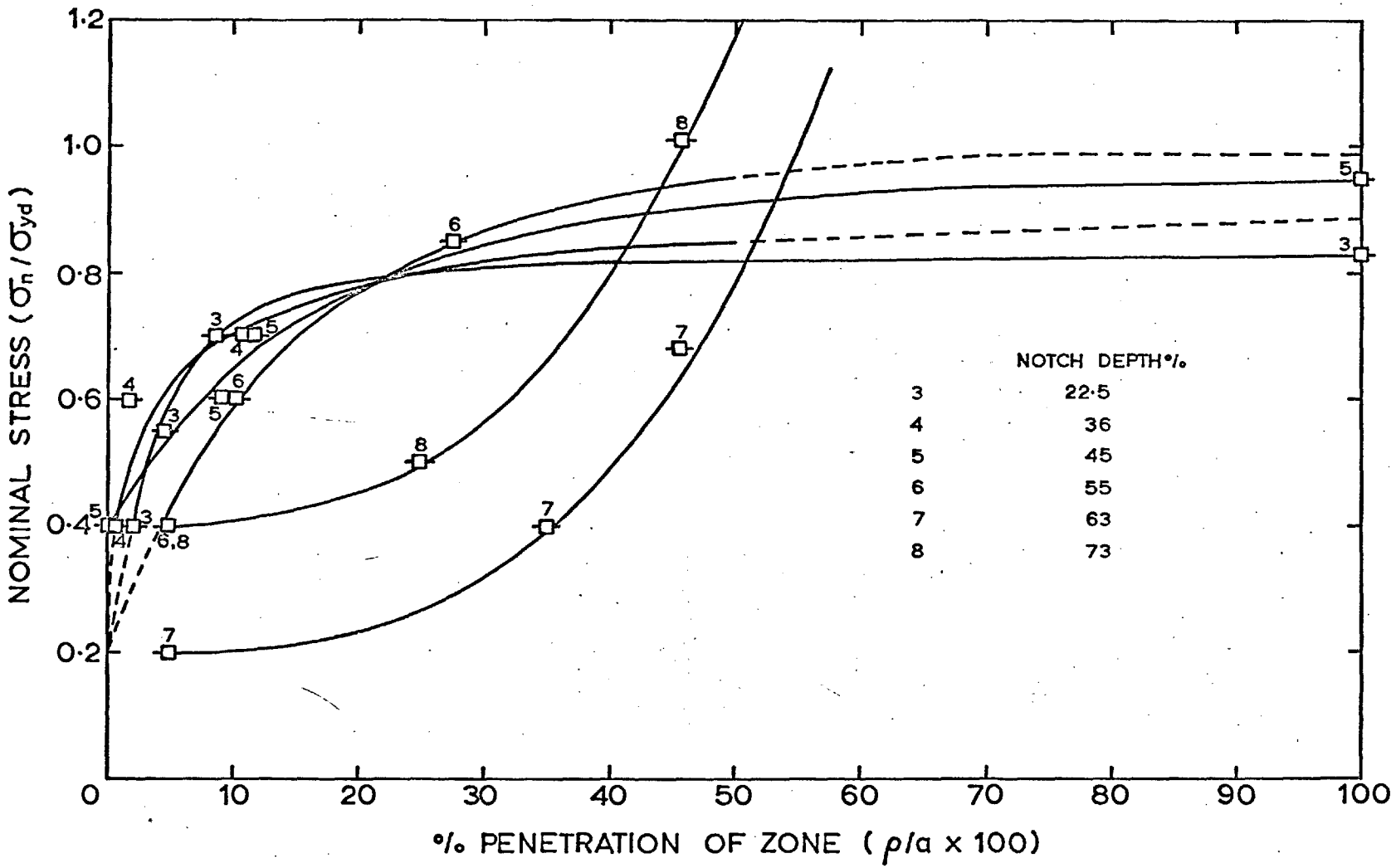

Fig.6.27. THE EFFECT OF NOTCH DEPTH ON PLASTIC ZONE DEVELOPMENT IN SPECIMENS WITH SHARP NOTCHES (Fine-grained 3% Si-Fe)

by the correspondingly small initial steep portions of the curves which bend sharply to show rapid deformation. This corresponds to the development and very fast growth of Lüders bands in unnotched specimens.

The 45% and 55% curves show similar characteristics. The initial steep parts show comparable slopes but these are longer than in shallower notches.

The initially slow rate of growth corresponds to the local deformation by wedge and R-hinges. This local deformation is directly associated with the transverse stress, which by restricting the displacement of the notch while the notch arms are allowed to move freely, causes the formation of the R-hinges (Fig. 6.24). The form and the mode of the R-hinges are also largely determined by the magnitude of σ_y along the y-axis, because high transverse strains are known to bring about out-of-plane (plane stress type) shear by restricting shearing in the plane of the specimen. Increasing σ_y from zero at the notch root should suppress the initially 45^o plane shear-type portion of the R-hinge, until at some distance below the notch where σ_y reaches a peak, the R-hinge changes to a plane stress mode. This corresponds to the outermost (along the x-direction) parts of the arcs, where R-hinges are parallel to the y-axis. The change of mode of the R-hinge is seen very clearly in some of the large grained

specimens having no active dislocation sites near the notch (the presence of dislocation sources in the locally stressed area tends to bring about crystallographic slip) - Fig. 6.35 (b). A reversion to the R-hinge direction would depend largely on whether the transverse stress continues increasing towards the inside of the specimen or having reached a peak, it decreases. It would appear, therefore, that the intercept on the y-axis from the points at which the R-hinges curve inwards, i.e., roughly the tip of the wedge W_1, in Fig. 6.24, is associated with the σ_y peak.

The stress analysis in chapter 7 indicates that the σ_y peaks are higher and they extend farther into the specimen notch depth (Figs. 7.14, 7.15, 7.16) which suggests a possible explanation for the increasing amount of yielding by the primary mode observed for deeper notches.

Curves for the 62% and 73% notches show a completely different tendency. The primary mode is easy, i.e., larger penetrations are possible at comparatively low stresses. The progress of these zones to the central axis, however, is increasingly difficult. The most likely reason for this is that the transverse stress continues to increase with distance towards the longitudinal axis, so that R-hinges are forced to progress by out-of-plane sliding, which is a difficult process in Si-Fe in the range of grain sizes

investigated. In other words, strictly speaking, there is no secondary mode as defined for the other notches.

(b) Theoretical predictions of the extent of zones.

Curves of σ_n/σ_{yd} vs. yield penetration from theoretical formulations of the plastic zone size in equilibrium with the applied stress, are plotted in Fig. 6.28.

Values of the zone size, ρ, for different notch depths were calculated from the DUGDALE formula (equation 6.1), expressed as a percentage of the half-waist and plotted against σ_n/σ_{yd} in Fig. 6.28 (b).

$$\frac{\rho}{d} = \sec\left(\frac{\pi\,\sigma_n}{2\,\sigma_{yd}}\right) - 1 \qquad (6.1)$$

where d is the notch depth, σ_n is the nominal stress and σ_{yd} the field stress in tension.

The curves of σ_n/σ_{yd} vs. zone penetration from the computer analysis (Fig. 7.20) have been reproduced in Fig. 6.28 (a).

The two sets of theoretical curves differ in two obvious respects:

A. The DUGDALE formula yields higher stresses for general yield in the shallower notches than in the deeper notches with the change in slope from initiation of yield to general yield becoming more gradual. The computer analysis, on the other hand, shows almost an opposite behaviour.

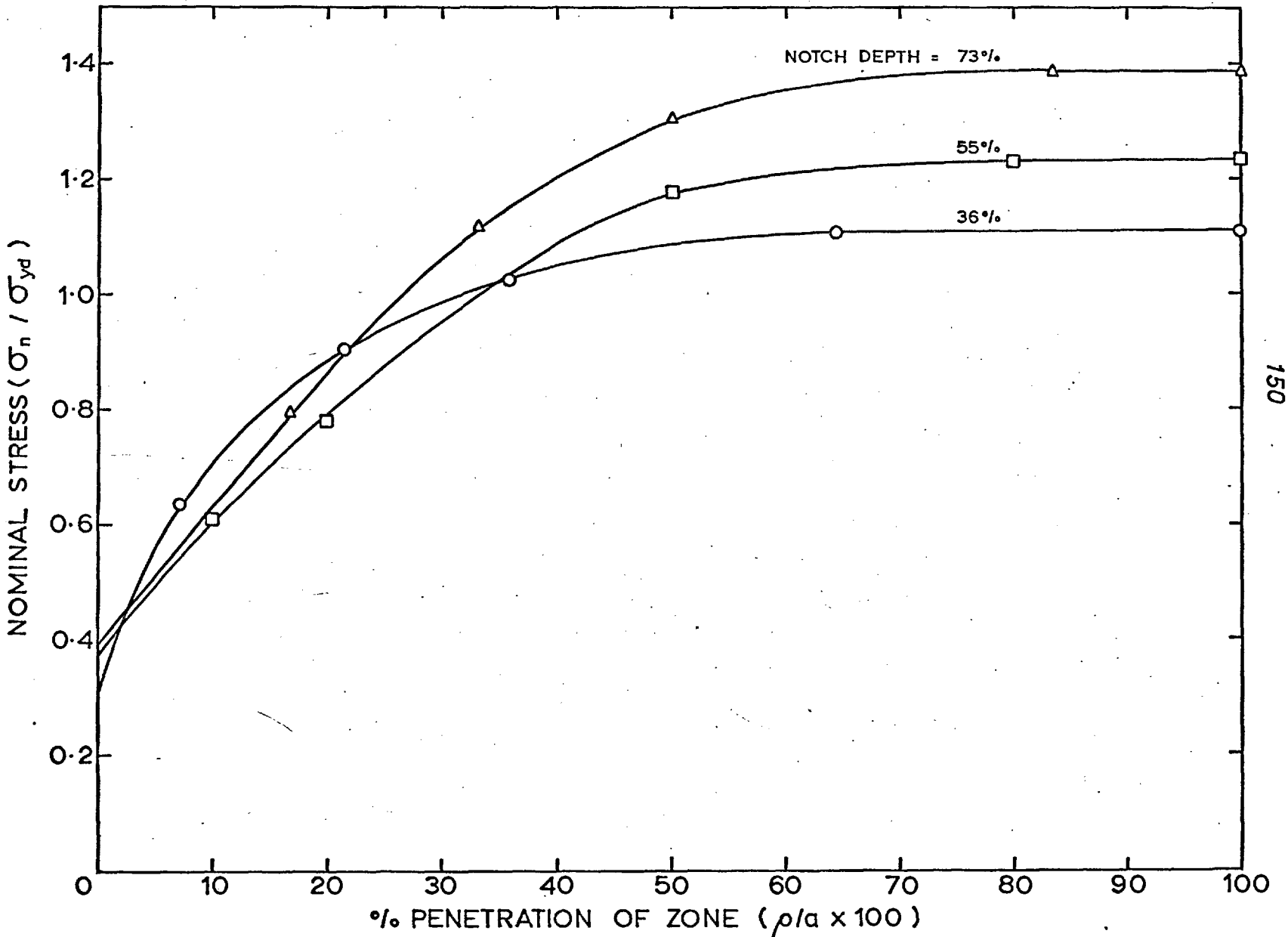

Fig. 6.28.(a). THE EFFECT OF NOTCH DEPTH ON PLASTIC ZONE DEVELOPMENT IN SPECIMENS WITH SHARP NOTCHES (Predicted from Stress Analysis in Ch. 7)

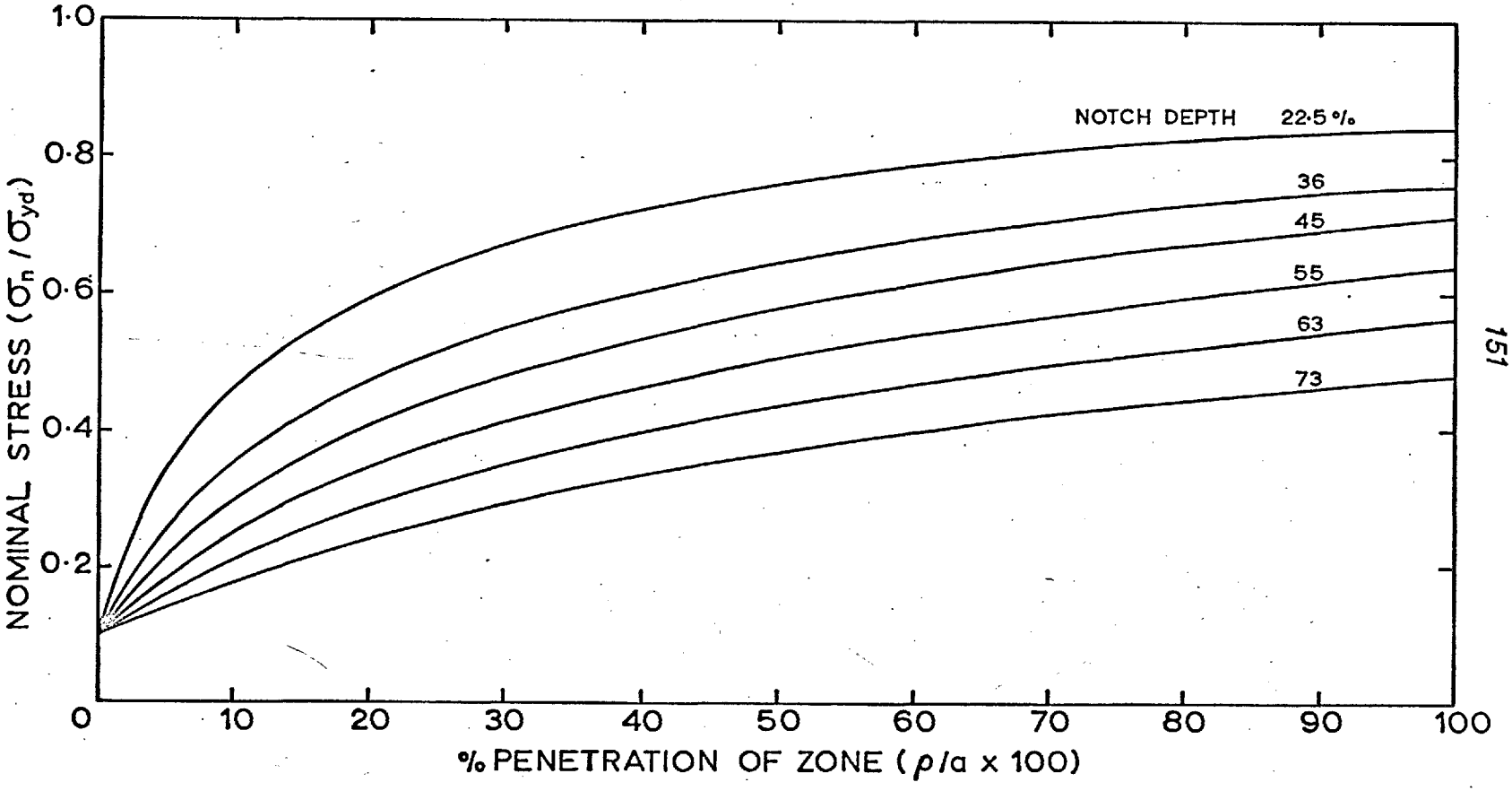

Fig. 6.28. (b). EFFECT OF NOTCH DEPTHS ON PLASTIC ZONE DEVELOPMENT IN SPECIMENS WITH SHARP NOTCHES (predicted from Dugdale's analysis)

B. The range of stresses over which the plastic zones progress from the nctch root to the central axis as predicted by DUGDALE's formula falls between σ_n/σ_{yd} = 0.1 and 0.85, whereas the predicted range from the computer analysis is roughly between σ_n/σ_{yd} = 0.3 and 1.4.

A comparison of the theoretical and experimental curves in Fig. 6.27 shows that on both counts (A) and (B), there is much better agreement of the experimental results with the theoretical predictions in Fig. 6.28 (a). For instance,

(a) All the curves show two distinct stages of yielding by the change in slope - an initial stage of slow growth of primary zones and a rapid secondary zone development stage.

(b) As in the experimental curves the 36% notch shows a small region of primary development followed by a gradual transition to the secondary stage. The 55% notch, on the other hand shows a larger primary yield region and a more sharp transition. Also, whilst yielding in the 55% notch starts at a later stage than in the 36% notch, because of a lower concentration factor, higher stresses are needed for general yielding.

In these respects, disagreement with the curves predicted by DUGDALE's relation is not a real one because the DUGDALE model is based on an infinite sheet in which the effect of the

stresses generated at one notch would not be felt at the other notch. It has been suggested that the model can be assumed to include a finite sheet width, provided the slit did not exceed a depth of 20% (FROST and DUGDALE (105). Since the computer analysis takes the finite geometry of the specimen into account, it should be expected to predict the nature of the curves better.

Stress values for successive stages of zone development for the shallow notched specimens (upto a depth of 36%) are perhaps predicted better by the DUGDALE curves than by the curves from the numerical analysis (Fig. 6.28 (a)). It must, of course, be kept in mind that the zone sizes have been represented by a convenient parameter, i.e., the depth of penetration in the negative y-direction, which does not take account of the actual zone shape. The thin plane-stress type zones described by DUGDALE were found to occur in steel (DUGDALE (9) and in this investigation - Figs. 6.21, 6.22, 6.23) and their progress along the slit axis is much more rapid even at comparatively low stresses. The zone shapes found to occur in Si-Fe, on the other hand, have much more lateral spread and their degree of correspondence with those computed by the finite-difference method is very good. Penetration of these zones along the notch axis requires a much larger area of slip and this should involve larger

stresses. The agreement in the range of stresses to bring about a zone spread from zero to 100% for some of the notches (22.5% and 36%) between the experimental curves (Fig. 6.27) and the DUGDALE predictions might well be fortuitous.

A feature which stands out in the experimental curves cannot be understood by either set of theoretical curves. This is that with increasing notch depth the primary mode of deformation is easier. In the experimental curves this is shown by an increased length and a reduced slope of the initial, primary region of the curves. This trend should make possible a notch depth where there is almost a linear relationship between the nominal stress and the zone size (73% notch in Fig. 6.25). The deep sharp notches, in fact, show a reversed slope in the primary region (Figs. 6.26,6.27). Although the theoretical curve for the 73% notch (Fig. 6.28 (a)) does show an extended primary region which is almost linear, it does not show a reduced slope or the reversed slope in Fig. 6.27. The reason for this is simply that the possibility of different modes of yielding, or of strain hardening due to the development of wide band fronts, is not envisaged by either of the models.

6.3.3 The Effect of Notch Depth.

The effect of increasing depth of notch is, basically, to permit deeper penetrations of the wedge into the material. This has been illustrated in section 6.2.2 and is borne out by the curves presented in the previous section; it is presumably a direct result of the stress concentration at the root of the notch, and the distances at which the effect of the $(\sigma_x)_{max}$ is felt. The reason for this is obscure and perhaps lies in the more fundamental properties discussed later in this section. At present, it seems to be a good starting point to attempt an explanation of the observed effects from the observation that wedge penetration is deeper for deeper notches. A diagrammatic representation of the effect of notching on the yield mode is presented in Fig. 6.29. It illustrates through the use of the deformation mechanism envisaged, how the deformation patterns are influenced by increasing depths of notching.

The yielding shown in Fig. 6.29 (a) is typical of the shallow notches. It is found at notch depths of up to 22% (Fig. 6.11 (a), (b)) in blunt or intermediate sharp notches and even up to 36% in the sharp notch (Fig. 6.15). The wedge zone is confined to a very short distance below the notch and the R-hinges associated with it are very small.

When a stress state is attained which is conducive to general yield it occurs through the medium of S-hinges. The σ_y was small with its peak at a very short distance below the notch.

Fig. 6.29 (b) shows how the marked difference in yielding observed in the 45% and 55% notches is possible. Larger wedges with accompanying relaxation by R-hinges makes the local deformation spread like a ripple from the notch root before the general mode of yielding starts with a consequent reduction of the large, mostly elastic core seen in the shallower notches. This should indicate that deformation below the notch becomes much easier for these notches. Curves of notch depth vs R.A. (Figs. 5.1-5.3) after failure support this observation. The S-hinges and R-hinges are less easily distinguishable in this geometry because the R-hinges attending the deep wedge open out considerably and secondary shear lines fork out from these (Figs. 6.13 (b), (c), 6.16, 6.17).

Fig. 6.29 (c) shows a complete absence of the secondary shear zones (Figs. 6.10, 6.18). The wedge development is rapid as shown by the graphs (Figs. 6.25-6.27) in section 6.3.2. Deformation is contained in the notched area and takes place entirely by the primary mode.

The wedge development

The wedge seems to be the result of a tearing effect due to the high σ_x developed under the root of a notch. Easier wedge growth with deeper notching is difficult to understand. From NEUBER's (1) elastic solutions, one would expect that stress concentrations reach a maximum for depths of 22% and 36% (Fig. 5.7). By the law of stress gradients (NEUBER), then, the longitudinal stress must decrease from its peak value very rapidly for the 22% and 36% notches and consequently the strain is very localized. But for successively deeper notches, because their σ_x peaks would be lower and the diminution is less rapid, the distribution would be such as to have higher stresses at the central axis.

The theoretical analysis using the von Mises criterion does, in fact, predict deeper penetration of the wedge for deeper notches (Figs. 7.8, 7.9, 7.10).

6.3.4 The Effect of Root Radius.

Increasing the root radius means that the stress concentration is lower and the effect of the maximum stress is distributed over a larger root surface. Consequently the wedge is much wider with less penetration than the sharp notches for comparable applied stress levels. As a result

of this and the longer root surface R-hinges are wide, have a lower curvature and appear to grow into the specimen, mainly in the notch direction rather than spreading outwards.

The patterns for larger root radii, therefore, resemble the zones seen by HAHN and ROSENFIELD (83) (compare Figs. 6.8 (b) and 6.12 (b) and 6.15). This is purely a geometrical effect and coincident patterns can in fact be obtained simply by superimposing the pattern of a deeper blunt notch on that of a shallower and sharper notch as illustrated in Fig. 6.30 (a), (b). This, of course, can only be done when the notches are deep enough for the local mode of deformation to take effect. For very shallow notches this does not arise, because yield is by the secondary mode with very little local deformation.

Thickness of specimen

The importance of the thickness of the specimen might be stressed at this point with respect to the local hinges. If the root radius (which is roughly equal to RR', Fig. 6.30 (c)) were of the order of the thickness 't' or larger, then conditions would be ideal for the local accommodation zones to develop by out-of-plane (plane stress-type) sliding with resultant slip traces almost perpendicular to the tensile axis. As the r/t ratio gets smaller, the out-of-plane sliding becomes more difficult at R and R' so that

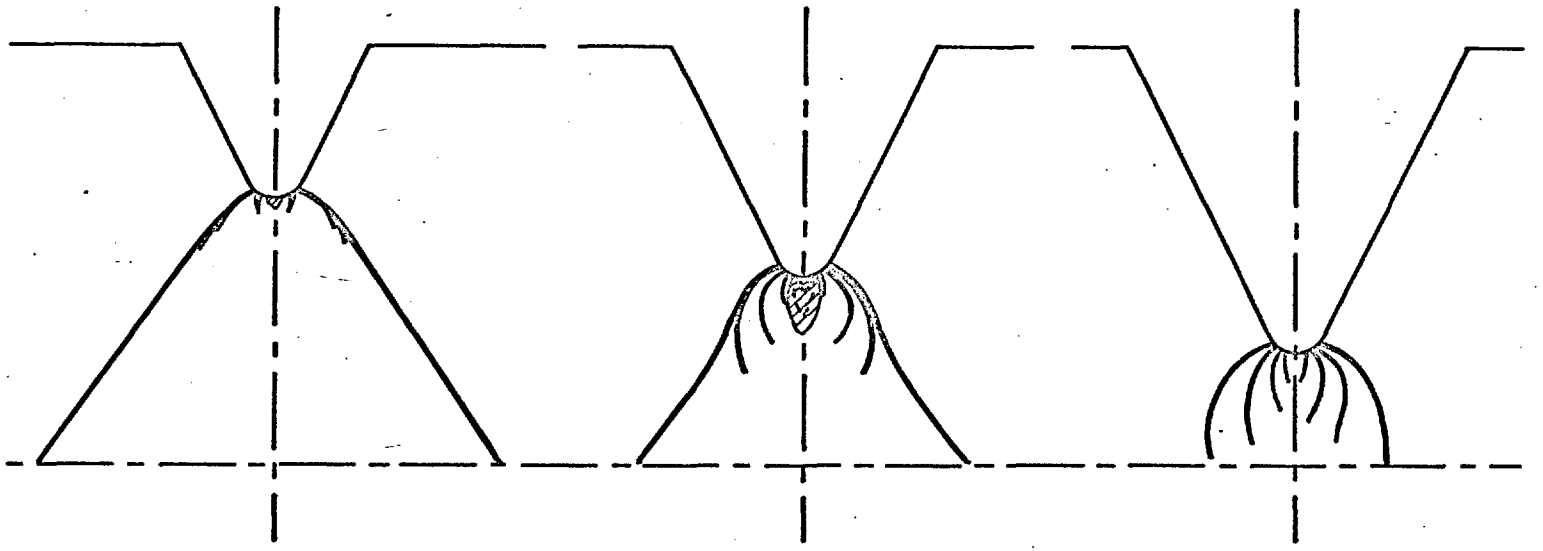

Fig.6.29. THE EFFECT OF NOTCH DEPTH ON DEFORMATION MODES.

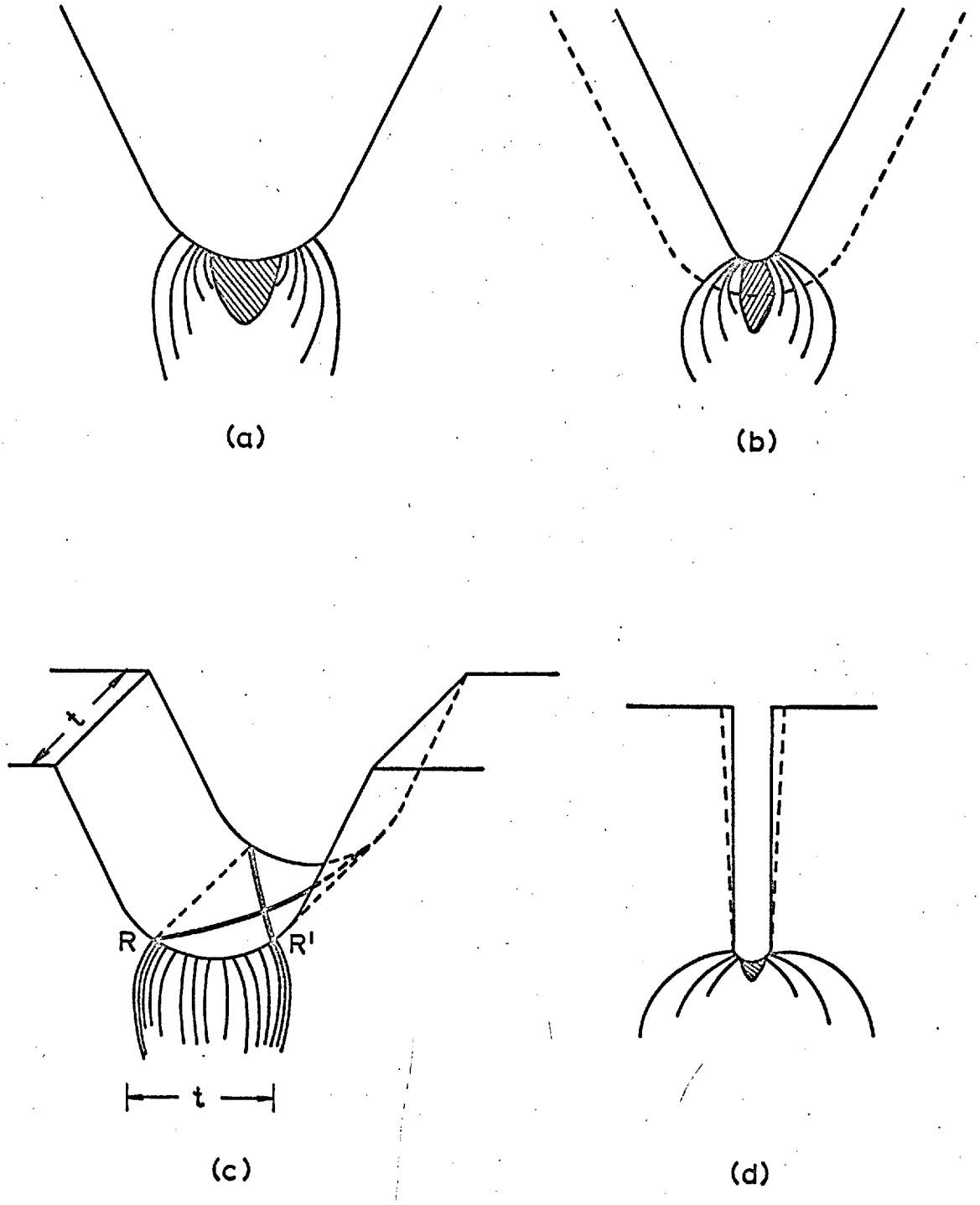

Fig 6.30. THE EFFECT OF (a) and (b) ROOT RADIUS, (c) THICKNESS AND (d) FLANK ANGLE ON THE LOCAL YIELD MODE.

the accommodation zones travel along the R-hinges (plane strain-type) until the arcs have spread to a distance roughly t apart. They can then spread in a plane stress manner provided that (a) the local strain (wedge) warrants further relaxation, (b) the flank angle is not too large, and (c) the notch is not too deep for 45° plane shear to start by forking out from the R-hinge. Specimen 4M3 (Fig. 6.8 (b)) shows the development of the zone expected for a notch with a fairly large radius ($r/t = 0.3$) and specimen 4M4 (Fig. 6.8 (c)) shows a later stage where 45° plane shear is starting to fork out on the left.

Specimen 4'M3 (Fig. 6.12 (b)) shows R-hinges developing into a plane stress mode (very much like the patterns observed by HAHN (83)) but later being overtaken by a general yield mode (Fig. 6.12 (c)).

6.3.5 The Effect of Flank Angle.

A specimen with edge slits was strained to see if deformation would occur through the expected mode. A sufficient notch depth (55%) was used to obviate secondary 45° plane shear and a large enough root radius ($r/t = 0.3$) to check whether R-hinges would directly develop into, and progress by, a plane stress mode.

Fig. 6.31 shows the pattern developed under this particular geometry. The deformation zone is confined to the axis of the slit, as expected, because

(i) the large r/t ratio prevents the development of the arcs of the R-hinge (6.3.4, Fig. 6.30 (c)) and,

(ii) the perpendicular arms of the slit restrict any R-hinge present from continuing a circular path below the tip of the wedge.

By reducing the root radius of the edge slit, it should be possible to bring about deformation by R-hinges, while still maintaining an overall plane stress mode locally. It is easy to visualize that the effect of a displacement of the flanks of the slit in the tension direction would not be felt at any appreciable distance below the notch (Fig. 6.30 (d)). The primary deformation thus takes place by R-hinges which follow a wider path with less tendency for them to curl inward as seen with V-notches of comparable depth and root radius. It is very likely that this then progresses in a plane stress manner - until a general yield mode can take over (as in 4'M4, Fig. 6.12), and unless a very deep notch is used whereby the general yield is excluded.

It should be stressed at this stage that the deformation mode is directly determined by the geometry of the notch and the specimen thickness, and only indirectly by the yield

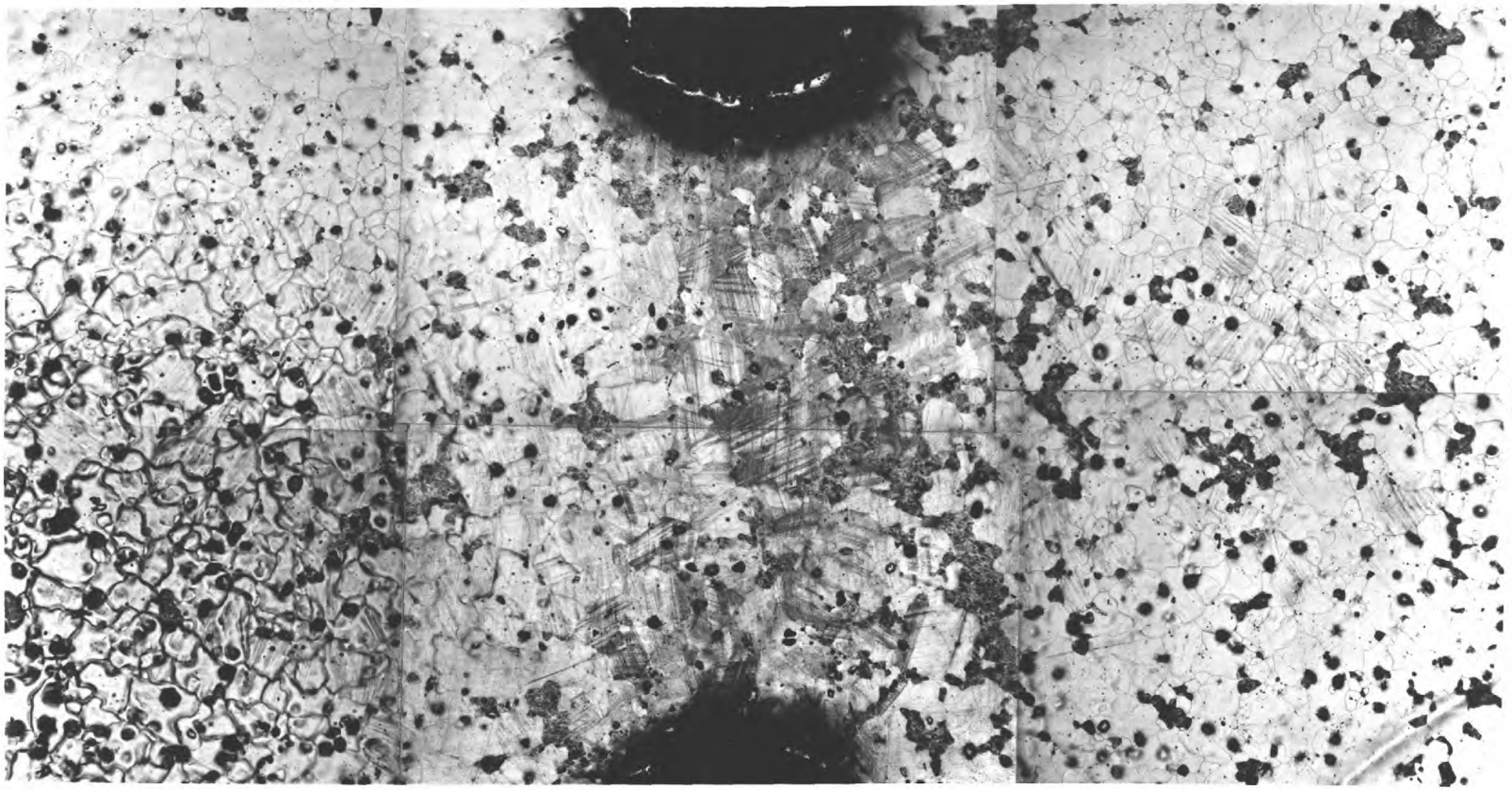

Sample M6 (d = 55%, r/t = 0.3, σ_n/σ_{yd} = 1.06). x 35

Fig. 6.31. Deformation pattern in an edge-slitted specimen of 3% Si-Fe (r = 0.015").

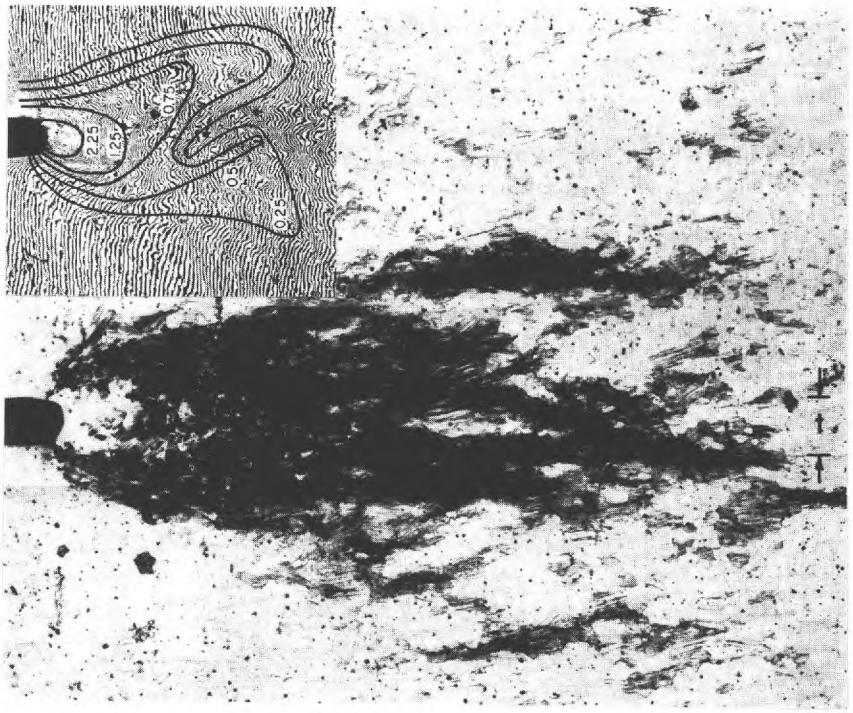

(a) d = 20%, r/t = 0.2, σ_n/σ_{yd} = 0.81. x 17.5

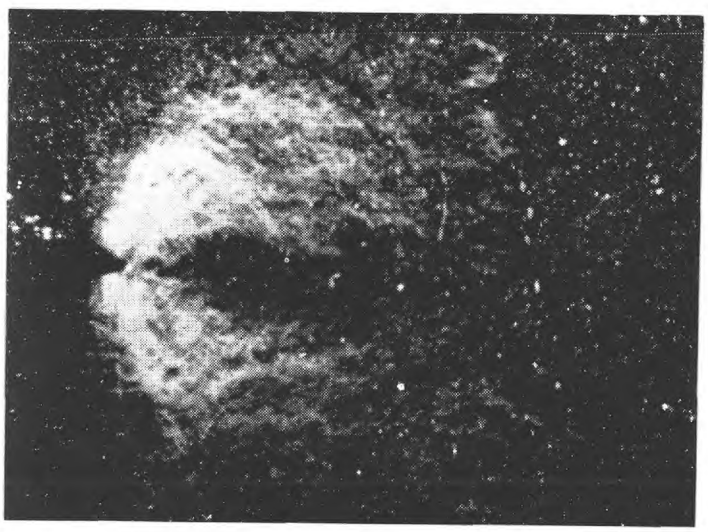

(b) d = 20%, r/t = 0.015, σ_n/σ_{yd} = 0.81. x 6

Fig. 6.32. The effect of varying the root radius/thickness ratio on deformation patterns in Si-Fe specimens with edge-slits. (HAHN and ROSENFIELD (83)).

characteristics of the material (6.3.7). The plane stress type patterns reported by HAHN are a direct result of the particular geometry of his specimens. One of his samples with a comparable r/t ratio ($\simeq$0.2) showed a pattern (Fig. 6.32 (a)) very similar to that of specimen M3 (Fig. 6.31). With decreasing r/t a wider spread of the zone is expected and was observed by HAHN (Fig. 6.32 (b)). The persistence of the plane stress mode observed in Fig. 6.32 (b) is probably coincidental - due to a particular combination of root radius, thickness and flank angle - as was found in specimen 4'M3 (Fig. 6.12 (b)). A sharper root radius would probably have brought about general yielding in a substantially plane strain mode as in 4"M4 (Fig. 6.15), and in fact closer to the far-reaching zone shapes predicted by STIMPSON and EATON (106) (whose relaxation calculations are based on a slit with zero root radius) rather than the zones confined to the slit axis, predicted by the DUGDALE-MUSKHELISHVILI (9) model.

6.3.6 The Effect of Grain Size.

The coarse-grained material had a lower dislocation density because of the higher annealing temperatures used. Consequently grain boundaries were found to play an important part as active sources of dislocation.

Owing to the large grain size, slip over large distances was affected by the orientation of grains, but at low stresses the zone shapes and the mode of deformation were consistent with the ideas developed for the fine-grained material (Fig. 6.33) However, even in some of the lightly stressed specimens, the local deformation zones, although basically having the same slip directions, appear different. This may happen where one of the grains, having a favourable orientation, shows crystallographic slip (Fig. 6.34 (a)), whereas in another case the grain orientation is such that only non-crystallographic slip is possible (Fig. 6.34 (b)).

Plastic deformation near the tip of a crack or notch can occur by the motion of dislocations either nucleated at the crack tip (GILMAN (107) in LiF) or emitted from sources near the crack tip and by the tip itself (TETELMAN and ROBERTSON (108) in Si-Fe).

From theoretical considerations, FRIEDEL (109) has concluded that nucleation of deformation actually at a crack tip is a difficult process. This should suggest that active sources fairly near the tip of a notch (where stresses may exist that are sufficient to operate the sources there), would initiate slip before this can occur actually at the root of the notch itself. In this respect, favourably oriented grain boundaries along the path of the R-hinges

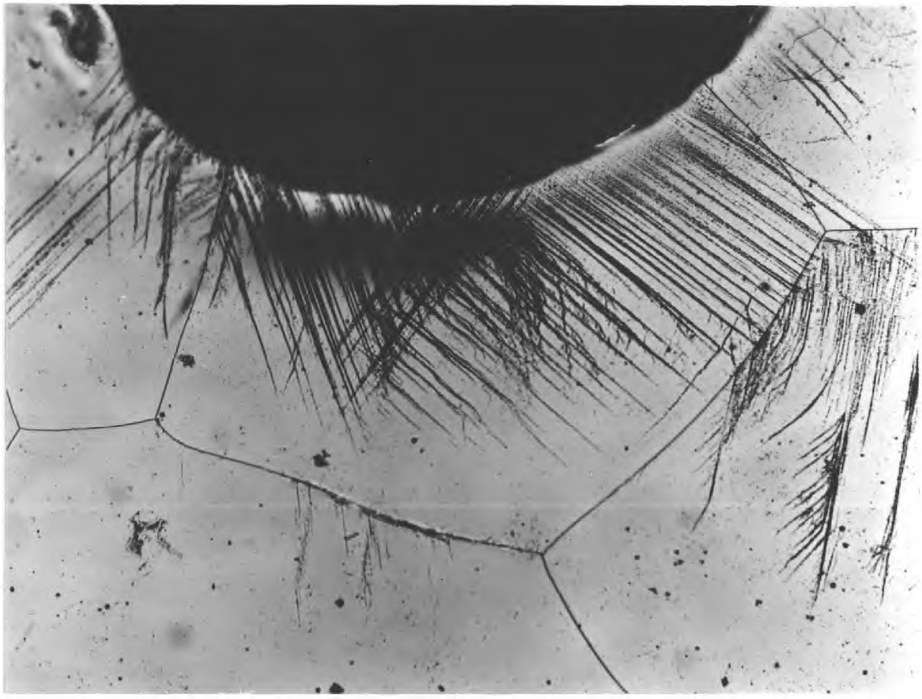

(a) Sample 4F3 (d = 36%, σ_n/σ_{yd} = 0.50). x 125

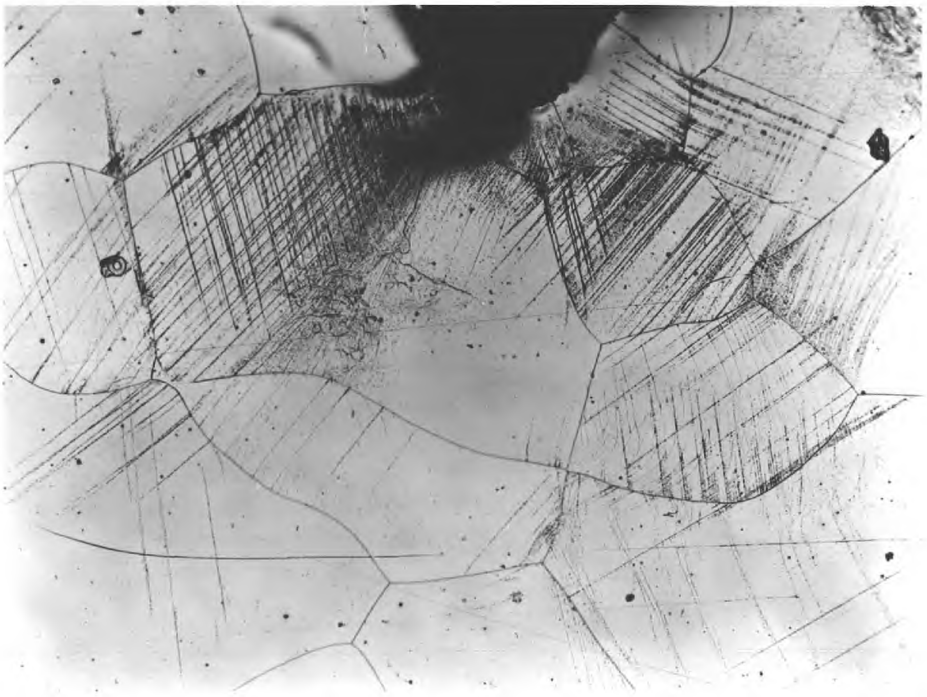

(b) Sample 2"C2 (d = 22.5%, σ_n/σ_{yd} = 0.59). x 120

Fig. 6.33. Local yield zones in coarse grained Si-Fe showing formation of wedge and R-hinge type zones under (a) a blunt notch and (b) a sharp notch.

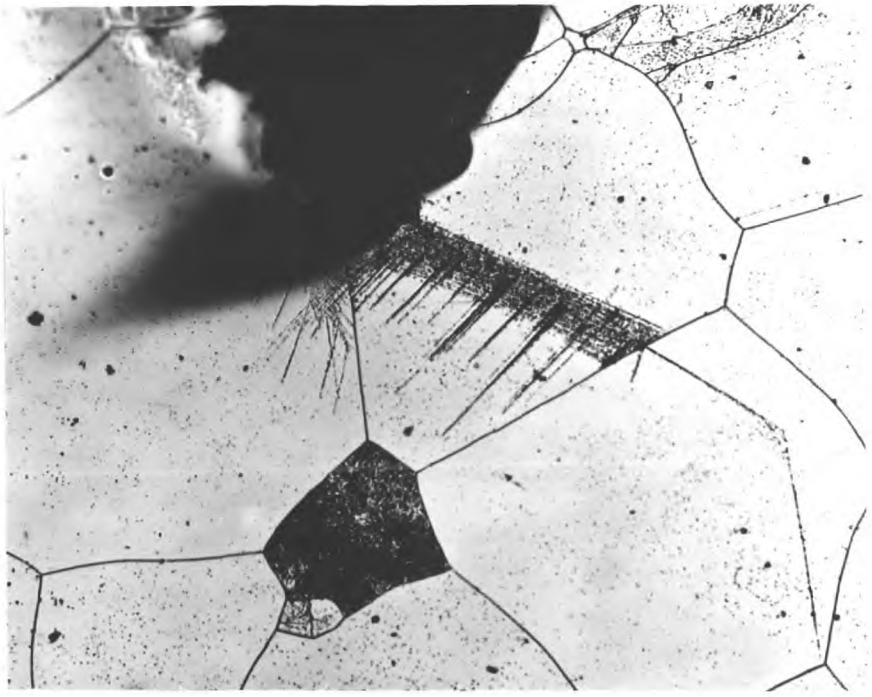

(a)

Sample 3"C2 (d = 22.5%, σ_n/σ_{yd} = 0.60). x 125

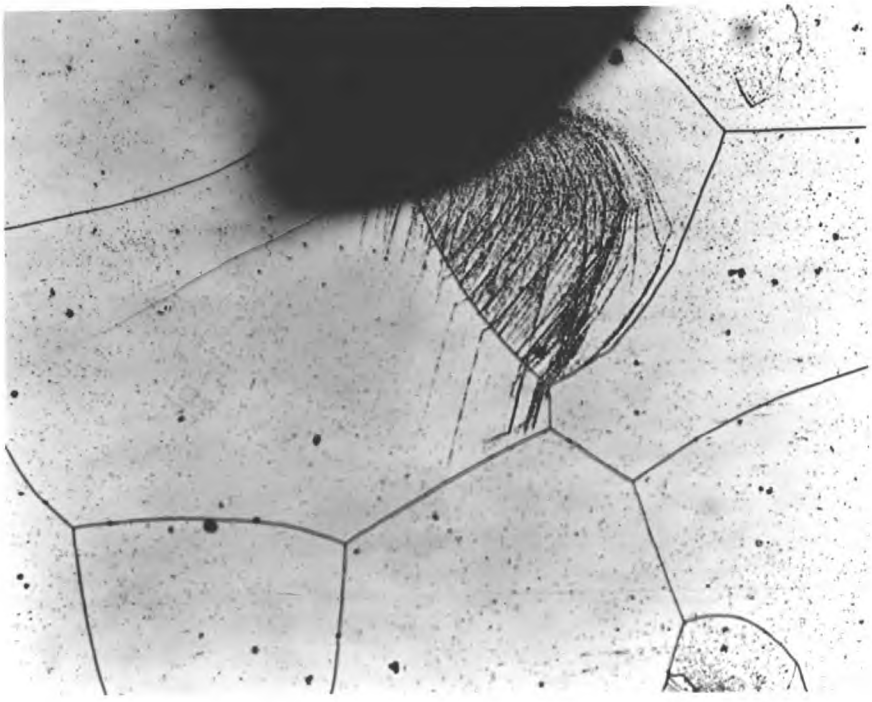

(b)

Fig. 6.34. Local yielding at opposite notches in a coarse grained Si-Fe sample. (a) and (b) show slip band formation in two grains of different orientation.

envisaged proved to be excellent sources of dislocations. Grain boundaries "A" and "B" in Fig. 6.35 (a) would emit dislocations which would be attracted to the central plane of the notch. A grain boundary very close to the notch, "C" (Fig. 6.35 (a2)) on the other hand, would emit dislocations away from the notch in the direction of the R-hinge.

If there are no favourably oriented grain boundaries within the range of the R-hinges, then slip is nucleated at the root of the notch and progresses in a non-crystallographic manner giving rise to R-hinge-type zones (Fig. 6.35 (b)).

6.3.7 The Effect of Material (Steel) on Zones.

The way in which the behaviour of the yield zones is affected by the nature of the material in notched specimens is discussed on the basis of observed patterns in high-nitrogen steel (6.2.3)

The Fry's etchant used does not reveal individual pits or delineate slip bands sufficiently clearly to warrant any detailed discussion on the nature and development of the bands. Broadly, the primary or local mode of yielding was very similar to that found in silicon iron (i.e., by wedge and R-hinges), whilst the secondary or general yield followed a plane stress mode.

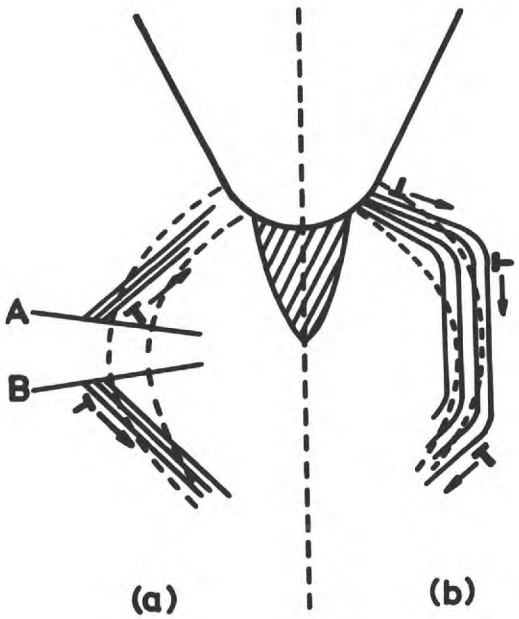

Hypothetical R-hinges (dashed) and wedge (shaded) superimposed on observed slip traces

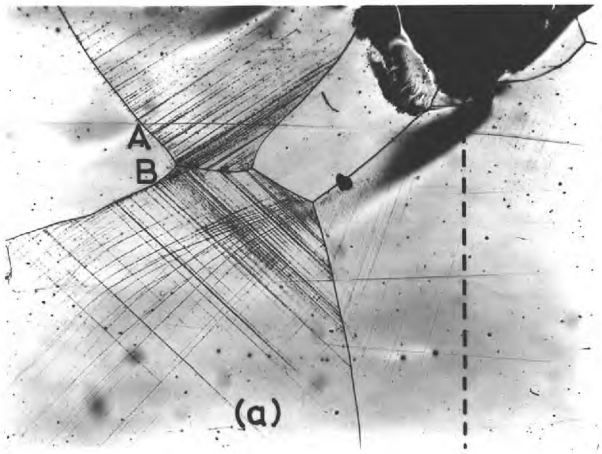

Sample 2"C2 (d = 9.0%, σ_n/σ_{yd} = 0.45). x 140

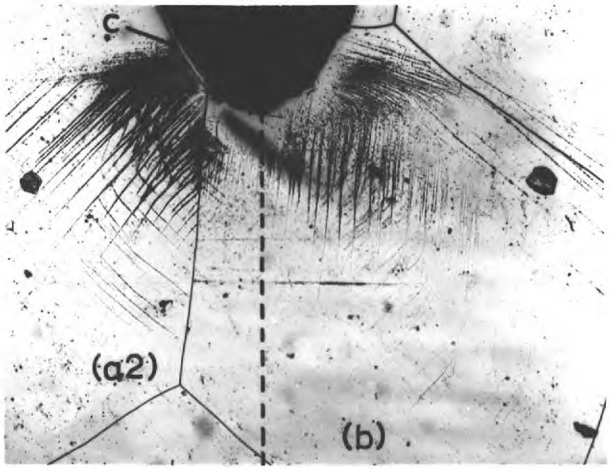

Sample 4'F2 (d = 36%, σ_n/σ_{yd} = 0.40). x 140

Fig. 6.35. Possible modes of slip band formation, (a) from grain boundary dislocation sources A, B, C, and (b) from notch.

The effect of the material on notch-yielding can be brought out by considering the way in which the behaviour of mild steel differs from that of Si-Fe under three headings.

(i) Initiation: In all notches of comparable depth and radius, higher values of σ_n/σ_{yd} were needed to start yield in steel.

(ii) Propagation: The zones propagate to the central longitudinal axis at lower σ_n/σ_{yd} ratios and much more rapidly than in Si-Fe.

(iii) Yield Mode: Although the local yield mode was similar in the two materials, the R-hinges in steel show a much smaller tendency to curve in towards the notch axis. The secondary mode starts earlier in steel and is distinctly plane-stress in type.

From a consideration of the yield characteristics in unnotched specimens, differences in yield modes due to notching in the two materials were expected and have briefly been mentioned in section 6.1.3. The observed differences mentioned above are, however, discussed here in greater detail and it is intended to show that they can be attributed to the basic differences in the two materials. These are:

(a) In steel, there is strong pinning, while in Si-Fe pinning is weak because of a higher density of active dislocation sources.

(b) There are more available slip planes in mild steel than in Si-Fe.

(c) Higher dislocation velocities are attained in steel than in Si-Fe.

The several aspects of yield behaviour can now be discussed in terms of these three material characteristics.

(i) Initiation of Yield

Ideally, slip should be nucleated at the root of the notch, when the $(\sigma_x)_{max}$ reaches a critical value (usually the macroscopic yield stress) required to unpin dislocations or to allow them to attain a critical velocity (10^{-3} cm/sec).

One would expect then, that in specimens having the same notch geometry (and therefore the same stress concentration factor), the first sign of slip would occur at identical values of σ_n/σ_{yd}. The fact that this was not found to be so, nust stem from reason (a) - i.e., dislocation pinning in relatively unimportant in silicon iron. A high density of active sources (weakly pinned dislocations) allows the process of "bowing-out" of dislocations before a critical value of $(\sigma_x)_{max}$ can be reached under the notch.

Strong pinning in steel keeps dislocations locked in place until the $(\sigma_x)_{max}$ equals the lattice friction stress.

(ii) Propagation of Yield

Because of a low density of mobile dislocations, sharp bands occur in steel with no attending relaxation in neighbouring grains. Steps of constant stress on the load-deflection curves show the rapid propagation of bands at relatively low σ_n/σ_{yd} values. Since this occurs when the applied strain rate is caught up by the plastic strain rate $\dot{\epsilon}_p$,

$$\dot{\epsilon}_p = \rho_m bV$$

where ρ_m is the density of mobile dislocations, b their Burgers vector and V their average velocity, it can be assumed that higher velocities are attained in steel than in silicon iron.

(iii) The Yield Mode

The effect of increasing transverse stress, as has been discussed previously, is to restrict shear in the plane of the specimen. If, however, a large number of slip planes are available, as in steel (6.1.1), yielding can continue by shear on a different set of planes.

Immediately below the notch, where σ_y is zero, R-hinges in steel start and progress in the same manner as in Si-Fe (Figs. (c) 6.21-6.23). When the local deformation reaches a stage where R-hinges open out to a distance t/2 from the notch axis, rather than curving in towards the notch axis,

as in Si-Fe, they continue parallel to it in a plane stress manner (Fig. 6.22 (b), (d) - hinge on the right side of the notch, Fig. 6.23 (b), (d)). If, however, the R-hinges cannot spread to a distance, roughly t/2 from the notch axis (as in shallow notches), the plane stress mode is initiated by S-hinges (Figs. 6.21 (b), (d), 6.22 (d) - left side of the notch).

In very shallow notches, where high values of σ_y are not attained, S-hinges show less tendency to change to a different mode of yielding and both plane shear and out-of-plane shear are observed (Fig. 6.20 (b)).

6.3.8 Correlation of Notch Strength and Deformation Mode.

Introduction of the notch brings about heterogeneous yielding and the etch-pit patterns provide direct evidence of this.

The very shallow notches while maintaining a largely uniform mode of yielding still direct yielding to take place from the notch along directions of maximum shear stress (secondary plane shear), thus enclosing a partially elastic diamond-shaped core between the notches. As the notch depth increases, within this range, the preferential yield in the secondary shear direction increases and the core has less plasticity.

This elastic core seems to be a useful parameter to describe the strength and ductility properties of the notch, since it is, in effect, an inverse measure of the amount of deformation in the waist of the specimen.

The core contains an increasing amount of elastic material up to a notch depth of 22.5%. The localized deformation, consisting of the wedge and the R-hinges, is negligible up to this stage, but as notch depth increases beyond 22.5% a point is reached at which there is an appreciable growth of R-hinges into the elastic core. This happens between 22.5% and 36% in the fine-grained Si-Fe and it coincides with the first reversal in the notch strength and ductility curves in Figs. 5.1 and 5.2. This tendency of decreasing notch strength continues through the intermediate notches (45% and 55%) as the elastic core gets further reduced until eventually no elastic core remains.

It may be inferred from this that increasing development of the primary mode weakens the notch - provided that the stress state is substantially bi-axial. This is understandable, because the far-reaching secondary shear zones originating from S-hinges disperse the displacement at the root over a large area away from the notched section and is therefore not sufficiently large locally to weaken the notch. If, on the other hand, the relaxation zones were to spread

inwards along the notch axis - as, for instance, the plane stress type zones envisaged by DUGDALE (9) and reported by HAHN (93) COTTRELL (76) - the notched section would be weakened considerably. The particular notch geometries used in this investigation which showed Dugdale-Muskhelishvili (D-M) type zones were in fact the weakest notches.

It is interesting to note that with increasing root radius the reversals in notch strength (Fig. 5.1) occurred for smaller depths. This is confirmed by the occurrence of the D-M type zones at lower depths for notches of larger root radius (compare $^{4}M^{4}$, $4'M4$ and $4''M4$, Figs. 6.8, 6.12 and 6.15).

In the deep notches the initial rate of deformation is rapid (Figs. 6.25-6.27) until the entire elastic core is annexed. Subsequent deformation involves a high rate of strain-hardening, particularly because the high stresses and sharp gradients of stress in the notched section prevent relaxation by zones spreading in the longitudinal direction. This accounts for the sharp rise in strength from a depth of 63%. Besides this it is conceivable that a certain amount of triaxiality exists at the base of the deep notches because of the increased notched-width to thickness ratio.

CHAPTER 7

STRESS ANALYSIS

7.1 INTRODUCTION

7.1.1 Object

The ways in which a boundary-value problem, such as the one under investigation, can be solved are many. It is generally recognized that the most difficult step in the whole process of engineering analysis is that in which a mathematical model is substituted for a real physical system.

In this investigation the primary object of the engineering analysis was to determine the form of the plastic zones due to varying notch shapes and their progression with increasing applied stress in order to have a basis for comparison with the experimental results. The choice of the method of solution was influenced by this and by the possibility of developing a convenient programme for the analysis.

7.1.2 Literature Review

The development of high stress concentrations at crack tips and notch roots, often leading to brittle fracture called for much experimental and theoretical investigation

on the nature of non-uniformity in the stress and strain fields present near the root.

Some of the more pertinent references are mentioned here to provide a background information on available solutions for stresses and strains associated with cracks and notches in plates.

(i) Elastic Solutions

The earlier solutions proposed were purely elastic.

INGLIS (110), in 1913, devised a solution for non-uniform stress and strain fields along elongated holes and cracks in thin plates. Since then the problem has been treated in a number of ways. WESTERGAARD (111) using a complex variable stress function arrived at the same result as INGLIS, but in a more easily useable form. GRIFFITH (112), investigating the cracking phenomenon, derived an equation for the maximum stress at the tip of a stable crack in a brittle material through strain energy considerations. NEUBER (1) developed methods for exact stress calculations and presented nomographs for computing elastic stress concentration factors for various notch profiles.

Purely elastic solutions, however, are not very useful as they predict infinite stresses at the crack tip, whereas in practice plastic flow occurs around the crack tip ensuring that the stress is finite everywhere. Further, the plastic

region makes the crack effectively larger so that the crack tip is in effect displaced relative to its initial position.

(ii) Plastic Solutions

Exact analysis of most problems of plastic flow is extremely difficult because the governing eqations are not linear. However, approximate methods have been used to obtain solution by estimating yield zones near the crack tip from exact elastic solutions and then incorporating simple approximations to allow for the presence of the plastic zone - SNEDDON (113).

Some of these elastic solutions have been tabulated by DIXON (114), and this allows the derivation of approximate plastic zones simply by finding where a chosen yield criterion is obeyed (DIXON (115), ROOKE (116)).

By introducing a plastic work factor in the place of the surface tension term in GRIFFITH's equation, OROWAN (117) extended GRIFFITH's theory to the case of a crack in steel to obtain stress concentrations at the crack tip. IRWIN (118) carried this further to include certain ductile materials.

For small stresses these approximations hold, but when the stresses are comparatively large yield zones are underestimated leading to error. Thus a rigorous approach was called for andthis was obtained to a large extent from numerical analyses.

(iii) Numerical Solutions

Numerical methods of solving elastic-plastic problems have become popular since ALLEN and SOUTHWELL (119) demonstrated the value of relaxation methods for solving that class of problem that involves boundaries or interfaces not initially known. JACOBS (120) (assuming plane-strain) and STIMPSON and EATON (106) (assuming plane-stress) have both carried out analyses of plastic zones using the relaxation method to allow for the effect of the plastic deformation on the stress distribution.

GAUS (121) working on the principles laid down by HRENNIKOFF (122) and McHENRY (123) developed a lattice model which was the physical analogue of an Airy stress function.

Recently, the availability of high-speed automatic computing facilities has encouraged the development of various other numerical methods of solution of the elasti-plastic equations formulated in terms of suitable stress functions.

Amongst them, notably, the "boundary collocation" method of solution has been applied by GROSS, STRAWLEY and BROWN (124) using the WILLIAMS (125) stress function and by KOBAYASHI (126) using WESTERGAARD's stress function. The collocation method consists in choosing a trial solution, which because of underdetermined parameters actually

represents a whole family of possible approximations. Solution depends on singling out the best approximation within the family by the use of various criteria.

BOWIE et alia (127, 128) have used the complex variable stress functions of MUSHKHELISHVILI (129) with the "conformal mapping" technique, whereby the specimen is represented by a unit circle on a complex plane functionally related to the specimen plane, to obtain their solution. They have reported certain advantages of the mapping technique over the collocation methods, such as the technique being adaptable to finite radius at the crack tip.

Practical iterative solutions for simple elastic-plastic problems have been developed and applied to various problems by MENDELSON and MANSON (130), MENDELSON and SPERO (131), DAVIS (132) and TUBA (133).

TURNER et al (134) formulated the "stiffness" approach for a plane triangular element in plane stress. The method enabled the differential equations describing equilibrium to be expressed in terms of displacements. The method employs a number of finite elements to describe the geometry of the specimen and is known as the "finite-element" method. Subsequently, many investigators have produced elements for different stress conditions.

7.2 GENERAL THEORY

7.2.1 Model

The method of solution adopted in this chapter involves the replacement of the continuous physical system by a pattern of discrete points, where the equilibrium is developed in terms of finite differences of an Airy stress function - $\chi(x,y)$. The theoretical formulation of the problem has already been given by ALLEN and SOUTHWELL (119). However, the main features are summarized in this section.

7.2.2 Assumptions

The general solution to an elasticity problem must satisfy three sets of equations: equilibrium, compatibility and boundary conditions.

The Airy stress function has been shown (119, 120, 106, 135) to provide a convenient solution for plane strain or plane stress problems. If a function $\chi(x,y)$ satisfies the biharmonic equation $\nabla^4\chi = 0$, then the equilibrium and compatibility equations are exactly satisfied for plane strain and approximately satisfied for plane stress conditions. The approximation in the plane stress problem occurs because for plane stress conditions it is assumed that

$$\sigma_z = \tau_{xz} = \tau_{yz} = 0$$

and that σ_x, σ_y and σ_{xy} are independent of Z. These assumptions imply that e_x, e_y, e_z and τ_{xy} are independent of Z and that γ_{xz} and γ_{yz} are zero.

For all the compatibility equations to be satisfied, the strain e_z must be a linear function of x and y, i.e., e_z must satisfy the equation

$$e_z = -\nu (\sigma_x + \sigma_y)/E = ax + by + c$$

where a, b, c are constants.

The condition is not always satisfied in plane stress problems. For thin plates, however, the solutions obtained from this approximation are reasonably good approximations to the exact solution.

It is assumed here that the specimen is thin enough to give a satisfactory plane stress solution.

The other assumptions involved in this method are:

(i) All boundary conditions refer to loads, and the distribution of stress is not dependent on the elastic constants.

(ii) All changes in the external dimensions of the body are negligible so far as the boundary conditions are concerned.

(iii) The von Mises yield criterion,

$$(\sigma_1 - \sigma_2)^2 + (\sigma_2 - \sigma_3)^2 + (\sigma_3 - \sigma_1)^2 = \text{constant}$$

determines the first occurrence of plastic straining and holds thereafter in the plastic region.

(iv) The material is taken to be elastic-perfectly plastic, the relation between shear stress and shear strain being that indicated in Fig. 7.1.

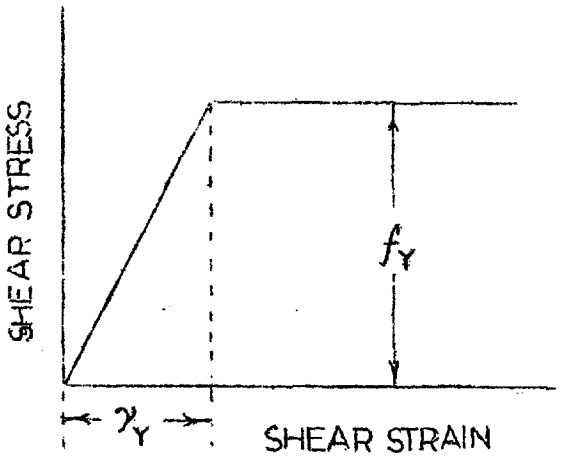

Fig. 7.1

(v) The validity of infinitesimal deformation theory, i.e., "incremental" principal strains have the directions of the principal stresses and these alter as the plastic region extends.

(vi) The plastic strain component is assumed to exist in an incompressible material, i.e., $(e_1)_p + (e_2)_p + (e_3)_p = 0$.

(vii) No element unloads, so that at each stage the developing plastic region encloses the previously existing one.

7.2.3 Boundary Conditions

The stress function boundary conditions have been derived in detail by ALLEN (135), ALLEN and SOUTHWELL (119), and is presented here in brief.

Along the entire outside boundary (see Fig. 7.2), we have

$$\frac{\delta \chi}{\delta x} = 0 \qquad (7.1)$$

$$\frac{\delta \chi}{\delta y} = \bar{\sigma}\, y \qquad (7.2)$$

where $\bar{\sigma}$ is the external applied stress. Integrating equation (2), we have

$$\chi = \tfrac{1}{2}\bar{\sigma}\, y^2 + c_1 \qquad (7.3)$$

At B_3,

$$\chi|_{y=o} = c_1 \qquad (7.4)$$

For this simply connected domain the constant will not enter into the stress formulation, so far simplicity, c_1 is taken to be zero. Thus along stressed boundary, B_2B_3

$$\chi = \tfrac{1}{2}\bar{\sigma}\, y^2 \qquad (7.5)$$

At B_2, where $y = 11$,

$$\chi = \frac{121}{2}\,\bar{\sigma} \qquad (7.6)$$

and

$$\frac{\delta \chi}{\delta y} = 11\,\bar{\sigma} \qquad (7.7)$$

therefore

$$\chi = 11\bar{\sigma}\, y + c_2 = \frac{121}{2}\,\bar{\sigma} \qquad (7.8)$$

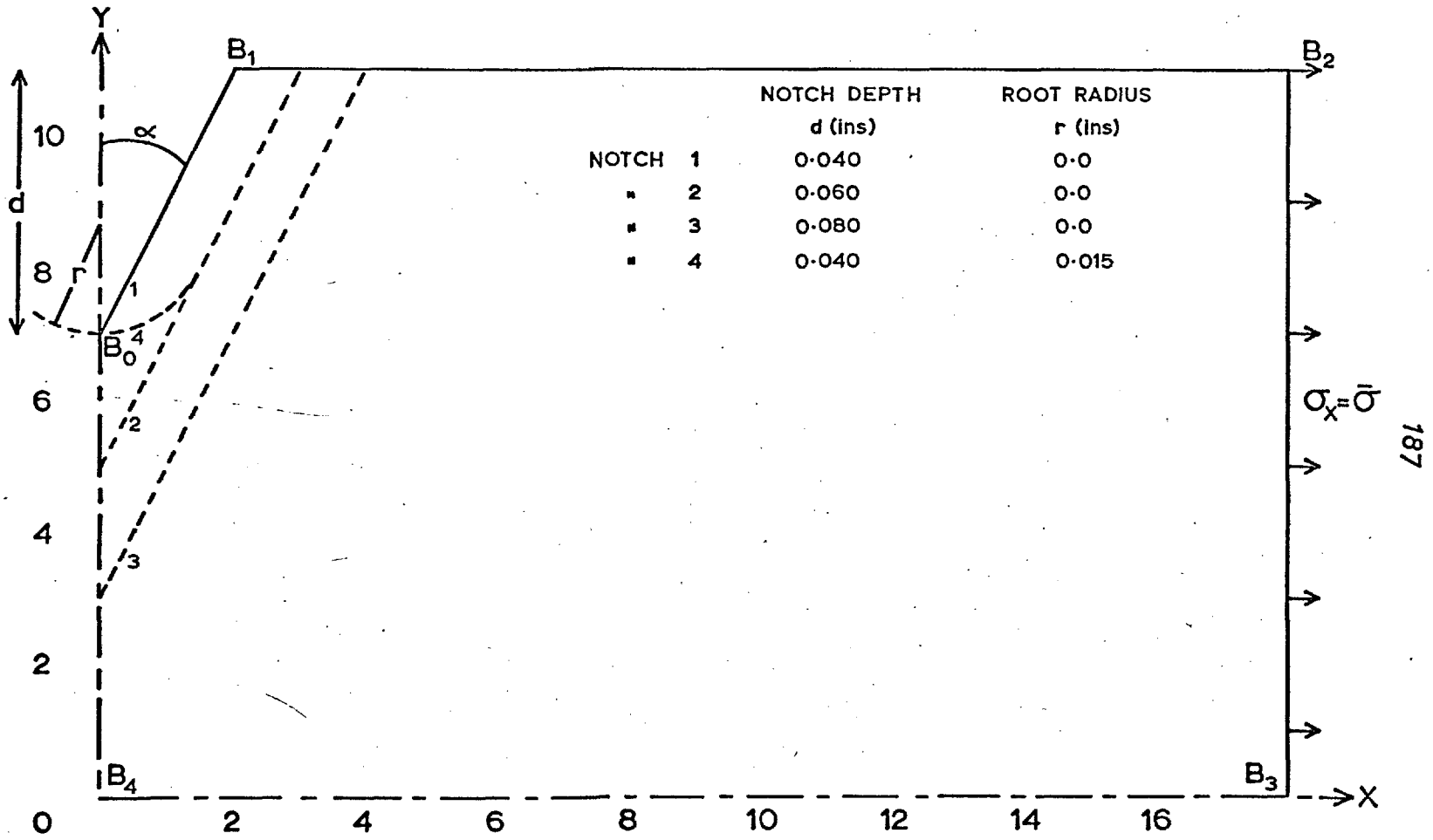

Fig.7. 2. SPECIMEN WITH V-NOTCHES UNDER PLANE STRESS TENSION

when $y = 11$,

$$c_2 = \frac{121}{2}\bar{\sigma} - 121\bar{\sigma} = -\frac{121}{2}\bar{\sigma} \qquad (7.9)$$

Substituting in equation (8),

$$\chi = 11\bar{\sigma}\, y - \frac{121}{2}\bar{\sigma} \qquad (7.10)$$

Thus along boundary $B_0B_1B_2$,

$$\chi = 11\bar{\sigma}\, y - \frac{121}{2}\bar{\sigma}$$

and along boundary B_1B_2,

$$\chi = \frac{121}{2}\bar{\sigma} \quad .$$

In the coarse-mesh iteration, an arbitrary value, $\bar{\sigma} = 48$, was chosen, for arithmetical convenience.

For iterating on the half-mesh it was found more convenient to increase dimensions of the specimen by a factor of 2 while using the same mesh size (length = 1). In the actual computational process, this simply entails the scaling down of χ-values on the coarse-mesh by a factor of 4 and re-iterating. This, of course, implies that the stress-values generated from this distribution of χ would have to be multiplied by a factor of 4^2 (= 16), since the calculation of stresses involves linear combinations of θ, ϕ and ψ which are second derivatives of χ.

7.2.4 Yield Criterion

The von Mises yield criterion can be expressed as:

$$(\sigma_1-\sigma_2)^2+(\sigma_2-\sigma_3)^2+(\sigma_3-\sigma_1)^2 \equiv 2\sigma_{yd}^2 \equiv 9\tau_{oct}^2 \qquad (7.11)$$

where σ_o is the yield stress in tension.

For plane stress this takes the form of an ellipse on the $\sigma_3 = 0$ plane:

$$\sigma_1^2 - \sigma_1\sigma_2 + \sigma_2^2 \equiv \sigma_{yd}^2 \equiv \frac{9}{2}\tau_{oct}^2 \qquad (7.12)$$

Also,

$$\sigma_1 = \frac{\sigma_x+\sigma_y}{2} + \sqrt{\left(\frac{\sigma_x-\sigma_y}{2}\right)^2 + \tau_{xy}^2}$$

and

$$\sigma_2 = \frac{\sigma_x+\sigma_y}{2} - \sqrt{\left(\frac{\sigma_x-\sigma_y}{2}\right)^2 + \tau_{xy}^2}$$

Substituting in equation (7.12), in terms of $\sigma_x, \sigma_y, \tau_{xy}$ the condition of plasticity becomes:

$$\sigma_x^2 - \sigma_x\sigma_y + \sigma_y^2 + 3\tau_{xy}^2 = \frac{9}{2}\tau_{oct}^2 = \sigma_{yd}^2 \qquad (7.13)$$

In terms of Airy's stress function,

$$\sigma_x = \frac{\partial^2\chi}{\partial y^2}; \quad \sigma_y = \frac{\partial^2\chi}{\partial x^2}; \quad \tau_{xy} = -\frac{\partial^2\chi}{\partial x\,\partial y}.$$

T he plastic (non-linear) field equation can then be written as:

$$\left(\frac{\partial^2\chi}{\partial y^2}\right)^2 - \frac{\partial^2\chi}{\partial y^2}\cdot\frac{\partial^2\chi}{\partial x^2} + \left(\frac{\partial^2\chi}{\partial x^2}\right)^2 + 3\left(\frac{\partial^2\chi}{\partial x\,\partial y}\right)^2 \leqslant \frac{9}{2}\tau_{oct}^2 \qquad (7.14)$$

with the equality holding when plastic yielding is reached.

In order to locate the plastic region by means of some convenient constant term the criterion (equation 7.14) is represented by special stress functions, θ, ϕ and ψ, in a simplified form:

$$D^2 \equiv \theta^2 + 3(\phi^2 + \psi^2) = 18\tau^2_{oct} \qquad (7.15)$$

where

$$\theta = \sigma_x + \sigma_y = \frac{\partial^2\chi}{\partial x^2} + \frac{\partial^2\chi}{\partial y^2}$$

$$\phi = -(\sigma_x - \sigma_y) = \frac{\partial^2\chi}{\partial x^2} - \frac{\partial^2\chi}{\partial y^2} \qquad (7.16)$$

$$\psi = -2\tau_{xy} = 2\frac{\partial^2\chi}{\partial x \partial y}$$

ALLEN and SOUTHWELL have shown that θ, ϕ and ψ can be superposed to give a composite pattern that shows the effect of a unit change of χ at a node inside a plastic region (Fig. 7.4).

7.2.5 Procedure

The procedure followed was similar to that of STIMPSON and EATON (106) in that the applied loading was kept constant to obtain an elastic χ-distribution and progressive plastic yielding was obtained by decreasing the critical yield stress. The Gauss-Seidel iteration method was used in obtaining the numerical solution instead of the relaxation (106) method which is more suited to hand computation.

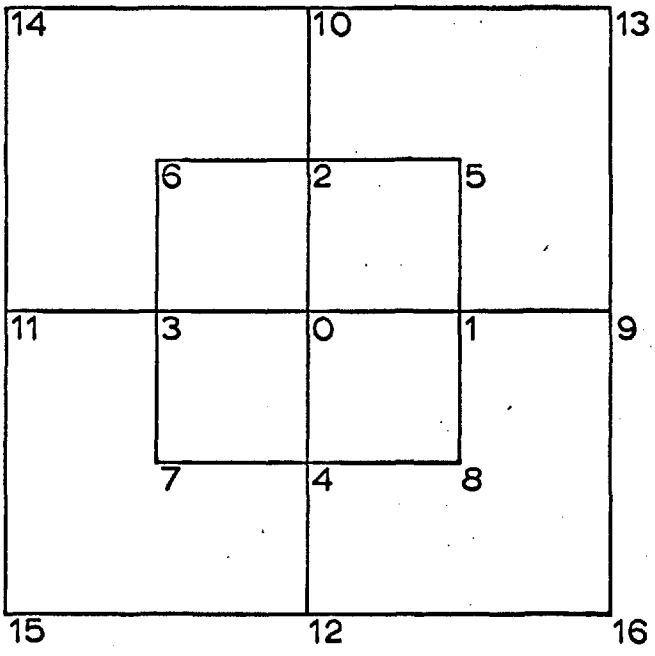

Fig.7.3. RELATIVE POSITIONS OF OTHER NODES WITH REFERENCE NODE "O"

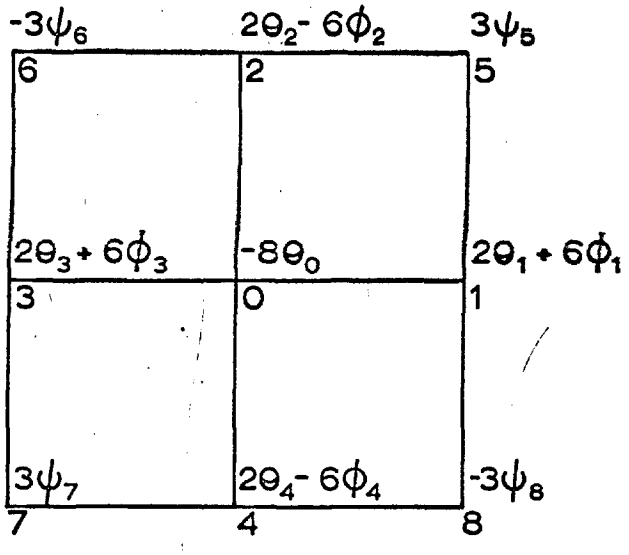

Fig.7.4. PATTERN GIVING EFFECT OF UNIT CHANGE OF χ AT A NODE "O" IN THE PLASTIC REGION

If the stress or strain gradients existing in the continuous material are small, the accuracy obtainable with even a coarse mesh will be fairly good. If the gradients are large, as in notch roots, a finer mesh is required to provide a sufficiently accurate picture of the distribution of strains. An investigation with a model of this type has value in that it is expected to give an accurate picture of the developing plastic enclaves and to some degree a quantitative estimate of stress values.

7.3 COMPUTER PROGRAM

The program developed uses Gauss-Seidel iteration by single steps to solve the linear biharmonic equation in the elastic region and the approximate plastic field equation in the plastic region.

In this section the continuous equilibrium formulation is reduced to a discrete formulation by simply replacing derivatives with finite-difference approximations. The procedure leads to a system of n simultaneous algebraic equations if n discrete points are involved.

The computational molecule representation of the governing differential equations are given in Figs. 7.5 (a) and (b).

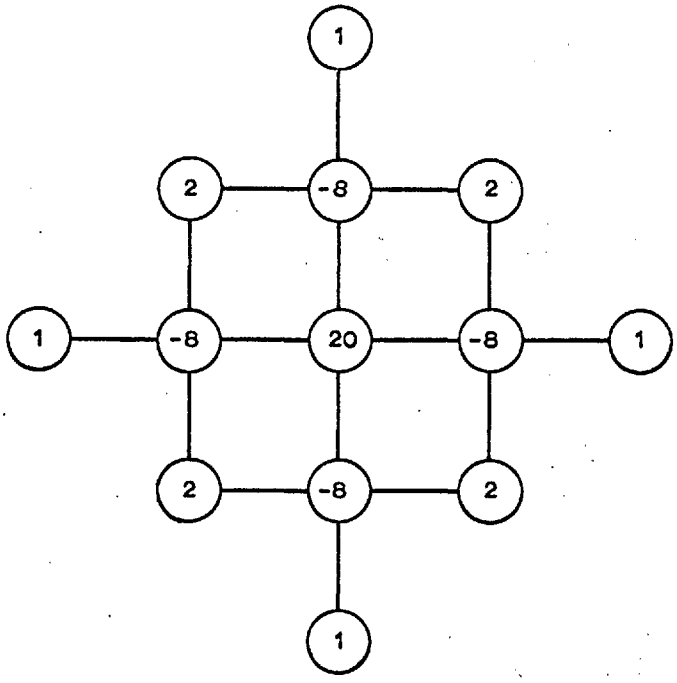

(a) Elastic

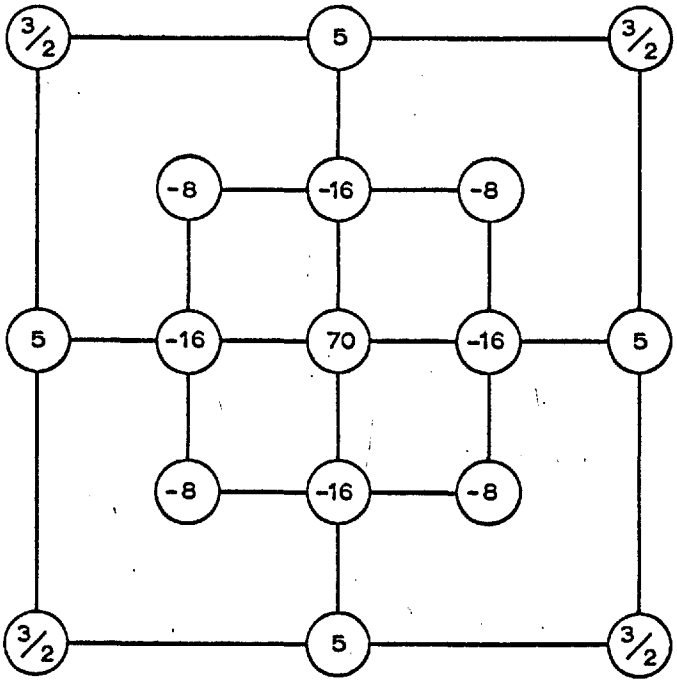

(b) Plastic

Fig. 7.5. COMPUTATIONAL MOLECULE REPRESENTATION OF FORMULA.

Written out the computational molecules take the form:

Elastic:-

$$\Sigma\chi_9 - 2\Sigma\chi_5 - 8\Sigma\chi_1 + 20\chi_o = 0 \qquad (7.17)$$

or

$$20\chi_o = 8\Sigma\chi_1 - 2\Sigma\chi_5 - \Sigma\chi_9 \qquad (7.18)$$

where $\Sigma\chi_1, \Sigma\chi_5$, etc. represent the sums of the χ values at the four symmetrical points typified by 1, 5, 9, etc. in Fig. 7.3.

Plastic:-

$$70\chi_o = 16\Sigma\chi_1 + 8\Sigma\chi_5 - 5\Sigma\chi_9 - \tfrac{3}{2}\Sigma\chi_{13} \qquad (7.19)$$

after substituting χ for θ, ϕ and ψ.

In the iteration process equations (7.18) and (7.19) are used to define an improved value of χ_o. The basic single step of iteration consists in replacing the current value of χ_o by the improved value:

$$\chi_o = \tfrac{1}{20}(8\Sigma\chi_1 - 2\Sigma\chi_5 - \Sigma\chi_9).$$

The latest improvements for the χ values on the right hand side are always employed.

Although a large number of equations and a large number of variables are involved, fairly rapid convergence was expected without the use of acceleration factors, because of the strong family resemblance among all single equations.

The computational procedure consisted in dividing the specimen into a convenient square network, feeding in computed values of χ at the boundary and zero at all internal nodes and then iterating the system to convergence. New and improved fictitious values outside the boundary were computed from boundary conditions at the end of each cycle of iteration for use in the following cycle.

The iteration cycle was programmed to follow a path travelling from the fixed boundary, B_1B_2 towards the longitudinal axis of symmetry. Dummy values were fed in at the axes of symmetry to make for easier convergence.

From the intermediate outputs it was found that a specified accuracy of 0.02/cycle in the coarse mesh and 0.002/cycle in the fine mesh was sufficient to bring about covergence. Between 1000 and 1400 cycles were needed to attain this specified accuracy in the coarse mesh (see Fig. 7.6). These iterated values, together with average values at intermediate nodes,were then fed into a finer network (half of coarse) and reiterated to convergence to give the final elastic solution. The number of cycles needed to reach the specified accuracy in this case was between 400 and 500 cycles, the specimens with the deeper notches requiring the fewer cycles.

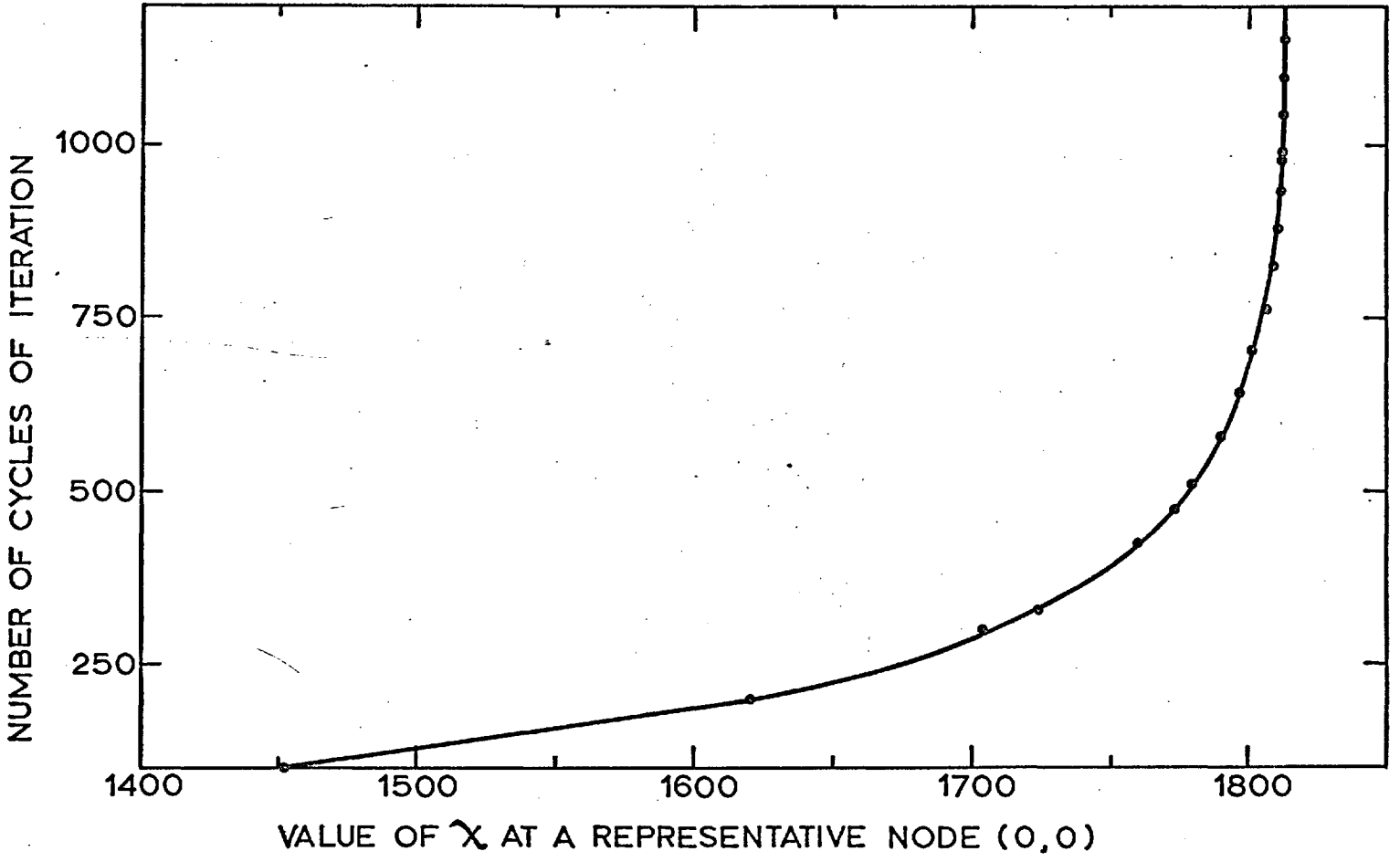

Fig.7.6. CONVERGENCE TEST TO DETERMINE DEGREE OF REQUIRED ACCURACY (d=0·080", r=0·015", Coarse Mesh)

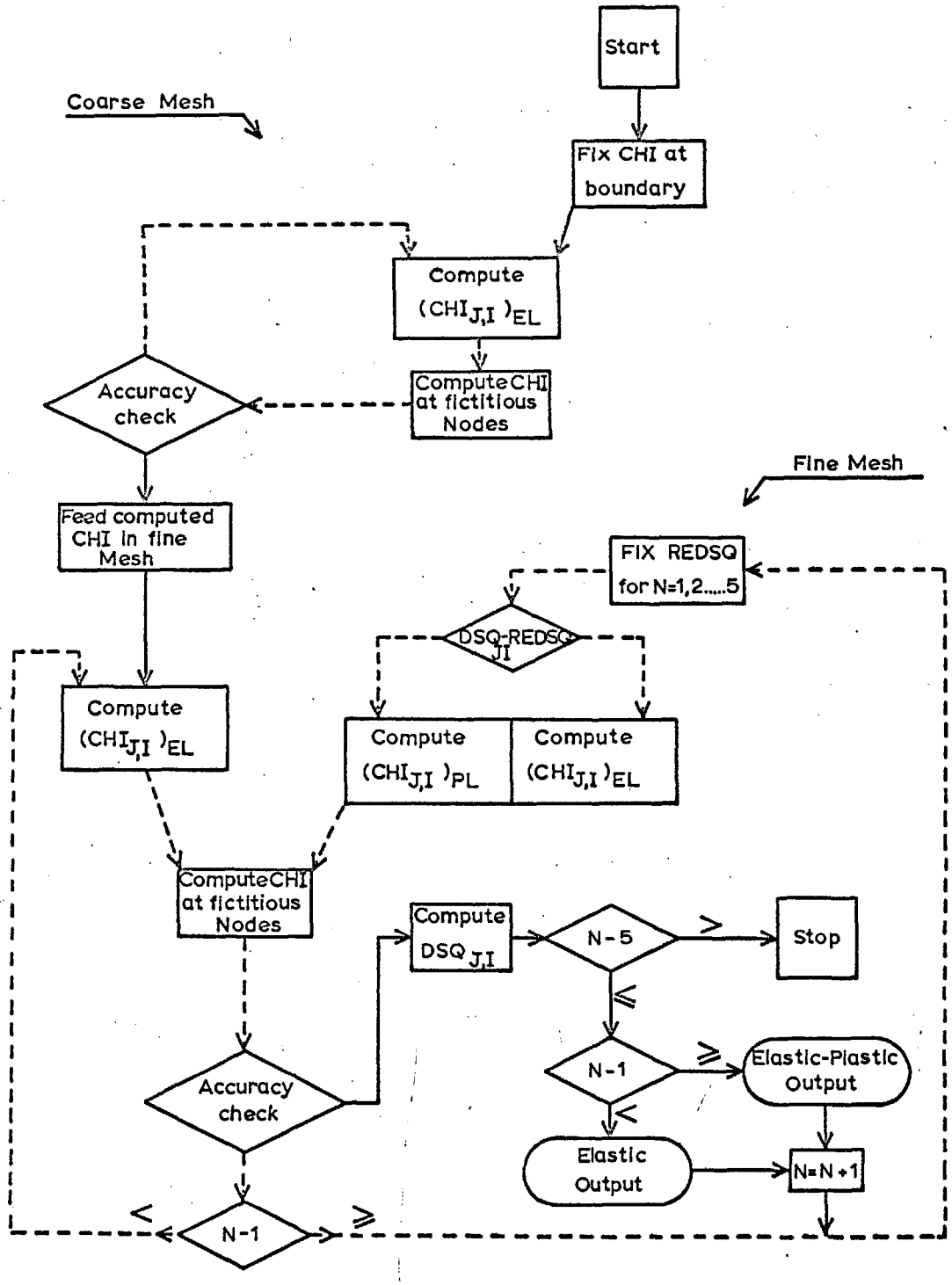

Fig.7.7 FLOW CHART FOR COMPUTER ANALYSIS

For the elastic-plastic analysis a decision process was programmed to store the maximum D^2 value (= REDSQ, say) along the X-axis for a particular penetration of plastic zone along the Y-axis, and compare it with the D^2 values of other nodes. A node with DSQ $\geqslant$ REDSQ would be in a plastic region resulting with the decision to recompute χ at that node according to the plastic field equation, while a node with DSQ $<$ REDSQ would have its χ value recomputed according to the elastic field equation. This process is again iterated to convergence so that values of χ in the plastic and elastic regions can be brought to a state of euqilibrium.

Normal stresses and the shear stress at each node were also computed for the elastic solution and the elastic-plastic solutions for various stages of zone development across the width of the specimen.

The flow sequence of the program is presented diagrammatically in Fig. 7.7.

7.4 RESULTS AND DISCUSSION

7.4.1 Plastic Enclaves

For a constant applied stress, $\bar{\sigma}$, at the right-hand boundary five stages of plastic enclave development were determined by selecting REDSQ (constant D^2) values from near

the notch to the central x-axis. Contours of constant REDSQ were then plotted for each plastic enclave to give the successive positions of the elastic-plastic interface for increasing ratios of $\bar{\sigma}$/REDSQ of $\bar{\sigma}/\tau_{oct}$, where τ_{oct}, the octahedral shear stress level, is related to REDSQ by equation 7.15.

Plastic enclave development along with the corresponding $\bar{\sigma}/\tau_{oct}$ value has been presented in Figs. 7.8 - 7.10 for all the notch profiles included in this stress analysis.

The enclave shapes agree very well with similar work (ALLEN and SOUTHWELL (119), STIMPSON and EATON (106)) and closely approximate the experimental zones presented in chapter 6. In the early stages, of course, the predicted primary zones do not show the R-hinge and wedge-type zones found in experiment, because the mesh size used in the solution is too coarse to resolve this degree of detail. However, the primary zone shapes are quite consistent with the deformation zones discussed earlier and the outer edges can be likened to the R-hinges whilst the tip of the wedge can be taken to be the intercept of the elastic-plastic interface on the y-axis.

(a) Shallow notches

In the sharp notch, from a very early stage ($\bar{\sigma}/\tau_{oct}$ = 1.0 in Fig. 7.8) the zones develop in wide angled directions

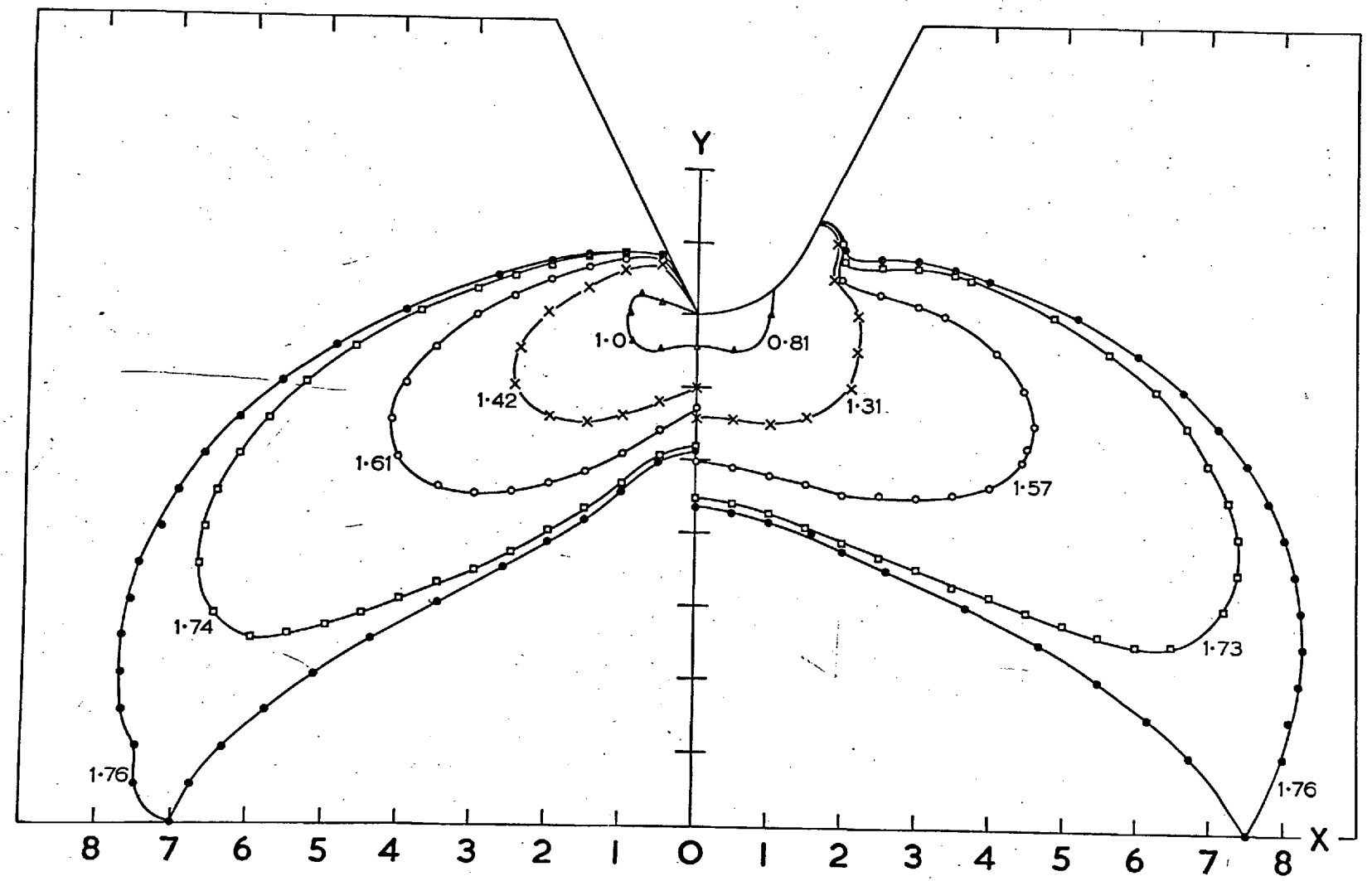

FIG. 7.8. PLASTIC ENCLAVES (36% NOTCH)

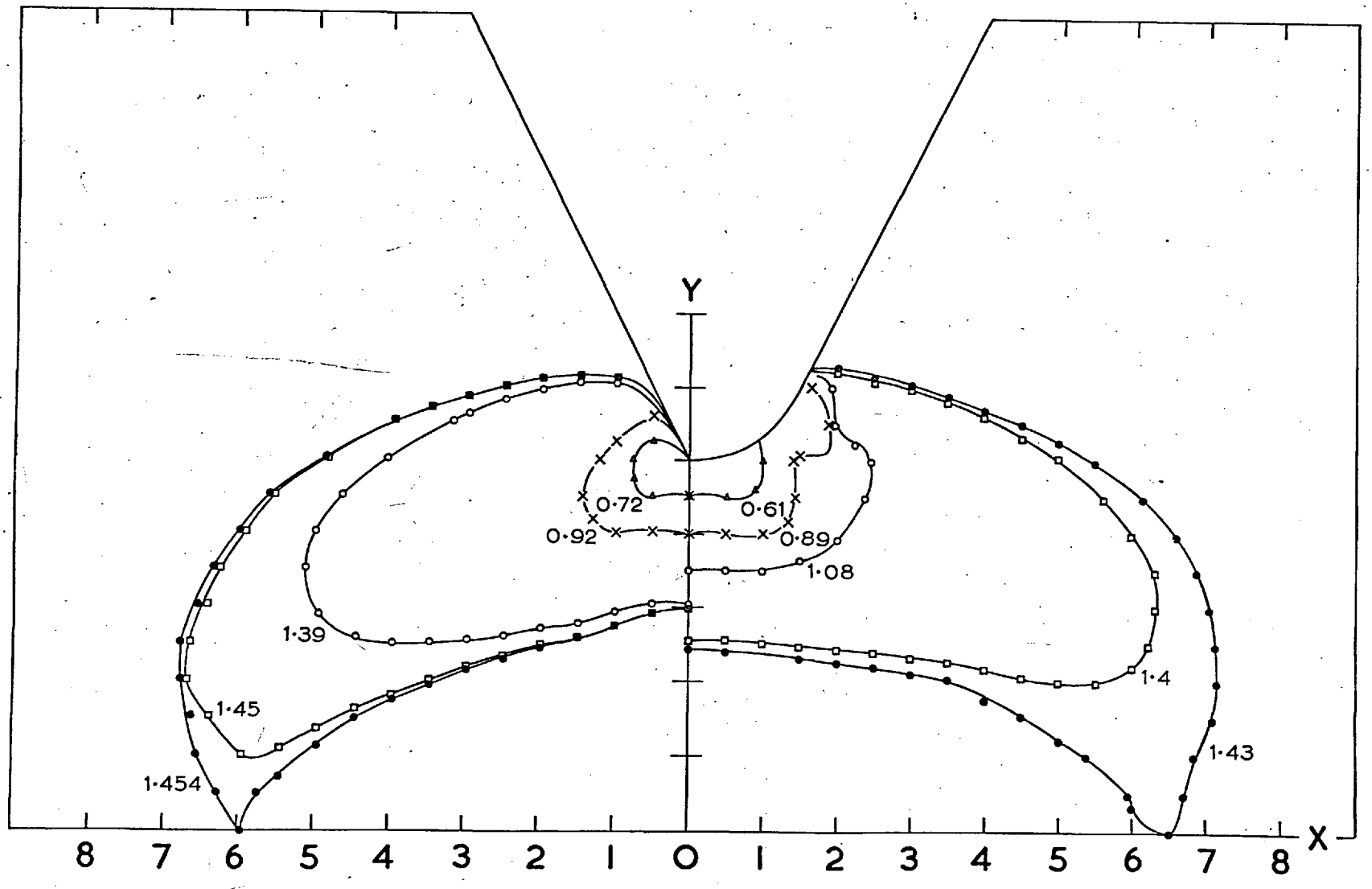

FIG. 7.9. PLASTIC ENCLAVES (55% NOTCH)

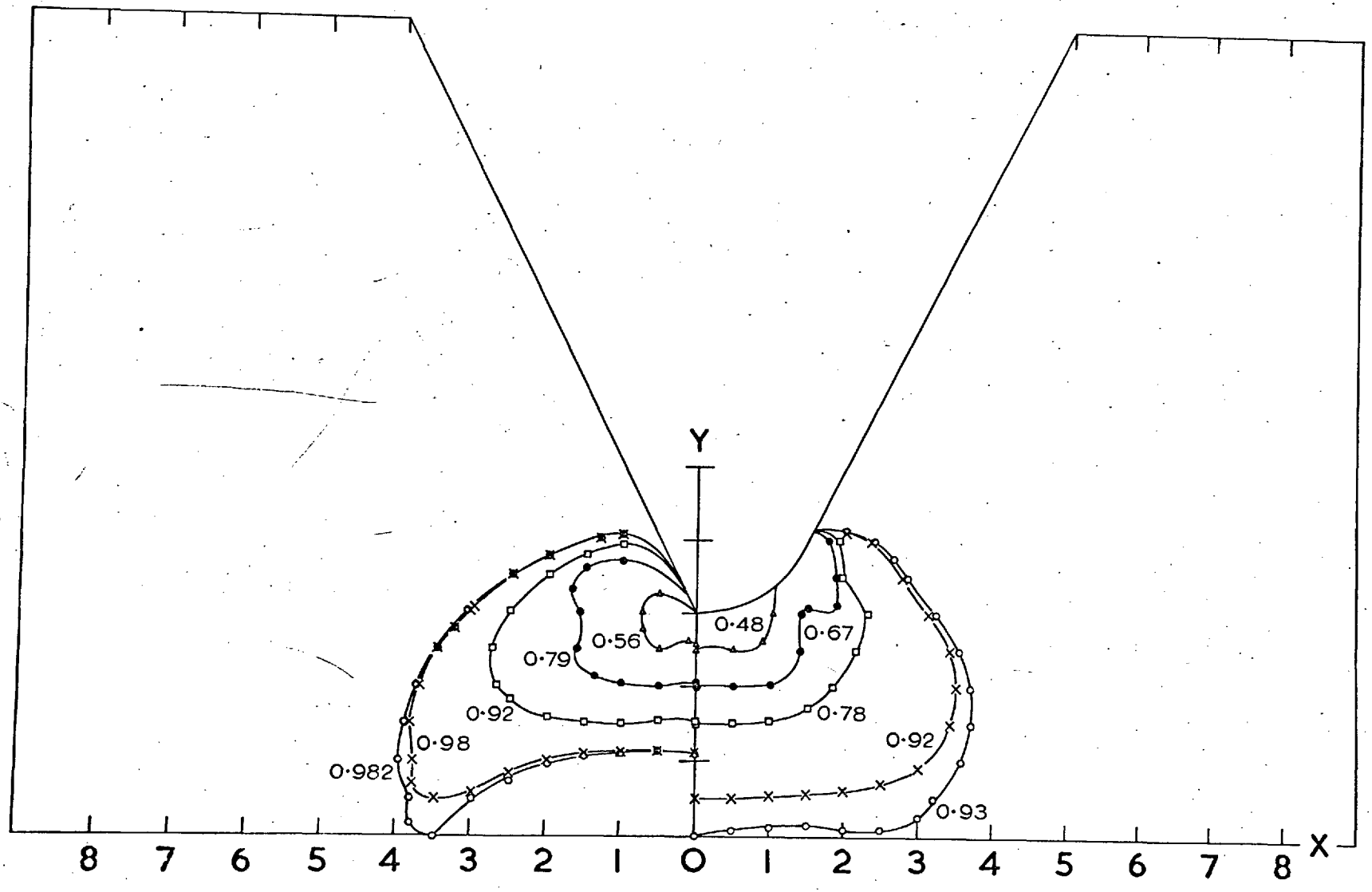

FIG. 7.10. PLASTIC ENCLAVES (73% NOTCH)

consistent with the early S-hinge formation in shallow sharp notches. Progress of the zone is thus largely in the secondary shear direction from the very beginning with very little primary R-hinge type formation and comparatively small wedge penetrations. The zones are very similar to those in Fig. 6.15.

The blunt notch on the other hand, shows larger wedge penetrations and the direction of development is much less wide angled than in the sharp notch up to a $\bar{\sigma}/\tau_{oct} = 1.31$. After this stage the direction of zone formation changes to the secondary direction in a manner very much like the forking out of secondary shear zones in sample 4M4, Fig. 6.8 (c).

(b) Intermediate notches.

As compared with the shallow notch the secondary development in the sharp notch of intermediate depth does not start till later and the shape of the plastic interface indicates the primary R-hinge and wedge-type development up to a $\bar{\sigma}/\tau_{oct} = 0.92$ (Fig. 7.9). The wedge penetration is also noticeably greater and the zone shapes are comparable to the experimental zones in Figs. 6.16 and 6.17.

In the blunt notches again the primary development is much more local to the notch axis and progresses further into the specimen ($\bar{\sigma}/\tau_{oct} = 1.08$ in Fig. 7.9) before there is

any sign of secondary zone formation.

An interesting feature is a second area of stress concentration apparent at the point where the curved root meets the straight flank in the blunt notches. At fairly low stress levels ($\bar{\sigma}/\tau_{oct}$ = 1.31 in Fig. 7.8, $\bar{\sigma}/\tau_{oct}$ = 0.89 in Fig. 7.9 and $\bar{\sigma}/\tau_{oct}$ = 0.67 in Fig. 7.10) plastic zones develop and grow separately from the zone below the notch. These are very similar to S-hinges which, however, are forced to grow in a plane stress manner because of the large root radius. At higher stresses these join the main body of the zone and become indistinguishable from it as it develops into general yield.

(c) Deep notches.

There is very little spread of the zones in the x-direction and much more development in the y-direction. However, the shape of these zones growing in the direction of the notch axis is characterized by their having large flat fronts. This type of primary development continues in the case of the sharp notch up to $\bar{\sigma}/\tau_{oct}$ = 0.92 and up to $\bar{\sigma}/\tau_{oct}$ = 0.93 in the blunt notch. The central elastic core, the size of which is governed by the secondary mode of deformation in a plane shear direction, is thus very small in the case of the sharp notch and practically non-existent in the case of the blunt notch.

The elastic-plastic interface for $\bar{\sigma}/\tau_{oct} = 0.78$ for the blunt notch in Fig. 7.10 compares very favourably with that in Fig. 6.10 and those for the sharp notch in Fig. 7.10 with the illustrations in Figs. 6.18 and 6.19.

Whilst the plastic zones predicted by this analysis correspond well with the experimentally etched zones in Si-Fe, agreement with those in mild steel is limited to that found during the early stages of primary zone development close to the notch. As shown earlier (chapter 6) the secondary zones in mild steel are thin and grow parallel to the notch axis and this mode of deformation is predicted by DUGDALE's analysis. Similar observations have been made by DIXON and VISSER by using photoelastic coatings. They found ALLEN and SOUTHWELL's relaxation predictions in good agreement with strain patterns in aluminium, but not in mild steel beyond a stress level $\sigma_n/\sigma_{yd} = 0.4$.

It seems, therefore, that whilst the model used in the relaxation analysis gives excellent approximations to some materials, it is not suitable for materials which exhibit a marked yield point instability as does mild steel.

7.4.2 Stress Distribution

To indicate the type and magnitude of the stresses existing in the specimen under applied stress levels a

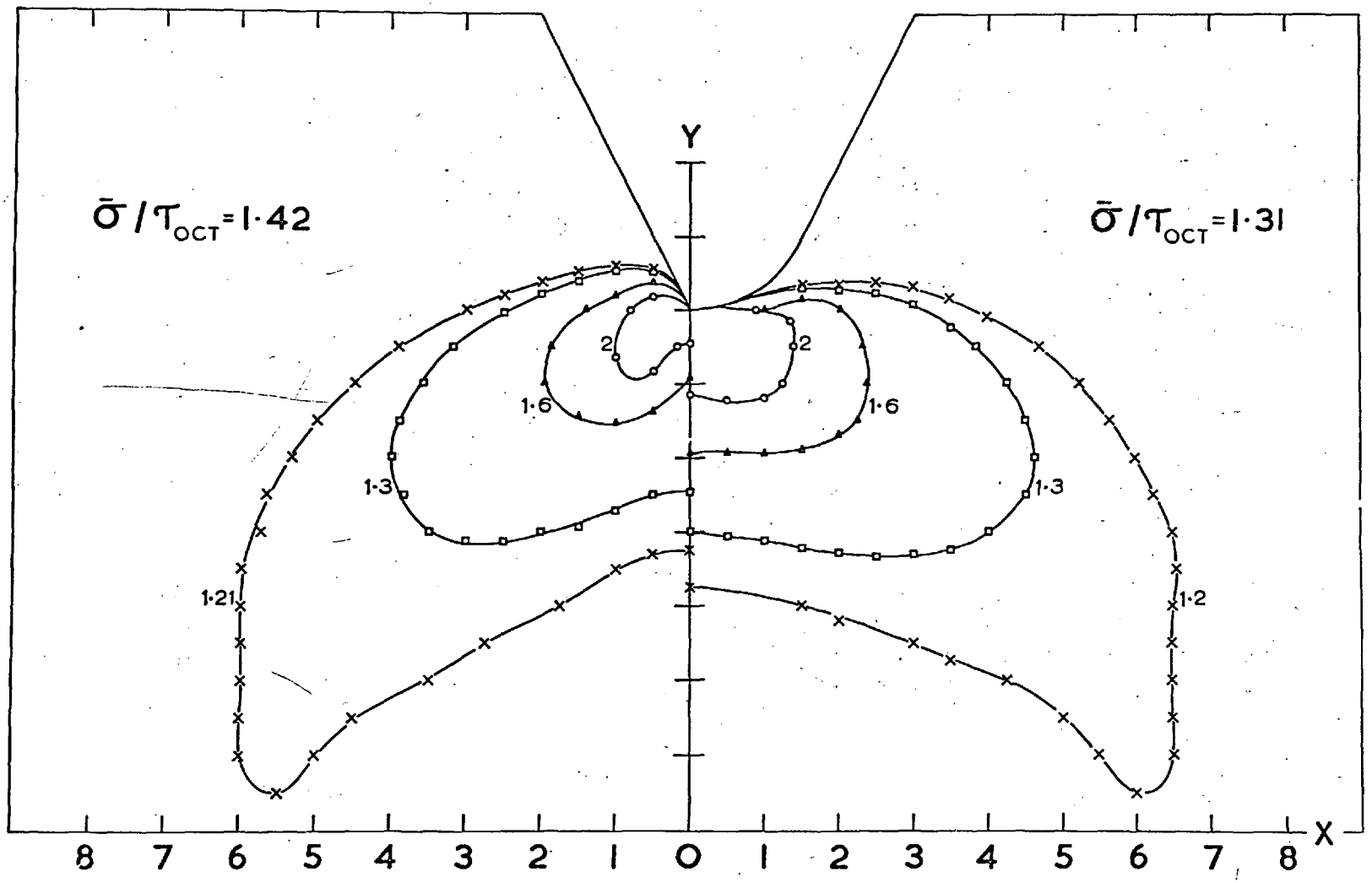

FIG. 7.11. $\sigma_x/\bar{\sigma}$ DISTRIBUTION FROM ELASTIC-PLASTIC ANALYSIS (36% NOTCH)

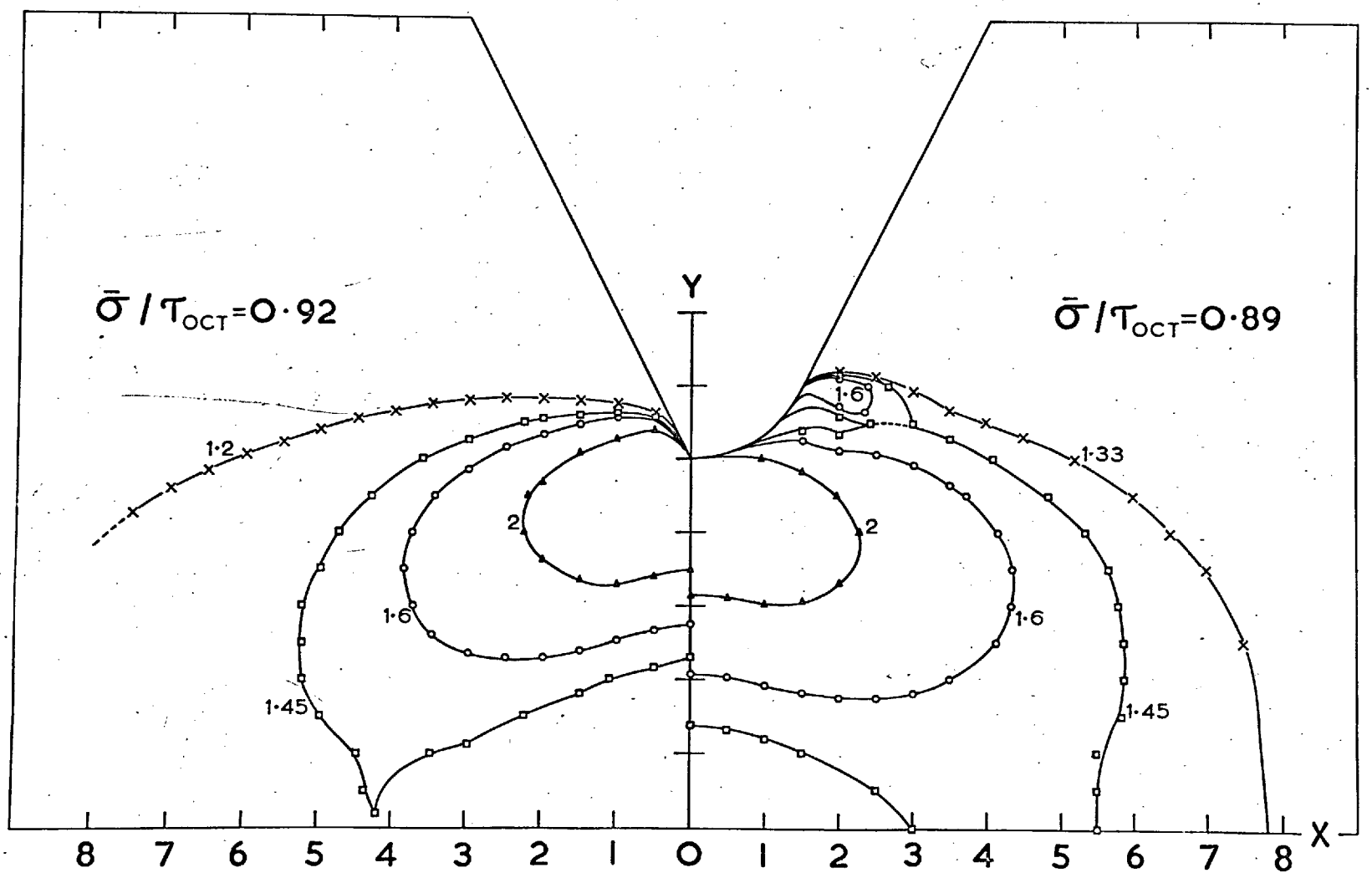

FIG. 7.12. $\sigma_x/\bar{\sigma}$ DISTRIBUTION FROM ELASTIC-PLASTIC ANALYSIS (55% NOTCH)

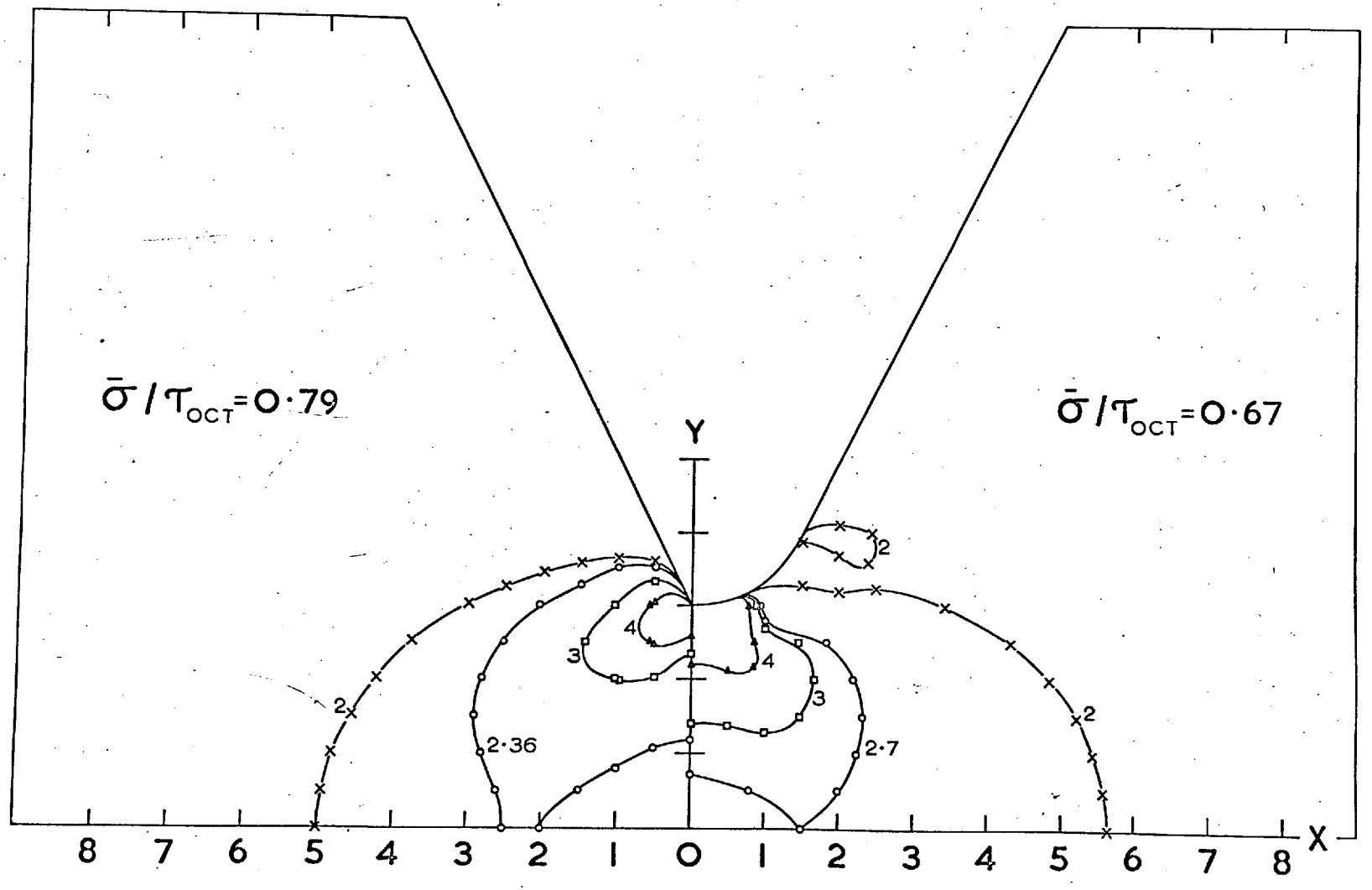

FIG. 7.13. $\sigma_x/\bar{\sigma}$ DISTRIBUTION FROM ELASTIC-PLASTIC ANALYSIS (73% NOTCH)

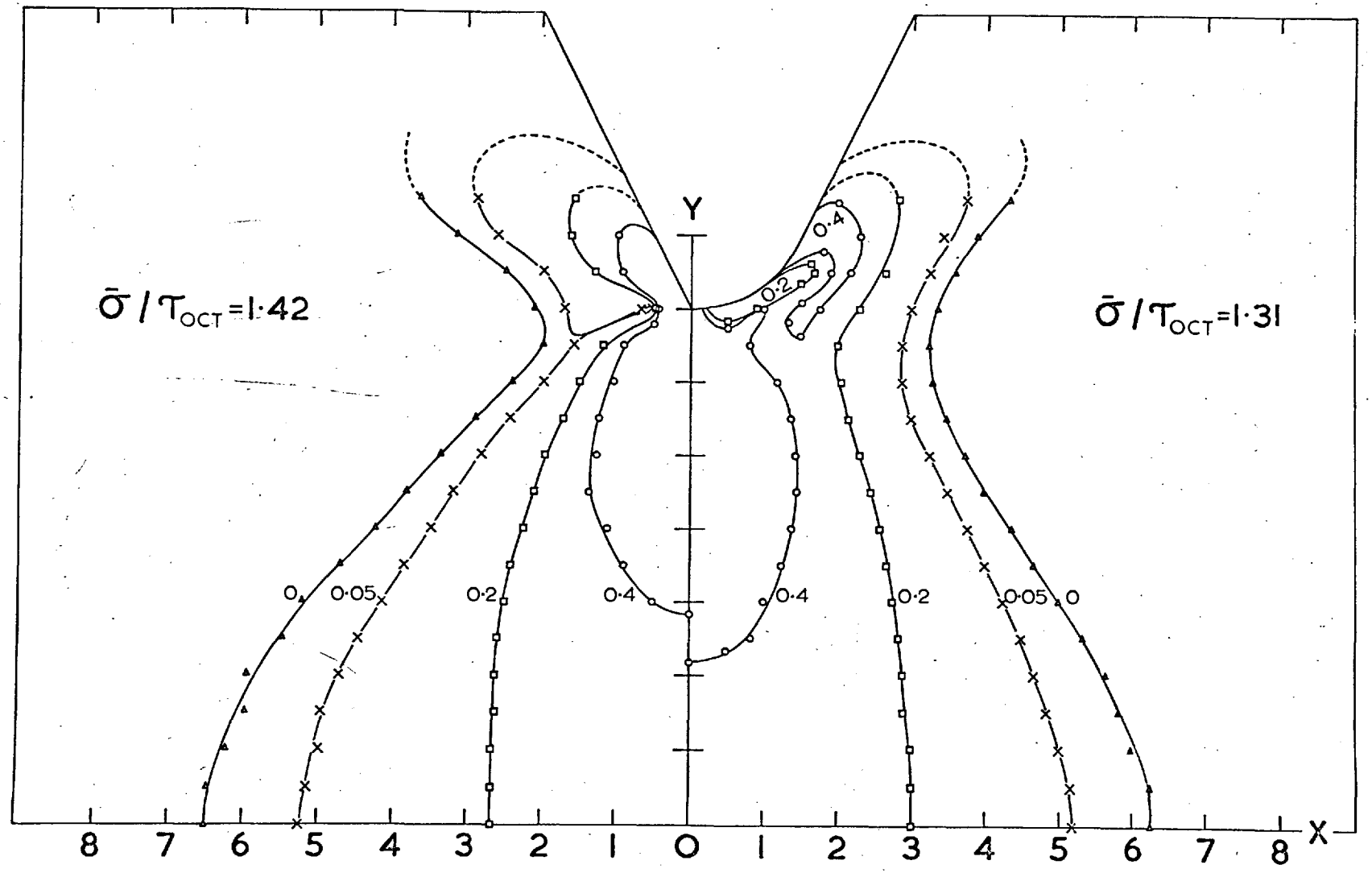

FIG. 7.14. $\sigma_Y/\bar{\sigma}$ DISTRIBUTION FROM ELASTIC-PLASTIC ANALYSIS (36% NOTCH)

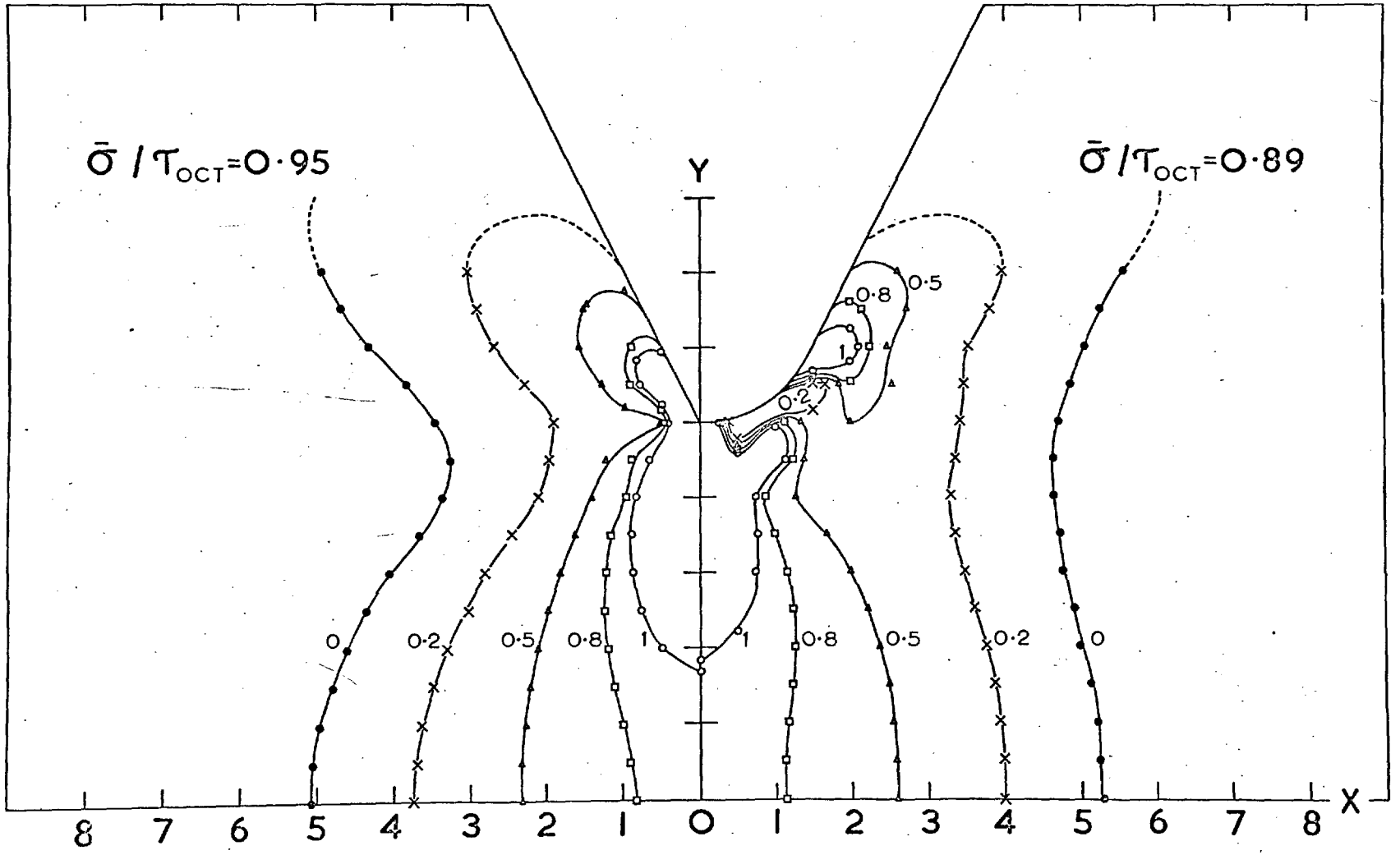

FIG. 7.15. $\sigma_Y/\bar{\sigma}$ DISTRIBUTION FROM ELASTIC-PLASTIC ANALYSIS (55% NOTCH)

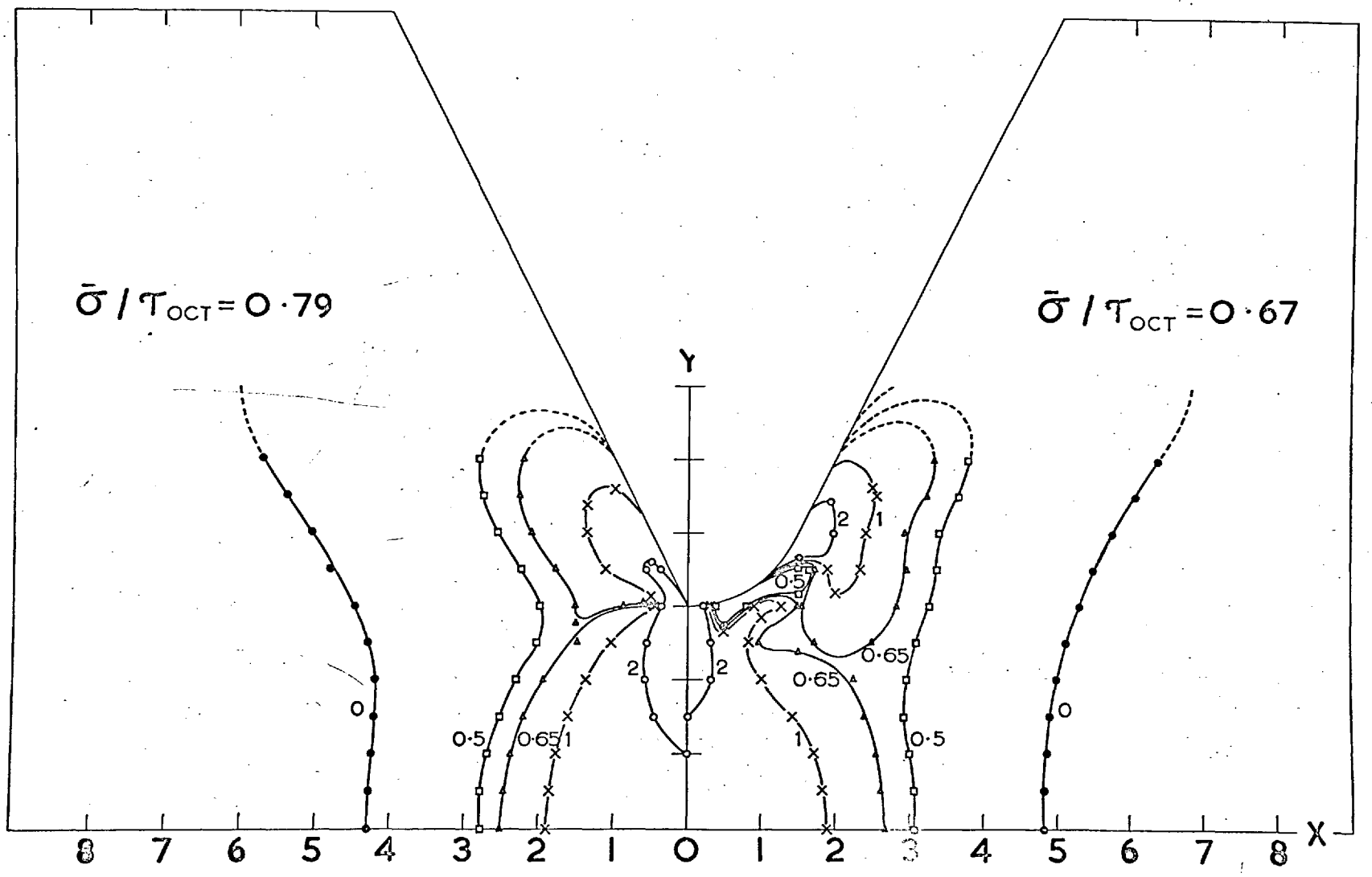

FIG. 7.16. $\sigma_Y / \bar{\sigma}$ DISTRIBUTION FROM ELASTIC-PLASTIC ANALYSIS (73% NOTCH)

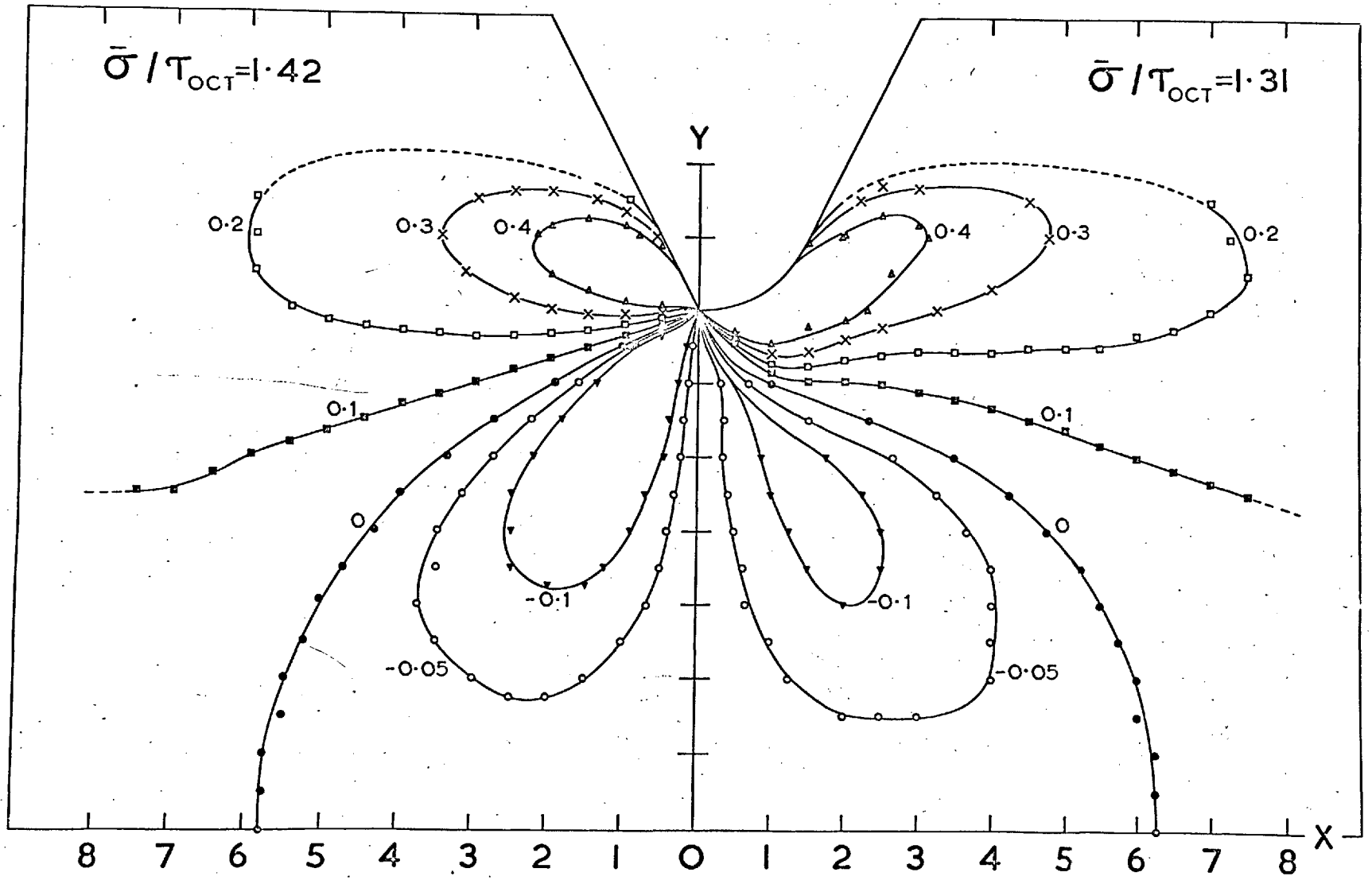

FIG. 7.17. $\tau_{XY}/\bar{\sigma}$ DISTRIBUTION FROM ELASTIC-PLASTIC ANALYSIS (36% NOTCH)

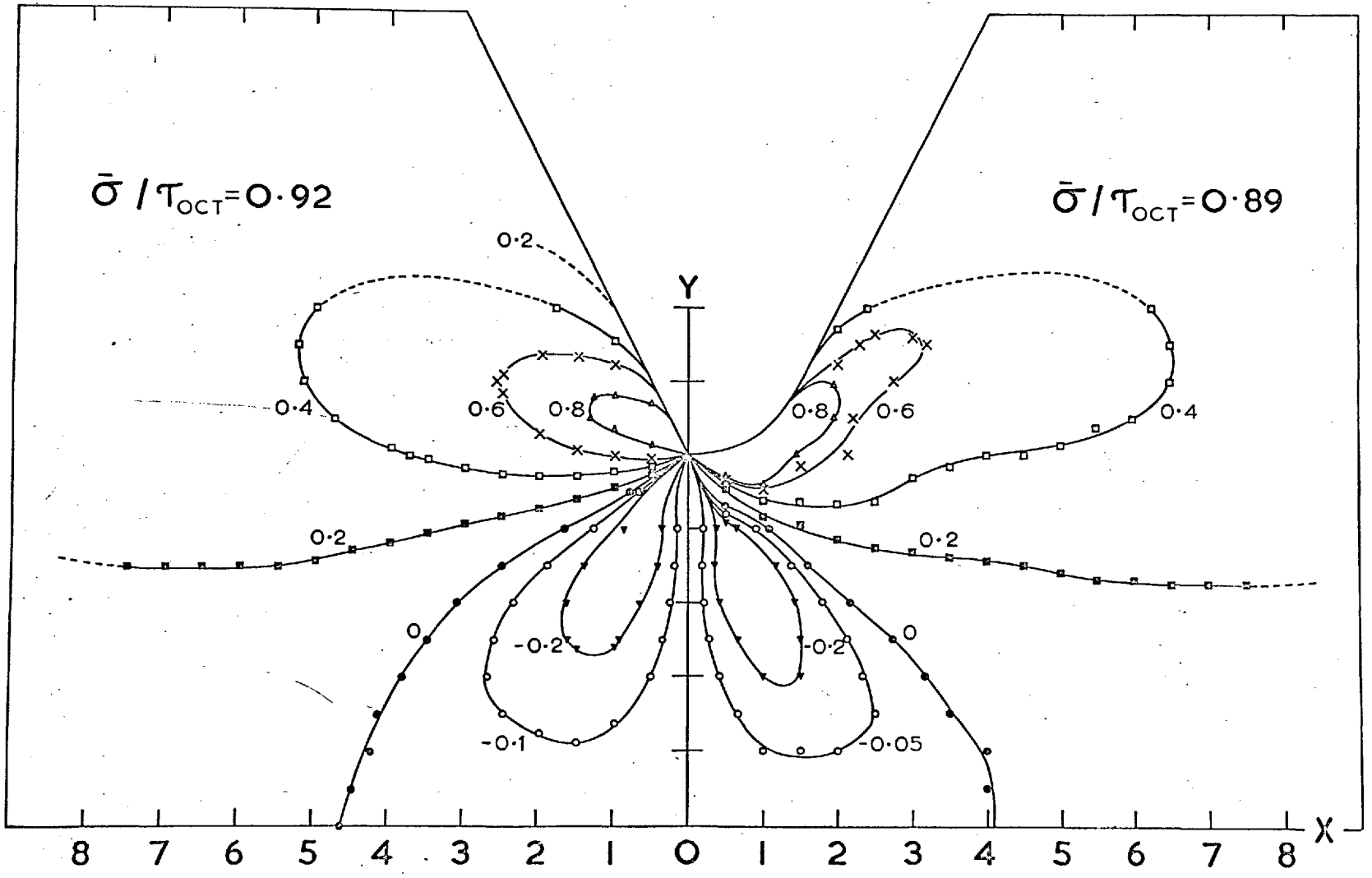

FIG. 7.18. $\tau_{XY}/\bar{\sigma}$ DISTRIBUTION FROM ELASTIC-PLASTIC ANALYSIS (55% NOTCH)

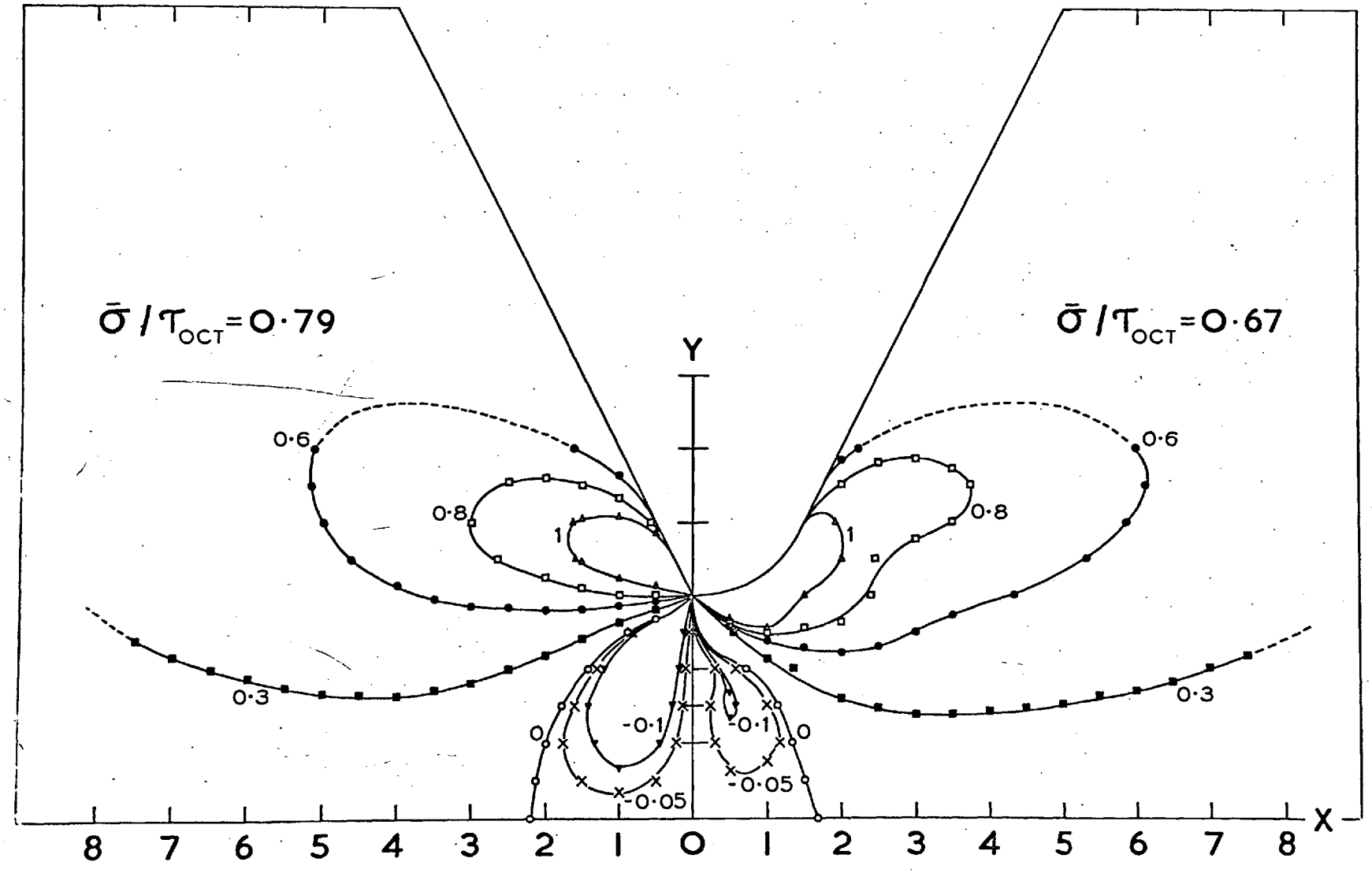

FIG. 7.19. $\tau_{XY}/\bar{\sigma}$ DISTRIBUTION FROM ELASTIC-PLASTIC ANALYSIS (73% NOTCH)

representative value of $\bar{\sigma}/\tau_{oct}$ has been chosen for each notch to illustrate the σ_x(Figs. 7.11 - 7.13), σ_y (Figs. 7.14 - 7.16) and τ_{xy} (Figs. 7.17 - 7.19) distributions.

An assessment of the accuracy of this method in determining the stress state is not within the scope of this work and has not been attempted. Suffice it to say that the distributions are typical and very similar to the elastic stresses except that there is a general shift of the higher stresses outward since the plastic region can not support them.

7.4.3 Zone Penetration with Increasing Stress Level

For comparison with the experimental results the $\bar{\sigma}/\tau_{oct}$ values for successive stages of zone development have been converted to σ_n/σ_{yd} ratios, where σ_n is the nominal stress at the waist and σ_{yd} the yield stress in tension.

From equation (7.11) the relation between σ_{yd} and τ_{oct} is given by

$$2\sigma_{yd}^2 = 9\tau_{oct}^2$$

or

$$\sigma_{yd} = 2.12\tau_{oct}$$

The nominal stress, σ_n, was obtained by plotting the elastic stress distribution at the waist and determining the average value of the longitudinal stress for each notch.

In terms of the ratio of the applied stress, $\bar{\sigma}$, at the right hand boundary of the specimen, these turned out to be, $\sigma_n/\bar{\sigma}$ = 1.35, 1.80 and 3.0, respectively, for the 36%, 55% and 73% deep, sharp notches.

As a representative case, results of the growth of plastic enclaves for the sharp notches with increasing stress level, σ_n/σ_{yd}, have been given in Table 7.1 and plotted in the graph in Fig. 7.20. The curves show two distinct stages of zone development - (a) an initial stage where there is a comparatively slow development and (b) a later stage of rapid growth. The two stages can be associated with the characteristically slow primary development by the wedge and R-hinges and with the rapid spread by secondary shear.

Fig. 7.20 shows that in the 36% notch yielding starts earlier and the change over from stage (a) to (b) is much more gradual than in the deeper notches. With increasing notch depth the initial part of the curves are longer indicating greater tendency of primary development and the transition from the primary to the secondary mode is also more distinct.

The nature of the curves bear a striking resemblance to the experimental curves (Fig. 6.27), particularly those for the 36% and 55% notches. The curve for the deepest notch did not agree with the experimental trend although the range of

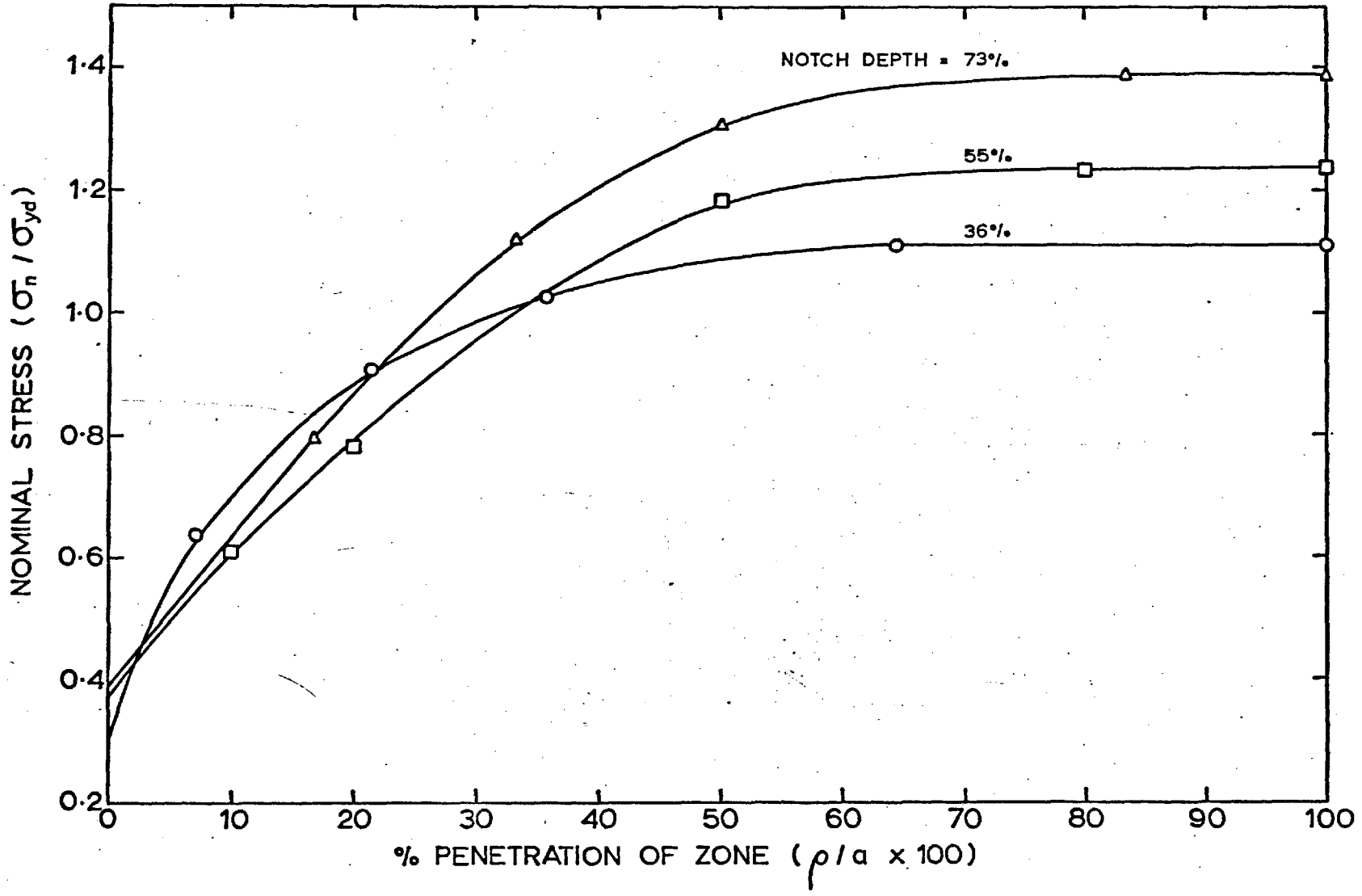

Fig. 7.20. THE EFFECT OF NOTCH DEPTH ON PLASTIC ZONE DEVELOPEMENT IN SPECIMENS WITH SHARP NOTCHES.

Notch Depth %	Zone Penetration %	$\frac{\bar{\sigma}}{\tau_{oct}}$	$\frac{\sigma_n}{\bar{\sigma}}$	$\frac{\sigma_n}{\sigma_{yd}}$
	7.14	1.0	1.35	0.64
	21.40	1.42	"	0.90
36	35.71	1.61	"	1.03
	64.29	1.74	"	1.11
	100.00	1.76	"	1.12
	10.0	0.72	1.80	0.61
	20.0	0.92	"	0.78
55	50.0	1.39	"	1.18
	80.0	1.45	"	1.23
	100.0	1.454	"	1.24
	16.67	0.56	3.0	0.79
	33.33	0.79	"	1.12
73	50.00	0.92	"	1.30
	83.33	0.98	"	1.39
	100.00	0.982	"	1.39

TABLE 7.1. Plastic Zone Development with Increasing Stress in Sharp Notches.

stresses from the start of yield to a full zone penetration is reasonably well predicted.

In comparing the predictions of the computer analysis with the experimental results for Si-Fe it is found that the predicted values of σ_n/σ_{yd} for corresponding zone sizes are higher (6.3.2). However, allowing for the assumptions made in the theoretical model, such as, a zero root radius, it is considered that the agreement is adequate.

CHAPTER 8

CONCLUSIONS

8.1 GENERAL

In order to describe the deformation in the elastic-plastic strain stage it was found necessary to distinguish two stages of zone development.

(a) The primary stage, is represented by comparatively slow yielding in the region of high non-uniform stresses close to the notch root. It is thus determined more by the degree of non-uniformity of elastic stresses than by material characteristics. It consists of a "wedge" and associated "R-hinges."

(b) The secondary stage is of rapid yielding in a general mode at a certain distance below the notch root where the stress distribution is more uniform and close to that in unnotched specimens. It is thus dependent on the yield characteristics of the material. This was usually set off by "S-hinges" from the root in the case of shallow notches, or from R-hinges in deeper notches.

From the observed deformation behaviour it was found convenient to classify the notches into four categories according to their depth.

(a) Very shallow notches (up to 9%). The specimens yielded in much the same way as unnotched specimens.

(b) Shallow notches (between 9% and 36%). The deformation was mainly by the secondary shear from S-hinges.

(c) Intermediate notches (between 36% and 55%). Deformation was by the primary, passing on to the secondary mode.

(d) Deep notches (between 55% and 73%). Deformation was mainly by the primary mode.

8.2 SUMMARY OF CONCLUSIONS AND FUTURE WORK

1. The effect of notching was to direct yielding along preferential directions. To describe the manner of yielding in the elastic-plastic strain stage these directions have been labelled as primary modes (wedge and R-hinges) and secondary modes (plane shear at 45° to the tensile axis and out-of-plane shear in planes at 45° to the specimen plane).

2. The formation of these zones depends in a complex way on first, the notch geometry and specimen thickness (which determine the elastic stress distribution) and second, the yield characteristics of the material (which are important in determining how the elastic stresses are redistributed). The mode of deformation determined, to a large extent, the subsequent strength and ductility properties of the notched specimens.

3. From considerations of stress distribution it was expected that the effect of increasing notch depth would be to raise the lateral stress, thereby resulting in a continuous increase in notch strength. Contrary to expectations, the experimental results showed a region of weak notches in the intermediate range, where strength decreased and ductility increased.

4. The decrease in strength is explained by taking into account the changes in the mode of yielding. It is suggested that if the notch shape were such as to allow the plastic zones to develop in a manner that minimizes the formation of an elastic core between the notches, then the notch ductility would increase, with a corresponding loss in notch strength.

5. Several factors can contribute to a decrease in strength in this manner.

(a) Increasing penetrations of the primary zones so that the secondary plane shear type zones are shifted to greater distances below the notch (as in the case of the sharper notches of intermediate depth in Si-Fe).

(b) A large enough root radius/thickness ratio to allow wide R-hinges to develop into the specimen in a plane stress manner (as in the case of blunt notches in Si-Fe, from a depth of 36% onwards).

(c) A small enough flank angle to permit easy progress of the zones in a plane stress manner (as in the case of the edge-slitted specimen shown in Fig. 6.31).

(d) A sufficient number of easy slip systems so that the presence of even low lateral stresses can help propagation of the zones in a plane stress manner (as in the case of mild steel).

6. The decrease of strength effected in this manner is temporary, as increasing concentration of deformation within a small area containing the notches rapidly leads to strain-hardening. Also the effect of increasing lateral stress continues to exert its influence, resulting in a reversion to the trend of increasing strength with increasing notch depth from a depth of about 55% upwards

7. It is expected that if any one mode of deformation could be maintained consistently in a non-strain hardening material, then increase in strength would be continuous with increasing notch depth. This is supported by the stress analysis, which in ignoring the mode of deformation and any change in the net width during deformation, indicates a continuous increase in strength with deeper notches. Also, in mild steel, where the secondary mode was not altered appreciably in the intermediate range, the decrease in strength was not as marked as in Si-Fe.

8. The sharpness of the root is relatively unimportant, provided it is finite, and provided it is not of an order such as to allow the formation of plane stress type zones.

9. From considerations of approximate limit loads, it was tentatively suggested that while mild steel obeyed the Tresca criterion of yielding, the von Mises criterion was more suited to Si-Fe. Results of the stress analysis were in sufficiently good agreement with experimentally etched yield zones to justify this assumption.

10. Initiation of yielding at the notch root was much earlier in Si-Fe than in mild steel, but the developing zones in the latter were sharp and traversed the specimen rapidly in a plane stress manner. In contrast, the slip bands in Si-Fe spread slowly in the plane shear direction with accompanying relaxation in neighbouring grains. The difference in the modes of deformation is attributed to a larger number of active dislocation sources in Si-Fe and a lower mobility of the slip dislocations.

11. From observations of etch patterns, load-deflection curves and other tensile data, it seems that on reducing grain size in Si-Fe, its yield behaviour approaches that of mild steel. Indeed the investigation of SUITS and CHALMERS (61) indicates that a very fine grained (20μ in diameter) Si-Fe can exhibit yield point instability and that Lüders

bands, nucleated at stress concentrators, such as fillets, can develop in a manner similar to "cross bands" in mild steel, while deformation contributed by the material outside the band remains small up to the upper yield stress.

In such a case it is conceivable that the deformation zones in notched specimens of Si-Fe would be similar to those found in mild steel. This aspect requires further investigation and similar work on very fine grained Si-Fe should prove interesting in this respect.

High strength materials, lower test temperatures and higher strain rates would bring about conditions that help to retain the stress non-uniformity due to notches into later stages of yielding, and thus would be expected to favour the primary yielding. Future work to determine the effect of these parameters on plastic zone formation would be valuable.

REFERENCES

1. H. NEUBER: "Theory of Notch Stresses", Translation David Taylor Model Basin, U.S. Navy, 1919.
2. A.P. GREEN, B.B. HUNDY: J. Mech. Phys. Solids, 4, 128, 1956.
3. M.M. FROCHT: J. App. Mech., 2, A-67, 1935.
4. J.R. DIXON: J. Mech. Phys. Solids, 10, 253, 1962.
5. J.F. KNOTT, A.H. COTTRELL: J. Iron and Steel Inst., 201, 244, 1963.
6. R.T. WILSHAW: Ph.D. Thesis, London, 1964.
7. J. GRIFFITHS: Ph.D. Thesis, Camb. 1965.
8. G. SACHS, J.D. LUBAHN, J. EBERT: Trans. ASM, 34, 517, 1945.
9. D.S. DUGDALE: J. Mech. Phys. Solids, 8, 100, 1960.
10. G. SACHS, J.D. LUBAHN: Trans. ASM, 31, 125, 1943.
11. H.A. LECQUEAR, J.D. LUBAHN: Welding J., 5, 585, 1954.
12. G. SACHS, J.D. LUBAHN: Trans ASM, 33, 340, 1944.
13. R.L. KENYON, R.S. BURNS: Trans. ASM, 21, 577, 1933.
14. H.E. DAVIS, E.R. PARKER, A. BOODBERG: Proc. ASTM, 47, 1947.
15. S.YUKAWA, J.G. McMULLIN: ASME Preprint 61-Met 2, 1961.
16. F.W. BARTON, W.J. HALL: SSC Report No. SSC-147, Washington, National Research Council, 1963.
17. J.A. HENDRICKSON, D.S. WOOD, D.S. CLARK: Trans ASM, 50, 656, 1958.

18. D.R. JENKINS, H.E. GASCOIGNE, L.W. WOLF, S.K. CLARK: WADD Tech. Report 60-234, Wright-Patterson AFB, Ohio, 1960.

19. B.L. AVERBACH, D.K. FELBECK, G.T. HAHN, D.A. THOMAS, Eds.: Fracture. John Wiley, N.Y., 1959.

20. L.E. GRINTER: J. Eng. Mech. Div., Proc. ASCE, 87 No. EM2, 1961.

21. V. WEISS, J.G. SESSLER: "Analysis of the Effects of Test Temperature on the Notch Strength of High-Strength Sheet Alloys." ASTM Preprint 80d, 1961.

22. V. WEISS, J.G. SESSLER, P. PACKMAN, G. SACHS: WADD Tech. Report 60-310, Wright-Patterson AFB, Ohio, 1960.

23. N. BROWN, R.A. EKVALL: Acta Met, 10, 1101, 1962.

24. P.J. WORTHINGTON, E. SMITH: Acta Met, 12, 1277, 1964.

25. A.H. COTTRELL: Report of the Bristol Conf. on Strength of Solids, Phys. Soc., London, 30, 1948.

26. J.R. LOW, Jr., M. GENSAMER: Trans AIMME, 158, 207, 1944.

27. J.C. FISHER, H.C. ROGERS: Acta Met, 4, 180, 1956.

28. E.O. HALL: Proc. Phys. Soc. Lond., B64, 747, 1951.

29. N.J. PETCH: J. Iron and Steel Inst., 174, 25, 1953.

30. H. CONRAD, G. SCHOEK: Acta Met, 8, 791, 1960.

31. F. de KAGINCZY, W.A. BACKOFEN, B. KAPADIA: Fracture, p65, John Wiley, N.Y., 1959.

32. A.N. STROH: Advance in Physics, 6, 418, 1957.

33. W.M. BALDWIN Jr.: Acta Met, 6, 139, 1958.

34. H. SCHWARTZBART, J.R. LOW, Jr.: Trans. AIMME, 185, 637, 1949.

35. J.J. GILMAN, W.G. JOHNSTON: Dislocations and Mechanical Properties of Crystals, p116, John Wiley, N.Y., 1957.

36. J.S. KOEHLER: Phys. Rev., 86, 52, 1952.

37. W.G. JOHNSTON, J.J. GILMAN: J. App. Phys., 30, 129, 1959.

38. D.F. STEIN, J.R. LOW, Jr.: J. App. Phys., 31, 362, 1960.

39. J. HOLDEN: Acta Met, 8, 424, 1960.

40. D. HULL: Introduction to Dislocations, Pergamon Press 1965.

41. G.T HAHN: Acta Met, 10, 727, 1962.

42. T. TAKENTI, S. IKEDA: J. Phys. Soc. Japan, 18, 488, 1963.

43. J.D. ESHELBY, F.C. FRANK, F.R.N. NABARRO: Phil. Mag., 42 351, 1951.

44. A.H. COTTRELL: Trans. AIMME, 212, 192, 1958.

45. I. CODD, N.J. PETCH: Phil. Mag., 5, 30, 1960.

46. R.W. ARMSTRONG, I. CODD, R.M. DOUTHWAITE, N.J. PETCH: Phil. Mag., 7, 45, 1962.

47. D.V. WILSON, J.A. CHAPMAN: Phil. Mag., 8, 1543, 1963.

48. P.J. WORTHINGTON, E. SMITH: Acta Met, 14, 35, 1966.

49. P.J. WORTHINGTON: Acta Met, 14, 1015, 1966.

50. J. HESLOP, N.J. PETCH: Phil. Mag., 1, 866, 1956.

51. A.R. ROSENFIELD: J. Inst. Met., 91, (3), 104, 1962.

52. V.D. KUZNETSOV: Solid State Phys., 2, 1941.

53. H. MUIR, B.L. AVERBACH, M. COHEN: Trans. ASM, 47, 380, 1955.

54. D.A. THOMAS, B.L. AVERBACH: Acta Met., 7, 69, 1959.

55. N. BROWN, K.F. LUKENS: Acta Met., 9, 106, 1961.

56. V.M. FINKEL, V.N. BEREZOVSKIY: Fiz. metal. metalloved., 20, (4), 597, 1965.

57. M.A. SHTREMEL: Fiz. metal. metalloved., 13, 6, 938, 1962.

58. W.D. BRENTNALL, W. ROSTOKER: Acta Met., 13, 187, 1965.

59. J.M. ROBERTS, N. BROWN: Trans. AIMME, 218, 454, 1960.

60. J.R. LOW, Jr., R.W. GUARD: Acta Met., 7, 171, 1959.

61. J.C. SUITS, B. CHALMERS: Acta Met., 9, 854, 1961.

62. D. McLEAN : Conf. on Relation of Properties to Structure. N.P.L., Lond., Jan. 1963.

63. W.E. CARRINGTON, D. McLEAN: Acta Met., 13, 493, 1965.

64. C. CRUSSARD: J. Aust. Inst. Met., 8, 3, 1963.

65. D.F. STEIN, J.R. LOW, Jr.,: Acta Met, 14, 1183, 1966.

66. R.P. CARREKER, Jr., R.W. GUARD: Trans. AIMME, 206, 178, 1956.

67. M.A. ADAMS, A.C. ROBERTS, R.E. SMALLMAN: Acta Met., 8, 328, 1960.

68. J.W. PUGH: Trans. ASM, 47, 984, 1955.

69. G.T. HAHN, W.S. OWEN, B.C. AVERBACH, M. COHEN: Weld. J., 38, 367S, 1959.

70. J.W. PUGH: Trans. AIMME, 48, 677, 1956.

71. N.J. PETCH: Acta Met., 12, 59, 1964.

72. G. LIANIS, H. FORD: J. Mech. Phys. Solids, 1, 1, 1959.

73. R.F. KOMHOLOV, G.V. USHIK: Izv. Akad. Nauk S.S.S.R. Otn. Mekhanika I Mashinostroeniye, 1, 111, 1959.

74. G.T. HAHN: Battelle Memorial Inst. Rep. SR-164, 1964.

75. von A. KOCHENDORFER, A. SCHURENKAMPER: Arch. f. Eisenhuwn, 32, 689, 1961.

76. B.A. BILBY, A.H. COTTRELL, K.H. SWINDEN: Proc. Roy. Soc., A272, 304, 1963.

77. J.F. KNOTT: Ph.D. Thesis. Camb., 196 2.

78. E.H. LEE: J. Appl. Mech., 19, Trans. ASME, 74, 331, 1952.

79. D.C. DRUCKER, W.N. FINDLEY: J. Appl. Mech., Trans. ASME, 493, Sept. 1965.

80. D.A. BATEMAN, F.J. BRADSHAW, D.P. ROOKE: Royal Aircraft Est. Tech. Note CPM 63, 1964.

81. J.R. DIXON, W. VISSER: "An Investigation of the Elastic-Plastic Strain Distribution Around Cracks in Various Sheet Materials." Proc. Int. Symp. Photoelasticity, Chicago, 231, 1961 (Pergamon Press, Oxford, 1963).

82. J.R. DIXON, J.S. STRANNINGAN: J. Mech. Eng. Sc., 6, (2), 1964.

83. G.T. HAHN, A.R. ROSENFIELD: Acta Met., 13, 293, 1965.

84. A.S. TETELMAN: Fracture of Solids, Ed. Drucker and Gilman, 461, 1962.

85. C.S. BARRETT, G. ANSEL, R.F. MEHL: Trans. Amer. Soc. Metals, 25, 702, 1937.

86. J. GRIFFITHS: Private communications, 1964.

87. C.E. MORRIS: Metal Progress, 56, 5, 5, 1946.

88. A. FRY: Stahl u. Eisen, 11, 1, 1093, 1921.

89. R.M. FISHER: Private communication, 1964.

90. D.C. DRUCKER: Proc. 2nd U.S. National Congr. of Appl. Mech., ASME, pp485-488, 1954.

91. H. CONRAD: JISI, 198, 364, 1961.

92. A.N. HOLDEN: Trans. Amer. Inst. Min. (Metall.) Engrs. 192, 182, 1952.

93. B. JAOUL: J. Mech. Phys. Solids, 9, 69, 1961.

94. G. POMEY, M. GRUMBACH: Unpublished results.

95. J.B. LEAN, J. PLATEAU, C. BACHET, C. CRUSSARD: C.R. Acad. Sci. Paris, 246, 2845, 1958.

96. D. GRIFFITHS, J.N. RILEY: Acta Met., 14, 755, 1966.

7. N. LOUAT: Proc. Phys. Soc. (Lond.), 71, 444, 1958.

98. B. SESTAK, S. LIBOVICKY: Acta Met., 11, 1190, 1963.

99. : J. Appl. Phys., 34, 2919,1963.

100. : Conf. on the Relation between Structure and Strength in Metals, N.P.L. 1963.

101. G.I. TAYLOR, C.F. ELAM: Proc. Roy. Soc., A112, 337, 1926.

102. R.P. STEIJN, R.N. BRICK: Trans. A.S.M., 46, 1406, 1954.

103. B. JAOUL, D. GONZALEZ: J. Mech. Phys. Solids, 9, 16, 1961.

104. B. SESTAK, S. LIBOVICKY: Czech. J. Phys., B12, 131,1962.

105. N.E. FROST, D.S. DUGDALE: J. Mech. Phys. Solids, 6, 92, 1958.

106. L.D. STIMPSON, D.M. EATON: Technical Rep. ARL 24, California Inst. Techn., 1961.

107. J.J. GILMAN: Trans. AIME, 209, 449, 1947.

108. A.S. TETELMAN, W.D. ROBERTSON: Acta Met., Trans. AIME 224, 775, 1962.

109. J. FRIEDEL: Averbach, B.L., Felbeck, D.K., Hahn, G.T., Thomas, D.A., Eds., Fracture, Wiley, N.Y., p498, 1959.

110. C.E. INGLIS: Trans. Inst. Naval Arch. (Lond.), 55, 1913.

111. H.M. WESTERGAARD: J. App. Mech., 6, 1939.

112. A.A. GRIFFITH: Trans. Roy. Soc. (A), 221, 1921.

113. I.N. SNEDDON: Proc. Roy. Soc., 187, 229, 1946.

114. J.R. DIXON: J. Roy. Aero. Soc., 66, 320, 1962.

115. : N.E.L. Rept. no. 71, National Eng. Lab., 1962.

116. D.P. ROOKE: R.A.E. Techn. Note CPM 29, 1963.

117. E. OROWAN: Repts. on Progress in Phys., 12, 214, 1948/49.

118. G.R. IRWIN: Trans. Am. Soc. Metals, 40A, 147, 1948.

119. D.N. de G. ALLEN, R. SOUTHWELL: Phil. Trans. Roy. Soc., A242, 49, 1950.

120. J.A. JACOBS: Phil. Mag., 41, 349, 1950.

121. M.P. GAUS: Committee Rept. om Project SR-137. SSC-129, Sept. 1961.

122. A. HRENNIKOFF: J. App. Mech., 8:4, A169, 1941.

123. D. McHENRY: J. Inst. of Civil Engrs., p59, 1943.

124. B. GROSS, J.E. STRAWLEY, W.F. BROWN, Jr.: NASA TN D-2395, Lewis Research Center, Aug. 1964.

125. M.L. WILLIAMS: J. App. Mech., 24, Trans. ASME, 79, 109, 1957.

126. A.S. KOBAYASHI: Boeing Co., Seattle, Wash., Document No. D-23551, Aug. 1964.

127. O.L. BOWIE : J. App. Mech., 31, Trans. ASME, 86, Series E, 208, 1964.

128. : J. App. Mech., 31, Trans. ASME, 86, Series E, 726, 1964

129. N.I. MUSKHELISHVILI: "Some Basic Problems of the Mathematical Theory of Elasticity." P. Noordhoff Ltd., Groningen, Holland, 1953.

130. A. MENDELSON, S.S. MANSON: ASME Paper No. 56-A202; NACA TN-4088 and NASA TR-28.

131. A. MENDELSON, S.W. SPERO: J. App. Mech., 29, Trans. ASME, 84, Ser. E, 151, 1962.

132 E.A. DAVIS: J. App. Mech., 30, Trans. ASME, 85, Ser. E, 210, 1963.

133. I.S. TUBA: Ph.D. thesis, University of Pittsburgh, 1964.

134. M.J. TURNER, R.W. CLOUGH, H.C. MARTIN, L.J. TOPP: J. Aero. Sci., 23, 9, 1956.

135. D.N. de G. ALLEN: Relaxation Methods, McGraw-Hill, London, 1954.

ACKNOWLDEGEMENTS

The work described in this thesis was carried out in the Department of Metallurgy of Imperial College, London, under the direction of Professor J.G. Ball, to whom I am grateful for the facilities provided. I wish to thank Mr. F.A.A. Crane who supervised the work and provided much encouragement, help and valuable discussion.

I also wish to express my thanks to Mr. T. Studley of the Steel Company of Wales for supplying the fine-grained Si-Fe material and the departmental work shop personnel for machining some of the notched specimens.

Finally I am grateful to the Imperial College computing centre for the provision of computing time.